TAMPEREEN TEKNILLINEN YLIOPISTO
TAMPERE UNIVERSITY OF TECHNOLOGY

Tapio Sorvajärvi

Advanced Optical Diagnostic Techniques for Detection of Alkali Vapors in High-Temperature Gases

Julkaisu 1177 • Publication 1177

Tampere 2013

Tampereen teknillinen yliopisto. Julkaisu 1177
Tampere University of Technology. Publication 1177

Tapio Sorvajärvi

Advanced Optical Diagnostic Techniques for Detection of Alkali Vapors in High-Temperature Gases

Thesis for the degree of Doctor of Science in Technology to be presented with due permission for public examination and criticism in Sähkötalo Building, Auditorium S2, at Tampere University of Technology, on the 22nd of November 2013, at 12 noon.

Tampereen teknillinen yliopisto - Tampere University of Technology
Tampere 2013

ISBN 978-952-15-3188-0 (printed)
ISBN 978-952-15-3197-2 (PDF)
ISSN 1459-2045

Abstract

Two advanced optical techniques for the detection of alkali vapors in high-temperature gases are introduced in this Thesis. Alkali vapors are released in solid fuel combustion and increase the maintenance costs of the power plant boilers. Especially, biomass and waste are challenging fuels for contemporary technology. Alkali related problems are controlled with proper fuel mixture ratios and additives that are mixed to fuels or sprayed into the boiler. However, the controlling increases the cost of the produced energy and the additives increase SO_2 concentration. In order to study the alkali formation mechanisms and to control alkali concentrations in power plant boilers, fast, accurate and highly sensitive detection techniques are needed.

This Thesis presents the fundamental absorption properties of the K, KCl and KOH vapors, reviews previously applied techniques for the detection of alkalis, and introduces two novel detection methods. The first method is based on the Photoacoustic Spectroscopy (PAS), that utilizes two branches of physics, namely optics and acoustics. A high-temperature PAS cell is introduced and applied to detect KCl and NaCl. Moreover, the possibility to apply the PAS cell to high-temperature salt-induced metal oxidation is discussed.

The second method, which was fully developed during this work, is called Collinear Photofragmentation and Atomic Absorption Spectroscopy (CPFAAS). CPFAAS provides the limit of detection below parts per billion and the dynamic range of eight orders of magnitude in the detection of alkali chlorides. Moreover, the detection time of the CPFAAS measurement is in the order of micro second, which enables the diagnostics of the fast changing processes, such as combustion. The technique is calibration free and is integrable to "see-through" applications. In this Thesis, CPFAAS is applied to determine potassium vapor concentrations from a laboratory cell, flue gases emanated from 10 mg fuel samples, and flue gases in intermediate and large scale combustion boilers. The presented applications, modeling and comparison with previously applied detection methods show that CPFAAS enables new detection and monitoring capabilities from corrosive high temperature gases.

Preface

This work was carried out in the Optics Laboratory of the Tampere University of Technology during the years 2008–2013. I gratefully acknowledge the financial support from The Graduate School of Tampere University of Technology, the Graduate School of Modern Optics and Photonics, all financial supporters of the ChemCom 2.0 (Chemistry in biomass Combustion) and FUSEC (Future Fuels for Sustainable Energy Conversion) projects, and Yrjö and Kalle Väisälä Foundation.

First, I would like to thank my supervisor Docent Juha Toivonen for providing me the opportunity to carry out my research, for guidance, and for being a motivating supervisor and adviser. You have had an ability to make me do my best and sometimes even more. I also thank my late supervisor Rolf Hernberg who encouraged me to start this work. I am extremely grateful to my former colleagues Ph.D. Albert Manninen and Ph.D. Jaakko Saarela for starting this journey with me in 2005. I have really missed those conversations we had and which led to those base ideas of this Thesis. I also thank my current colleagues Samu, Johan and Antti for sharing the everyday routine of the Ph.D. student with me. My special thanks goes to former and current co-worker Jussi F., Jaakko, Jussi R., Terhi and Jan. You have done a lot of work to put in practise all those crazy ideas I have had and which have led to our current knowledge. Thank you Miro and Hannu for sharing lunch hours. Overall, the atmosphere in the Optics has been superior and has help to carry on during the difficult moments. I'm also very grateful to Inkeri Vänskä, Hanna Kivisaari and Antti Lepistö for the job you have done to help me forward in my research.

Special thanks to people from Åbo Akademi Process Chemistry Center and Metso for providing fual analysis and facilities to carry out fruitful measurement campaigns.

I thank my parents Pirjo and Topi for your endless faith on me and those thousands of encouraging words that helped me to go through all these years of study. Finally, my beloved wife Anne and daughters Aada and Oona. You are my sun shines and the most valuable mental resources. Thank you for your understanding and your endless support during last years.

Tampere, November 2013

Tapio Sorvajärvi

Contents

List of publications

Paper 1 T. Sorvajärvi, A. Manninen, J. Toivonen, J. Saarela, and R. Hernberg, "Resonant photoacoustic cell for pulsed laser analysis of gases at high temperatures," Rev. Sci. Instrum. **37**, 123103 (2009).

Paper 2 T. Sorvajärvi, J. Saarela, and J. Toivonen, "Optical detection of potassium chloride vapor using collinear photofragmentation and atomic absorption spectroscopy," Opt. Lett. **37**, 4011–4013 (2012).

Paper 3 T. Sorvajärvi, and J. Toivonen, "Principles and calibration of collinear photofragmentation and atomic absorption spectroscopy," Appl. Phys. B. *available online* September (2013)
DOI: 10.1007/s00340-013-5633-9.

Paper 4 T. Sorvajärvi, N. DeMartini, J. Rossi, and J. Toivonen, "In-situ Measurement Technique for Simultaneous Detection of K, KCl and KOH Vapors Released Dusring Combustion of Solid Biomass Fuels in Single Particle Reactor ," Appl. Spectrosc. *accepted for publication* (2013)

List of figures

List of tables

List of symbols

CPFAAS	Collinear Photofragmentation and Atomic Absorption Spectroscopy
DFB	distributed-feedback
DOAS	Differential Optical Absorption Spectroscopy
ELIF	Excimer Laser Induced Fragmentation Fluorescence
IACM	In Situ Alkali Chloride Monitor
LIBS	Laser-Induced Breakdown Spectroscopy
OPO	Optical-parametric-oscillator
PA	Photoacoustic
PAS	Photoacoustic Spectroscopy
PEARLS	Plasma Excited Alkali Resonance Line Spectroscopy
PF/FD	Photofragmentation and Fragment Detection
PFF	Photofragment Fluorescence
PLIF	Planar Laser-Induced Fluorescence
ppb	Parts per billion (10^{-9})
ppm	Parts per million (10^{-6})
ppt	Parts per trillion (10^{-12})
ps-DIAL	Picosecond Differential Absorption Lidar
RIS	Resonance Ionization Spectroscopy

SI	Surface Ionization
SPR	Single particle reactor
TDLS	Tunable Diode Laser Spectroscopy
αL_{max}	Maximum absorbance due to the fragment atoms
α_{nm}	nth zero of the derivative of the mth order Bessel function divided by π
α_{rest}	Background extinction coefficient [1/m]
$\Delta\lambda_L$	Lorentz width of absorption line [m]
$\Delta\nu_D$	Doppler width of absorption line [Hz]
γ	Fragmentation efficiency
λ_f	Fragmentation wavelength [m]
ν_0	The center frequency of absorption line [Hz]
σ_X	Absorption cross section of substance X [m^2]
τ	Recovery time constant [s]
A_f	Cross section area of the fragmentation pulse [m^2]
C	Offset parameter in CPFAAS waveforms
c	Speed of light [m/s]
c_s	Speed of sound [m/s]
dx	Step resolution [m]
$E_{absorbed}$	Absorbed energy [J]
E_{in}	Input energy of the fragmentation pulse [J]
E_{out}	Output energy of the fragmentation pulse [J]
f_{nml}	Frequency of cylindrical resotor nml eigenmode [Hz]
h	Planck's constant [Js]
I	Intensity [W/m^2]
I_0	Initial intensity [W/m^2]
k	Boltzmann constant [J/K]
L	Sample length [m]
l	Index of longitudinal eigenmode

M	Molar mass [g/mol]
m	Index of azimuthal eigenmode
n	Index of radial eigenmode
R	Radius of the rasonator [m]
T	Ambient temperature [K]
X_{XY}^{impure}	Target molecule XY concentration in impure sample
X_{XY}^{pure}	Target molecule XY concentration in pure sample
Q	Quality factor of eigenmode

Chapter 1

Introduction

COMBUSTION is the most used technique in the world in energy production having a share of 91 % of total capacity. In 2010, 89 % of all combusted fuel was fossil based, which induced a net flow of 30 Gt of CO_2 into the atmosphere[1]. An increasing need for energy and the current trend of fossil fuels usage have been forecast to lead to a CO_2 level of 1000 part per million (ppm) and a global mean temperature rise of about 6 °C during the next 100 years if no new political actions are performed[2].

The European Union (EU) countries are committed to increasing their total share of the renewable energy sources in total energy consumption to 20 % by the year 2020[3]. The target of the directive is to reduce green house gas emissions and to enhance the sustainability of the energy supply. Wind power and photovoltaics are planned to increase the fastest in percentages, but in absolute amounts, solid biomass combustion will gain the largest growth in the EU[4]. Countries with large forest reserves, such as Finland, are able to fulfill the increased need for solid biomass with wood and the residues of the forest industry[5]. The other countries have to consider the usage of more challenging fuels, such as agricultural residues and sludge.

Biomass combustion has been found to accelerate high temperature corrosion and slagging due to the high content of alkali metals and chlorine in the fuel. In a combustion process the released alkalis and chlorine form alkali chlorides that react with the metal

surfaces of the boiler[6]. Especially problematic alkali chlorides are KCl and NaCl, which are found to react with chromium already at the temperature of 500 °C[7]. Thereby, the steam circulating in the superheater tubes of the biomass fired power plants is usually kept below that temperature. In order to increase the steam temperatures and, thus, the efficiency of the power plants, the concentration of the alkali chlorides has to be controlled. The reduction of the alkali chloride concentration is typically done by mixing sulfur-containing fuel, such as peat, with primary fuel or by spraying an additive like the water solution of ferric sulphate[8] or ammonium sulphate[9] to the flue gases. However, the controlling substances increase the price of the produced energy and too high sulfur concentration in the boiler increases SO_2 emissions. In order to find a balance between corrosion, operating costs, and SO_2 emissions; a real-time monitoring technique for alkali chlorides in the flue gases is needed.

Optical spectroscopy is a branch of science that studies interactions between light and matter. The interactions, such as light scattering, absorption and emission, are molecule specific and can be applied to the selective diagnostics of many kinds of samples. The most common optical technique is direct absorption measurement through a sample, where the target molecule concentration can be calculated by knowing the absorption cross section the molecule, and comparing the intensities of the incident and the transmitted light beam. Optical measurement techniques provide excellent sensitivity, good selectivity, and non-contacting measurement. In other words, they allow molecule specific trace gas detection without the need for physical sampling. Due to their good diagnostics capabilities, optical measurement techniques are used in many applications for example in power production[10], medical research[11], and environmental monitoring[12].

1.1 Aim and Scope of This Work

This work was launched in 2008 as a part of the activities of the Tampere University of Technology (TUT) Physics Department Optics Laboratory in a project called ChemCom 2.0 (Chemistry in Biomass Combustion). ChemCom 2.0 was funded by Finnish Technology Agency (Tekes) and many international companies. The project aimed to develop experimental methods and mathematical tools to gain improved understanding of fundamentals in biomass-, black liquor-, and waste combustion. Our

original task in ChemCom 2.0 was to a develop photoacoustic (PA) measurement technique to be applied to the detection of alkali and heavy metal salts, and to improve the understanding about their spectroscopic properties. However, the interest of our collaboration partners to measure alkali vapor concentrations directly from the furnaces of the boilers combusting biomass fuels made us to change our approach, and we started to develop a completely new measurement technique. The technique was meant to be capable of measuring alkali chloride concentrations from parts per billions (ppb) to hundreds of parts per million (ppm) *in-situ* through several meters wide furnaces. The first laboratory experiments with the new technique were made in the summer of 2009 and the first power plant tests took place in the fall of 2009. The excellent results encouraged to carry on the development work and since early 2010 we have focused on enhancing the reliability, the accuracy and the applicability of the new technique. The development work and the knowledge gained from the earlier photoacoustic studies led to this Thesis.

1.2 Structure of the Thesis

This Thesis is a compilation of the work done within a time period of five years, between 2008 and 2013. The Thesis consists of six introductory chapters and four peer-reviewed papers. The purpose of the introductory chapters is to introduce the reader to the topic, explain the principles of the applied techniques, and highlight main results of this work.

Chapter 1 describes the application area, our motivation for this research, and the structure of the work. The optical absorption properties of the studied alkali vapors are discussed in Chapter 2 . Chapter 3 introduces the principles of the previously applied techniques for the detection of alkali compounds and discusses their usage in different applications.

Chapter 4 and 5 introduce the techniques applied in this work. The first technique is based on the Photoacoustic Spectroscopy (PAS), that is applied to detect KCl and NaCl vapors in high temperature conditions. For this purpose, a resonant photoacoustic cell for high-temperature gas analysis is introduced. The response of the cell for both alkali chlorides is determined and its applicability in real-time corrosion research is discussed. The second technique is called Collinear Photofragmentation and Atomic

Absorption Spectroscopy (CPFAAS) which is developed during this work. Chapter 5 presents the principles of the CPFAAS technique, its calibration equations, applicability to multicomponent analysis and three combustion applications, where the CPFAAS has so far been used. The presented applications are selected such that they highlight the performance of CPFAAS in different conditions and the increased alkali chloride emissions due to the use of alternative biomass fuels. The previous techniques and the techniques introduced in this work are compared at the end of Chapter 5.

This work is summarized in Chapter 6. The peer-reviewed papers, which are the base of this work, are collected at the end of the book.

1.3 Author's Contribution

The Thesis includes four peer-reviewed journal papers. Paper 1 deals with a high temperature photoacoustic cell and Papers 2 - 4 present the theory and an application of the CPFAAS technique. The subjects of the papers and their key results are:

Paper 1

A resonant photoacoustic cell applicable to the high temperatures analysis of corrosive gases is introduced. The structure of the cell is described in detail and the signal processing in the case of laser pulse excitation is discussed. The performance of the cell is demonstrated by determining its sensitivity to corrosive KCl vapor. Moreover, the shape of the photoacoustic spectrum of KCl and the saturation behavior of PAS signal from KCl are determined. The sensitivity and the saturation behavior determined in this work give a good reference for further studies in Paper 2 and Paper 3.

Paper 2

The concept of the CPFAAS is verified. The measurements are done using the same sample cell that was used in Paper 1, which allowed the direct comparison of the techniques. The sensitivity of CPFAAS is measured with optimal 245 nm fragmentation wavelength. Moreover, the line profile of the released K atom fragments is determined. The line shape of the K atom fragments determined in this paper is utilized in Paper 3 and Paper 4 to evaluate the absorption cross section of K atom fragments.

Paper 3

The theoretical calculations needed to solve precursor molecule concentration from the waveforms measured using CPFAAS are presented and verified experimentally. The experimental results are compared to two independent reference techniques in order to verify the theoretical expressions. The measurements were done in a quartz cell in order to avoid KCl reactions with the cell material. The dynamic range of the CPFAAS measurement of KCl is determined to be 8 orders of magnitude based on the saturation behavior of KCl, determined in Paper 1, and the presented calculations.

Paper 4

A selective and simultaneous CPFAAS based detection of K, KCl and KOH is presented. The built experimental setup is demonstrated by measuring the release histories of all three K vapors emitted from 10 mg spruce bark samples combusted at the temperatures of 850 °C, 950 °C, and 1050 °C. Also, the spectral interference between KCl and KOH, and the release dynamics of the studied K vapors are discussed.

All the papers in this work are a result of collaboration and team work. The author's contribution to the papers is summarized in Table 1.1. The contribution is divided into three categories: **Preparation**, **Experiments**, and **Reporting**. Preparation includes the theoretical calculations, design, and measurement setup development; Experiments consists of the experimental work and signal analysis; and Reporting contains the preparation and finalizing the manuscript.

Table 1.1. Summary of author's contribution to articles included in this Thesis

Paper	Preparation	Experiments	Reporting
Paper 1	50 %	60 %	80 %
Paper 2	90 %	100 %	90 %
Paper 3	90 %	100 %	90 %
Paper 4	70 %	80 %	80 %

Chapter 2

Spectroscopy of Potassium Vapors

SPECTROSCOPIC properties of potassium atoms and main potassium compounds found in gaseous form in combustion conditions are presented in this chapter. The discussed properties are very similar to other alkali atoms and compounds, and are not discussed here in detail.

2.1 Potassium (K) atom

The potassium atom belongs to alkali metals and has one valence electron on its outer $4s$ orbital. It is very reactive element and is not found in metallic form in nature. The melting point and boiling point of potassium are 64 °C and 759 °C, respectively[13]. Potassium is an important nutrient and is therefore found abundantly in all living organisms. The main industrial use of potassium is in fertilizers. In 2011, 92 % of annual potassium production was consumed by fertilizer industry[14]. More than 70 % of potassium in fertilizers is in the form of potassium chloride[15].

The spectrum of atomic K is similar to that of the hydrogen atom and is ruled by the single valence electron. Optical transitions between different electron shells are unrestricted but the orbital angular quantum number l (l=0, 1, 2, 3 ... for s, p, d,

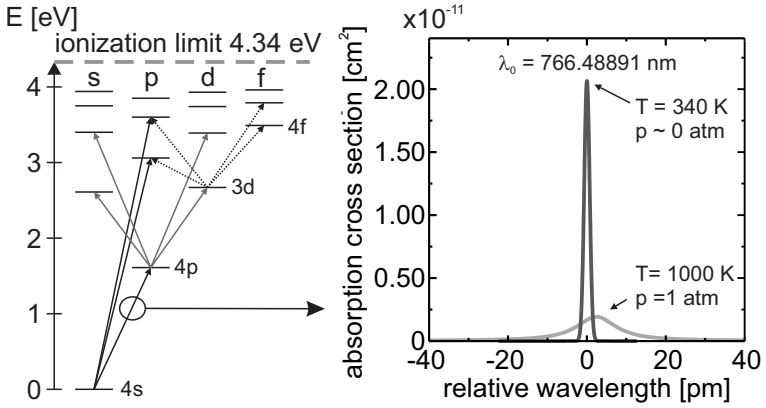

Figure 2.1 a) Diagram for atomic potassium energy levels and b) two absorption peaks modeled for a transition from the ground state $^2S_{1/2}$ to $^2P_{3/2}$ in two different conditions. Energy diagram is reconstructed based on the data presented in reference 18.

f,...) has to change by -1 or $+1$ in each transition. The first allowed transitions from the ground state and from the first excitation states are presented in Fig. 2.1 a).[16,17]

The ground state of potassium $4s$ has no fine splitting and is described with the term $^2S_{1/2}$. The upper levels are affected by the coupling of spin-orbit and angular momentum, and are split into two parts. Spectrally the fine structure is observed as two closely separated lines of potassium both arising from $4s$ orbital and ending up to $4p$ orbital. More specifically, these lines correspond to the transitions $^2S_{1/2} -^2 P_{1/2}$ and $^2S_{1/2} -^2 P_{3/2}$ known as D1 (769.9 nm) and D2 (766.5 nm) lines of potassium, respectively.[16,17]

The observed absorption lines of atoms are very narrow but still have a finite line width. The typical broadening mechanisms of the atomic lines are natural broadening, Doppler broadening, and pressure broadening (also known as collision broadening). Natural broadening sets a lower limit to how narrow the line can be at absolute zero temperature. In room temperature and at low pressure, the Doppler broadening is the dominating broadening mechanism. The Doppler width $\Delta\nu_D$ of atomic line can be calculated as

$$\Delta\nu_D = 7.16 \cdot 10^{-7} \nu_0 \sqrt{T/M}, \tag{2.1}$$

where ν_0, T and M are the center frequency of the atomic line, ambient temperature, and molar mass, respectively[19]. In atmospheric pressure, the pressure broadening is the most dominating effect inducing a Lorentzian profile for the atomic line. Coef-

ficients determining the line width of the pressure broadened line are atom specific. One simple way to approximate the width of the pressure broadened line $\Delta\lambda_L$ is to use a proportionality [20]

$$\Delta\lambda_L \propto pT^{-0.7}, \tag{2.2}$$

and an experimentally determined line width at known temperature and pressure p. For example, the Lorentzian line width for potassium D1 line has been measured to be 5.2 GHz at the pressure and temperature of 1 atm and 1170 K, respectively [21]. In addition to broadening, ambient pressure changes the absorption line by shifting it. The pressure shift of potassium D1 line is measured to be approximately 2.4 pm/atm at the temperature of 1170 K [21].

Figure 2.1 b) presents the modeled absorption spectrum of the potassium D2 line in two conditions. The narrower line with a higher peak value has been calculated using nearly vacuum conditions and the temperature of 340 K, which is a typical condition in atomic reference cells, and the broader line using the temperature of 1000 K and 1 atm pressure, which is more close to combustion conditions. For the narrower line the calculations result in a Doppler width of 0.82 GHz, and for the broader line a Doppler width of 1.42 GHz and a Lorentz width of 5.8 GHz. In wavelengths, the total line widths for low temperature and high temperature potassium are 1.6 pm and 12 pm, respectively. The line shift of high temperature potassium is 2.4 pm (1.2 GHz), when the D2 line is assumed to shift similarly to the D1 line. The maximum absorption cross section of the high temperature potassium is found to be 10.8 times smaller than that of the low temperature potassium.

2.2 Potassium Chloride (KCl) Molecule

Potassium chloride belongs to the group of alkali halides which are compounds of one alkali and one halogen atoms bonded together with an ionic bond. The bond length of KCl molecule is 2.67 Å [22]. KCl has a melting and boiling temperatures of 770 °C [13] and 1413 °C [23], respectively. The saturation vapor pressure of KCl at its melting temperature is 36 mbar (calculated using a commercial HSC 5.1 database reference 24) corresponding to 360 ppm in ambient pressure of 1 bar. In gaseous form, KCl occurs mainly as diatomic molecules, but four-atom dimers may also occur in certain conditions [22]. In combustion, KCl vapor is formed through the direct vaporization

of solid KCl or through chemical reactions between released potassium and chlorine containing species[25].

The most important spectroscopic properties affecting the optical detection of all alkali halides have been collected into Fig. 2.2. The figure presents the schematics of the potential energy surface of KCl. The vibrational constants of the alkali halides are commonly very low[22] (280 cm^{-1} for KCl), which makes their direct usage in the optical detection challenging. The vibrational bands have been determined using emission spectroscopy[26] or utilizing the information gained from the fluctuation bands[27,28], which are discussed more later in this section. In UV region the spectra of the alkali halides contain broad continuums (shown on left in Fig. 2.2) and lack a clear fine structure[29]. The electronic excitation states of the alkali halides are repulsive meaning that the UV photon absorption is followed by the dissociation of the molecule. Despite the ionic ground state $^1\Sigma^+$ of alkali halides their excitation states in near UV region are covalent and produce neutral atoms, which either settle on their ground or excited electronic state. The electronic state of the fragment depends on the ambient temperature and the energy of the excitation photon[30,31]. For example, the three lowest energy excitation states of KCl release atom pairs K($^2S_{1/2}$) Cl($^2P_{3/2}$), K($^2S_{1/2}$) Cl($^2P_{1/2}$), and K($^2P_{1/2}$) Cl($^2P_{3/2}$). The excitations are further divided in transitions from ionic ground state $^1\Sigma^+$ to covalent bound states $^1\Sigma^+$ or $^1\Pi$, corresponding to parallel and perpendicular transitions, respectively. These transitions are energetically closely separated and are observable as separate bands in the absorption spectrum only at temperatures below 300 K[32].

The lowest covalent excitation state of alkali halides settles energetically below the dissociation level of the ionic ground state, which cause the crossing of two states. The crossing states form a potential well where the molecule can be trapped. The trapping does not occur when the molecule is excited to $^1\Pi$ state. However, the excitation to $^1\Sigma^+$ state induces trapping when the crossing point of the ground and excited states locates at internuclear distances smaller than 8 Å[33]. The crossing point of the KCl-curves occurs at internuclear distance of 19.8 Å[29] when the trapping effect is negligible and each absorbed photon can be assumed to induce the dissociation of a molecule[34].

The UV spectrum and the absorption cross sections of KCl shown in Fig. 2.2 were originally determined in 1967[30]. The later studies showing the shape of the KCl spectrum as a function of temperature[35] and the spectrum of the pure monomers[36]

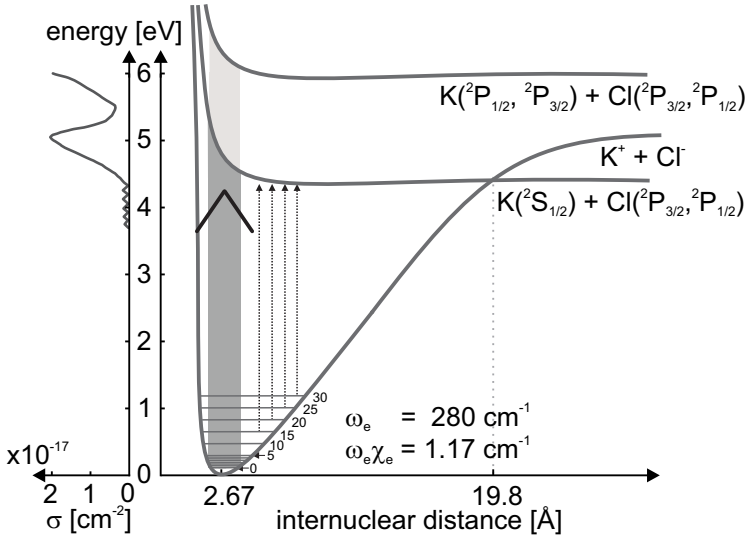

Figure 2.2 Schematics of potential energy surface of KCl. Vibrational levels are closely separated and they are only rarely applied in KCl measurements. The UV absorption spectrum shown on the left hand side corresponds to electronic transitions from ionic ground state to covalent excitation states. The covalent states are repulsive and induce the dissociation of the molecule to neutral atoms. The weak fluctuation bands observed around 4 eV originate from excited vibrational bands to the horizontal part of the repulsive excitation state.

have corresponded well to the original study. The broad continuum in the spectrum around 4.5 eV originates from the excitation from different vibrational levels of ground state of KCl to the steep edge of the repulsive state. Due to the close separation between the first two excitation stages, producing $Cl(^2P_{3/2})$ and $Cl(^2P_{1/2})$ atoms, they are indistinguishable. The continuum starting from 5 eV toward higher energies originates from the excitation to upper repulsive states that excites neutral K atoms to p orbitals or to higher orbitals[37]. The higher orbital excitation has been studied for CsCl[31], whose spectrum is analogous to that of KCl.

The fluctuation bands of the alkali halides are observed at lower energies than where the first continuum starts as a few nanometers wide weak bands. The fluctuation bands originate from the transitions from the excited vibrational states of the ionic ground state to the horizontal part of the repulsive state. The observation of the fluctuation bands has enabled the estimation of the vibrational constant of some alkali halides in early studies[27] and the more accurate determination of the shape of the repulsive states of the alkali halides[38].

2.3 Potassium Hydroxide(KOH) molecule

Potassium hydroxide is a linear triatomic molecule containing potassium, oxygen, and hydrogen atoms[39]. Oxygen and hydrogen atoms are tightly bonded together and form a hydroxide radical with the bond length of 0.96 Å. The length of the ionic bond between K and O is in the order of $2.2 - 2.3$ Å.[40]. KOH is a very hygroscopic and reactive compound. Its melting point is 406 °C[13]. The vaporization of KOH is found to produce a huge portion of dimers close to its melting point temperature, which together with its reactivity make the study of KOH monomers challenging[41]. In combustion processes, KOH may be formed and cause high temperature corrosion when fuel contains an abundance of potassium[42].

To our knowledge the UV absorption properties of KOH have not been explicitly measured. However, it is said that KOH has dissociating absorption bands in the UV region and K-O bond dissociation energy have been determined to be 86 kcal/mol corresponding to the fragmentation wavelength of 330 nm[43,44]. The best approximation for the absorption cross section of KOH can be evaluated from that of NaOH having absorption maxima at 205 nm, 230 nm and 313 nm and peak absorption cross sections of $0.87 \cdot 10^{-17}\ cm^2$, $1.8 \cdot 10^{-17}\ cm^2$ and $0.59 \cdot 10^{-17}\ cm^2$, respectively at the temperature of 300 K[45]. According to its dissociation energies, KOH should absorb UV light around similar wavelengths[44].

Chapter 3

Measurement techniques for detection of alkali compounds

THIS chapter reviews the previously applied techniques capable of detecting alkali compounds in real-time in combustion conditions. The first four techniques are based on sampling. The sampling ones provide typically good selectivity and high sensitivity, but encounter challenges such as sampling line losses and the nucleation of alkali vapors. The rest are optical techniques and some of then can be applied *in-situ*. The comparison between the optical *in-situ* techniques below and the ones introduced in this work is done in Table 5.1 at the end of Chapter 5. Conventional sampling techniques (batch methods) requiring several hours sample collection time and off-line analysis are excluded from the review.

3.1 Sampling techniques

Molecular beam/mass spectrometry measurement is based on the sampling and ionization of the analyzed gas. The induced ions are channeled to a mass spectrometer indicating the mass spectrum of the sample. The analyses result in simultaneous information for example from K, KCl and KOH emission. The technique has been

applied in combustion research to measure the composition of flue gas from 20 mg to 50 mg grass samples in real-time. The measured readings in combustion experiments are calibrated by comparing them to the total release from a weighted KCl reference sample.[46]

Surface Ionization (SI) utilizes the fact that the alkali metals are efficiently ionized on the hot metal surface. If a sample contains particles or molecules, a fraction of them is melted and dissociated on the surface before the ionization. The emitted ions are collected and measured as a current[47]. The SI technique provides the limit of detection below ppb with 1 s time resolution. SI detects the total alkali flow, and makes no difference between K and Na atoms or, whether, the detected alkali originates from an atom, a molecule, or a sub-micron particle. The technique has been applied in laboratory measurement to study alkali release from 20 mg biomass samples[48] and in full-scale power plants[49]. SI calibration is done using gas with known alkali composition.

Plasma Excited Alkali Resonance Line Spectroscopy (PEARLS) is based on the mixing of a flue gas sample with a nitrogen plasma jet. The plasma dissociates the gases and particles in a sample to atoms and ions. The total amounts of alkalis are detected either by measuring the transmission of the alkali specific wavelengths through the gas jet or detecting the light emitted by alkali atoms recovering to their ground level. The detection limit of the device is 50 ppb in absorption mode and 2 ppb in the emission mode. PEARLS have been applied to the on-line diagnostics of total alkali concentration (g/m^3) in full-scale power plants. The calibration of the PEARLS technique is based on the absorption properties of the alkalis, which has also been confirmed with known sample gas flux.[20]

Impactor and cyclone sampling are selective for particles of different sizes and can be applied to preselect a sample for further analysis with off-line techniques. Traditionally, impactors are used to collect samples over longer times but a few modern aerosol instruments, such as Electrical Low Pressure Impactor (ELPI), are also capable of providing real-time aerosol particle size distributions. In combustion experiments it is found that sub-micron particles $0.19 - 0.3\ \mu$m collected from combustion boilers consists mainly on KCl and K_2SO_4[50]. This is due to the fine particle formation during sampling and cooling of the sample gas. One application of the fine particle separation and analysis has been a study of KCl sulphation in controlled laboratory conditions[51].

3.2 $In-situ$ techniques

Tunable Diode Laser Spectroscopy (TDLS) provides the absorption measurement over narrow spectral lines with high velocity and good accuracy. The tuning of the laser wavelength over the studied line reveals the shape and strength of the line and, thus, the concentration of the measured atom or molecule can readily be calculated. TDLS has been applied for the detection of potassium atoms from coal fired power plants operating at atmospheric and 10 - 16 bar pressures. A fast wavelength modulation at kHz frequency allowed the elimination of the transmission fluctuations through 300 mm and 140 mm flue gas channels in atmospheric and high pressure power plants, respectively. The detection limit for potassium atoms was found to be 10 ng/m^3 with a time resolution of 1.7 s.[21]

Planar Laser-Induced Fluorescence (PLIF) has been developed for the detection and mapping of the spatial distribution of Na atoms in the plume of burning particles. The technique utilizes vertically planar laser pulses that pass the plume of the burning particle and excite the sodium atoms on their path. The fluorescence light emitted by sodium atoms is imaged with an ICCD camera. The images are taken from the side of the plume with a viewing angle of 90° respect to the traveling direction of the laser pulse. The technique can be calibrated using known Na flux and direct absorption measurement. The detection limit of the technique is in the order of ppb for Na atoms.[52]

Differential Optical Absorption Spectroscopy (DOAS) utilizes the known absorption profiles of the measured species to deduce their concentrations from a measured spectrum. The spectra of the alkali chlorides are broad having no fine structure and can be measured with a broadband UV lamp and a UV sensitive spectrometer, as has been done in a device called In Situ Alkali Chloride Monitor (IACM)eveloped by Vattenfall Research and Development AB. Due to the similarity of the absorption spectra of KCl and NaCl, the technique measures their sum concentration (KCl + NaCl). An advantage of the technique in combustion research is its capability of simultaneously detecting the concentration of sulfur dioxide (SO_2). The detection limits of DOAS with a sample length of 5 m for alkali chlorides and SO2 are 1 ppm and 10 ppm, respectively.[36] The technique has been utilized in the detection of the alkali chlorides in power plants[53,54] and laboratory experiments[55].

Photofragment Fluorescence (PFF) techniques detects the alkali compounds by exciting them to repulsive excitation states that can simultaneously dissociate the molecule and excite the released alkali fragment. The excited alkali fragment is detected as it recovers back to its ground state through radiative relaxation, i.e. fluorescence. The PFF threshold wavelengths for the alkali compounds depend on the dissociation energy of the molecule and the excitation energy of alkali atom fragment. Typically, the PFF threshold wavelength of the combustion related alkali compounds is in the vicinity of 200 nm.[43]

PFF detection of alkali compounds is often done using pulsed ArF excimer laser emitting light at the wavelength of 193 nm and providing the pulse energies of tens of millijoules. PFF measurements combined with excimer laser source are also known in literature as **Excimer Laser Induced Fragmentation Fluorescence (ELIF)**[56–58]. Usually, ELIF detects the emission from K and Na atoms at two wavelengths and, thus, measures the sum of alkalis bonded to chlorides and hydroxides (KCl + KOH and NaCl + NaOH). However, alkali hydroxides have lower bond dissociation energy than alkali chlorides and a part of the alkalis released from them settle on higher excitation states when the fragmentation wavelength of 193 nm is applied. Thereby, the monitoring of multiple fluorescence wavelengths allows the selective detection of chlorides and hydroxides[59]. The detection limit of the ELIF technique has been found to be 0.1 ppb for Na and 0.05 ppb for K[60].

The PFF technique has also been applied to the quantitative detection of NaOH by using 355 nm laser pulses having a pulse width and pulse energy of 8 ns and 85 mJ, respectively. The high energy 355 nm pulses excites NaOH molecules first to their lowest repulsive state and then, before the molecule fragmentation, re-excite them to a higher repulsive state that produces excited Na atoms. The process is a called resonant two-photon excitation and the fluorescence intensity is proportional to the square of the laser intensity.[61]

The third PFF detection scheme utilizes two pulsed laser sources. The first pulse dissociates the studied molecule, and the second pulse excites the released alkali atoms. PFF arrangement with two lasers has been applied to study the low temperature spectra of the alkali compounds[32,45], for example.

Laser Induced Breakdown Spectroscopy (LIBS) is based on the focusing of a high intense laser pulse to a target point. The tightly focused laser pulse forms a plasma, when its intensity exceeds a certain threshold limit. The high-temperature plasma induces the dissociation of molecules and sub-micron particles and excites the released atoms to their excitation states. When plasma cools down, the atoms recover to their ground levels and emit light at the atom specific wavelengths. The analysis of the observed spectrum results in the atomic composition of the sample. In combustion research, the LIBS technique has been utilized in the detection of the total releases of K and Na from burning coal and biomass samples having the mass of a few tens of milligrams. The detection limit of the LIBS measurement has been found to be 2.9 ppb and 7.2 ppb for total Na and K, respectively.[62,63]

3.3 Other optical techniques

Resonance Ionization Spectroscopy (RIS) is mostly applied for the detection of atoms but is applicable to molecule detection as well, when the molecule is first fragmented. RIS is based on the optical excitation of an atom to an ion that is collected and detected as a current. Resonance ionization is a sufficiently strong effect since it utilizes the excitation levels of atoms as intermediate stages. Schemes for different RIS excitation paths and proposal for K excitation are given in reference[64]. One application of RIS is the detection of alkali atom fragment released in the photodissociation of the alkali halide molecule. This scheme has been demonstrated by measuring the photolysis spectrum of CsI for Cs production in the fragmentation wavelength range of 300 - 340 nm[65].

Picosecond Differential Absorption Lidar (ps-DIAL) measures backscattered light from short laser pulses propagating in a media. Using two closely separated wavelengths the background scattering of the light could be assumed to be the same at both wavelengths and any difference found in the backscatter intensities can be assumed to result from light absorption. The use of picosecond pulses enables a spatial resolution of <1 cm. ps-DIAL has been utilized for example to measure KCl vapor concentration profile in a heated metal tube.[66] The technique has potential for $in-situ$ boiler measurements, but to our knowledge it has been applied to measure only controlled samples in a laboratory so far.

Chapter 4

Photoacoustic Spectroscopy

PHOTOACOUSTIC Spectroscopy (PAS) is based on the conversion of light into a pressure wave or a pressure impulse. The phenomenon was first observed by A. G. Bell in the 1880s[67]. In his early experiments, Bell reflected a modulated sun light beam on an absorber and listened to the induced sound with an ear trumpet[68]. Nowadays, PAS provides one of the most sensitive gas measurements utilizing high power lasers and sensitive microphones. In this chapter, the principles of the photoacoustic detection are discussed and a couple of the most convenient acoustic transducer solutions are mentioned. A signal processing method used in this work is described and main results related to the detection of alkali chlorides are highlighted. The behavior of the acoustic resonator in the high-temperature and corrosive conditions is discussed at the end of the chapter.

4.1 Photoacoustic signal formation and detection

The principle of the photoacoustic (PA) measurement is categorized in Fig. 4.1 into three sections. The sections are the formation of sound, the sound wave, and the detection of sound. The formation of sound is based on the conversion from the absorbed light to increased sample pressure. The efficiency of the conversion depends on the

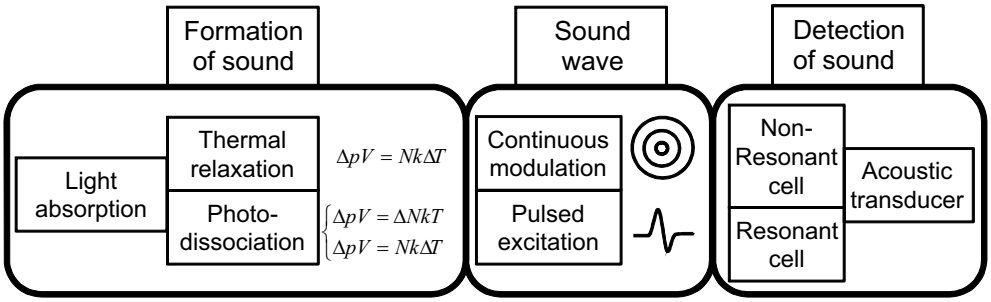

Figure 4.1 Main steps of photoacoustic wave formation and detection.

relaxation path of the excited energy level. The vibrational levels, excited typically with IR light, relax mainly via thermal relaxations, wherein the excitation energy converts directly into heat as the sample molecules are colliding[69]. According to the ideal gas law, the sample heating is observed as an increased pressure in closed systems. The excited vibronic levels, which are excited with VIS and UV wavelengths, may relax through thermal relaxations but also via radiative relaxation, which reduce the efficiency of heat and pressure formations[70]. UV and VIS light excitation may also lead to the fragmentation of the molecule, as was discussed in Chapter 2. The fragmentation increases the number of particles in the sample and, thereby, the pressure of the system. Moreover, the molecule fragmentation induces sample heating through two mechanisms. First, the fragments gain kinetic recoil energy as the molecule dissociates. The magnitude of the recoil energy roughly corresponds to the difference between the energy of the excitation photon and the bond dissociation energy of the target molecule. Second, the fragments may undergo chemical reactions with surrounding gases. The chemical reactions are typically slower than other pressure inducing mechanisms[71].

The pressure change becomes an acoustic wave when its amplitude is modulated periodically. The most typical modulation techniques in PAS are amplitude and wavelength modulation. The amplitude modulation is applied when the wavelength of the excitation beam is not tunable[72] or the absorption spectrum of the sample lacks the fine structure within the wavelength tuning range[73]. The amplitude modulation setup can be realized for example with a cw-light source and a chopper when the induced acoustic wave is found at the modulation frequency and at its higher harmonics. A drawback in the amplitude modulation is the background signal that occurs at the same frequencies as the actual signal. The wavelength modulation applies the wave-

length tunability of the light beam and the narrow absorption peaks of the target molecule. The wavelength modulation is realized by sweeping the excitation wavelength back and forth over a sample absorption peak when the actual signal occurs at twice the modulation frequency and the background signal from broadband absorbers, such as measurement chamber windows, at the modulation frequency. The modulating waveform can be selected to optimize the sensitivity or the selectivity of the PA detection[74]. The excitation can also be done by applying a pulsed light source when the induced free-space signal occurs as a short pressure impulse and contains a broad band of frequencies[75].

PA waves are typically excited in chambers providing good acoustic isolation against ambient background noise. The chambers are operated in resonant or in non-resonant mode. The non-resonant operation can be understood as the excitation and detection of the acoustic wave without utilizing the amplification provided by the eigenmodes of the chamber structure[69]. In the resonant mode operation, the PAS signal is detected at the frequency corresponding to the resonance frequency of the chamber. The resonant properties of the chamber can be enhanced by properly selecting the wall materials and by polishing the walls. The acoustic chambers optimized for resonant operation are also known as acoustic resonators. The use of the acoustic resonator enhances the sensitivity of the PAS detection with orders of magnitude but requires a proper resonant tracking system so that the detection accuracy remains[72,76]. In single pulse PAS, the induced impulse excites all acoustic resonances covered by its frequency spectrum. The amplitudes of the pulse-excited resonance modes depend on the initial frequency spectrum of the pressure impulse and the traveling path of the laser pulse with respect to the profiles of the resonator eigenmodes. For example, if a laser pulse travels through a cell along a nodal point of a resonance mode, that mode is not excited. The single pulse excited oscillations decay exponentially due to the resonator losses[76,77].

The absolute detection limit in the PA measurement depends on the amplitude of the induced pressure wave, and the sensitivity and noise characteristics of the acoustic transducer detecting the pressure wave. The amplitude of the wave can be increased by using a high power excitation beam[78], exciting the acoustic wave in a laser cavity[79] or by optimizing the structure of the resonator[76,80]. The detection of the pressure wave is optimized by selecting the most convenient acoustic transducer. Many applications utilize condensed or electret microphones due their robustness, low price, broad and

flat frequency response from a few hertz up to 100 kHz, and relatively good sensitivity being in the order of mV/Pa[81]. However, there are other options when special requirements such as very small detector size, ultra high sensitivity or low electric noise are needed. An example of a small and low priced acoustic detector is a quartz tuning fork[82], which provides good sensitivity and low noise characteristics when the detection frequency is tuned to its resonance at 32770 Hz. Cantilever microphones enable extremely good sensitivity in non-resonant detection with low signal frequencies[83]. Optical microphones are good options when low electric noise is needed[84,85]. An interesting option for the acoustic transducer is an electromechanical film which can be stacked in order to enhance its sensitivity[86] or be used to cover the inner walls of the PA resonator to minimize the asymmetries of the acoustic resonator[87].

4.2 Photoacoustic cell for high temperature gas analysis

PAS experiments are in general performed in near room-temperature conditions due to the technical limitations of the acoustic transducers. High temperature gas analysis is also possible but requires a special acoustic chamber design. One possibility is to use a "heat-pipe" design that applies the second longitudinal mode of a metal tube. In "heat-pipe" cell, the PA wave is excited at the heated center part of the tube and detected at the water cooled end of the tube.[88,89]. Another possibility is to excite a PA wave in a hot sample chamber or in a resonator, and detect it through a narrow signal tube connected with the measurement volume[90,91].

The design of the PA chamber developed in this work is presented in Fig. 4.2. The chamber consists of an acoustic resonator, buffer volumes on both sides of the resonator, and cooling tubes that allow one to keep the chamber windows at room-temperature. The pressure signal is recorded with a microphone through a signal tube. The interior of the red box is placed in an oven that can be heated up to 1000 °C. The laser beam travels through the chamber without interacting with the chamber walls along a channel having an inner diameter of 6 mm. More specific description of the chamber is given in **Paper 1**.

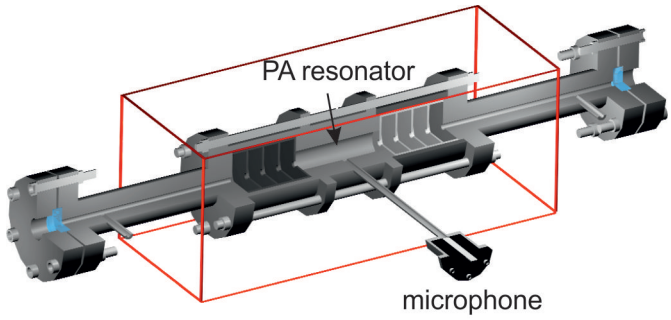

Figure 4.2 Photoacoustic chamber developed for the analysis of high temperature gases. The interior of the red box is placed in an oven and heated. The PA wave is excited in the resonator and detected through a signal tube with a condensed microphone.

The photoacoustic chamber and a light source are known together as a PA cell[76]. In this work, the high temperature PA chamber was used together with a pulsed optical-parametric-oscillator (OPO) laser. The laser emits 5 ns pulses the wavelength of which is tunable from 210 nm to 2300 nm. The output pulse energy is approximately 1 mJ at UV wavelengths. The laser pulses were aligned to travel along the center axis of the resonator, which favored the excitation of the radial modes of the resonator. The excited eigenmodes were recognized utilizing an equation describing the eigenfrequencies of the lossless cylindrical resonator[76]

$$f_{nml} = \frac{c_s}{2}\sqrt{\left(\frac{\alpha_{nm}}{R}\right)^2 + \left(\frac{l}{L}\right)^2}, \tag{4.1}$$

where n, m and l are the indices expressing the orders of the radial, azimuthal and longitudinal modes, respectively. R denotes the radius of the resonator and L is its length. The symbol α_{nm} denotes the nth zero of the derivative of the mth order Bessel function divided by π. c_s is the speed of sound in the resonator. The decay rates of the pulse excited oscillations depend on the resonator specific quality (Q) factors. The Q-factors are determined as a relation of resonance frequency and the width of the observed resonance peak in the frequency domain at height of $1/\sqrt{2}$, i.e. the quality factors can be calculated using a relation $\mathrm{Q}_{nml} = f_{nml}/\Delta f_{nml}$.

An example of the photoacoustic waveform detected from the developed PA cell and its frequency spectrum are shown in Fig. 4.3. The waveform was detected from KCl sample gas at the temperature of 659 °C using the excitation wavelength and pulse

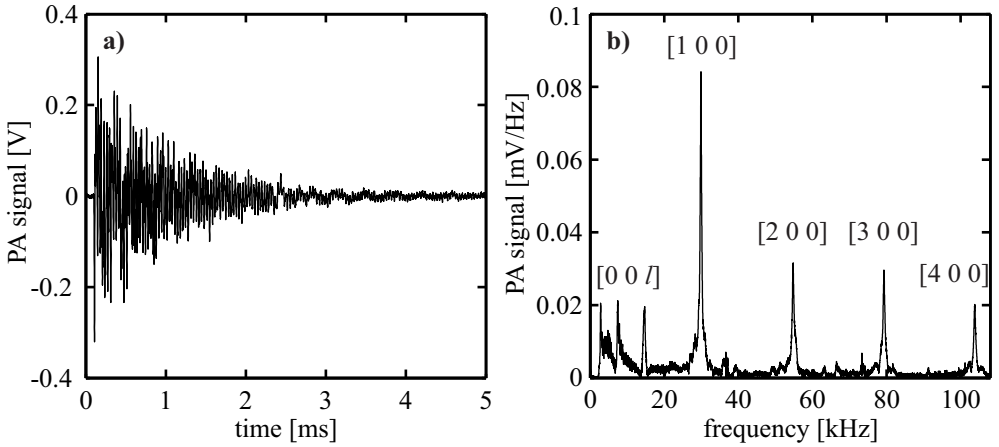

Figure 4.3 Example PA signal in a) time and b) frequency domains. The signal has been measured from KCl vapor at 659 °C using 245 nm wavelength and pulse energy of 300 μJ.

energy of 245 nm and 300 μJ, respectively. The sample gas was produced by placing quantity of KCl powder in the buffer volumes where it sublimated and diffused to the other hot sections of the resonator. The saturated vapor pressure of KCl at the measurement temperature was calculated to be 20 ppm using a thermochemical HSC 5.1 database[24].

The frequency spectrum in Fig. 4.3 b) shows that the recorded waveform consists mainly on four radial and three longitudinal eigenmodes. The lack of azimuthal modes verifies that the laser beam has traveled along the center axis of the resonator where all azimuthal modes have a nodal point. The excitation of the longitudinal modes indicates that the sample vapor was distributed inhomogeneously through the resonator volume. In other words, the diffusion of the vapor from the buffer volume was imperfect. More homogeneous sample distribution is achieved by placing the sample powder inside the resonator (see **Paper 1**).

The frequency spectrum can be used to calculate the amplitudes of the first periods of the oscillations, the Q-factors of the eigenmodes and the oscillation phases of the modes (see **Paper 1**). The calculated data can be used further to model the original waveform. The modeled and the original waveforms are drawn in Fig. 4.4 for comparison. The modeled signal is calculated from all seven observed eigenmodes. The figure also indicates how the first radial mode alone follows the recorded waveform.

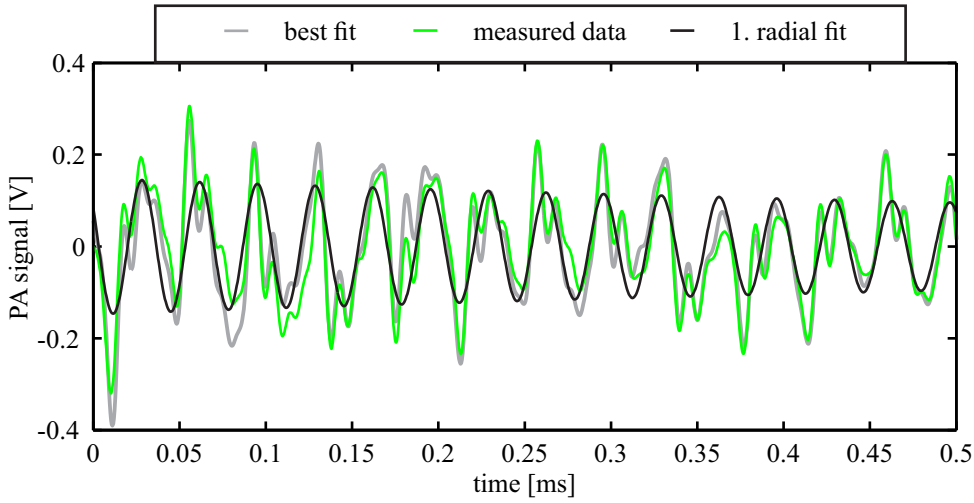

Figure 4.4 Photoacoustic signal presented together with its waveform fits calculated using three longitudinal modes and four radial modes (best fit) and only the first radial mode. The figure presents the signal oscillations over the first 0.5 ms after the first wavefront has reached the microphone.

The modeled waveform is observed to correspond well to the measured data, which verifies the modeling method. There are small differences at the very beginning of the waves because the weak modes were ignored in the modeling. However, after 0.3 ms from the beginning of the signal, fit and the original waveform are almost identical. Figure 4.4 also indicates that the first radial mode is the dominating mode in the resonator, and it determines the oscillation trend of the observed wave. The first radial mode explains approximately 33 % of the total magnitude of the detected oscillations at $t = 0$. The response of the PA cell is determined in the next section for the first radial mode which has the best signal to noise ratio.

4.3 Photoacoustic response of KCl and NaCl

The developed PA cell was applied to detect KCl and NaCl vapors in high temperature conditions. The salt powders were inserted in the acoustic resonator to ensure a homogeneous gas concentration through the measurement volume. The Q-factor of the first radial mode was in the range of 100-130 during the measurements. The Q-factor was determined in every measured condition.

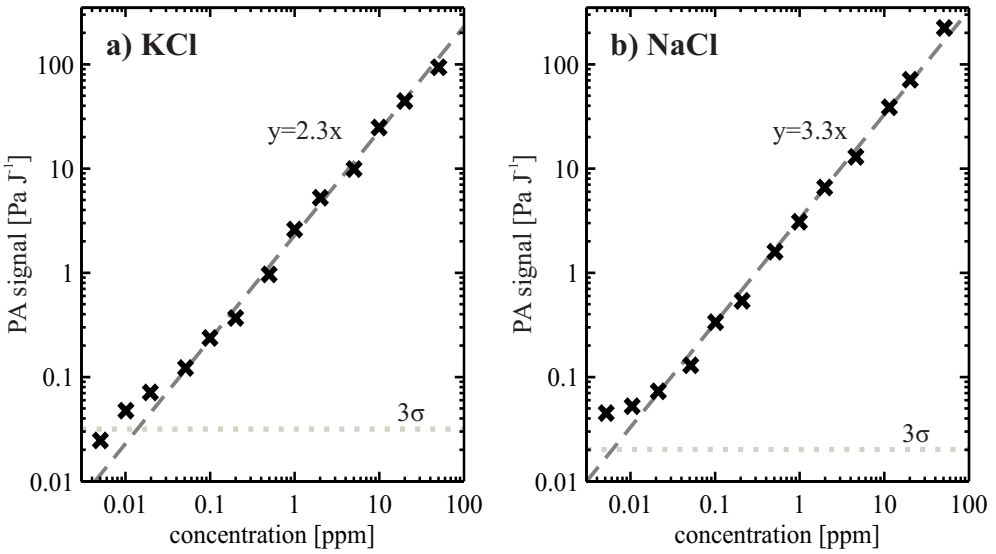

Figure 4.5 Normalized amplitude of the first radial mode detected from the different concentrations of a) KCl and b) NaCl. The extrapolated detection limits are 15 ppb and 6 ppb for KCl and NaCl, respectively.

The PA responses of KCl and NaCl vapors are presented as a function of sample concentration in Fig. 4.5. The PA responses were calculated by normalizing the amplitudes of the first radial eigenmode with a microphone response (4.13 mV/Pa), an amplification gain (10^4) and laser pulse energy. Potassium and sodium chloride vapors were measured using the excitation wavelengths of 245 nm and 237 nm, and average pulse energies of 300 μJ and 470 μJ, respectively. The excitation wavelengths corresponded to the absorption maxima of the KCl and NaCl vapors. The applied pulse energies were the maximum values that could be coupled to the resonator without wall interactions. 3σ noise levels were determined at the temperature of 470 °C as a standard deviation of frequency spectrum in the vicinity of 27 kHz multiplied by three. The selected frequency region corresponds to the frequency of the first radial eigenmode at the temperature of 470 °C in N_2. The 3σ noise levels were normalized with the Q-factors of 130 observed at 470 °C and with average pulse energies applied in the corresponding measurements.

The slopes of the PA responses were determined to be 2.3 $\mathrm{PaJ^{-1}ppm^{-1}}$ for KCl and 3.3 $\mathrm{PaJ^{-1}ppm^{-1}}$ for NaCl. The detection limits were determined as crossing points between the linear fits and the 3σ noise levels. The detection limits of KCl and NaCl

were found to be 15 ppb and 6 ppb, respectively. The measured points deviated slightly from the linear fit at small sample concentrations due to a noise peak which originated from the Q-switch of the pulse laser and located in the vicinity of the PA signal peak in the frequency spectrum.

The usage of the high pulse energies maximises the PA signal and shows the absolute sensitivity of the PA cell. However, the high pulse energies may saturate the absorption when the linearity between PA signal strength and excitation pulse energy is lost. The strength of the PA signal from KCl and NaCl as a function of the pulse energy is shown in Fig. 4.6. The curves were measured from sample concentrations of 20 ppm when the signal to noise ratio was good even at small pulse energies, and the light absorption was less than 5 % through the 8.5 cm long resonator.

The nonlinear behavior of PA response at high pulse energies E_p is described with a saturation equation having the form of $PA_{signal} = C_1[1 - exp(-E_p/C_2)]$. The saturation equation is derived from a standard rate equation of the two level system [92] assuming fast molecule dissociation (no stimulated emission) and slow recombination of the fragments (no spontaneous emission). The fitting coefficients C_1 and C_2 were

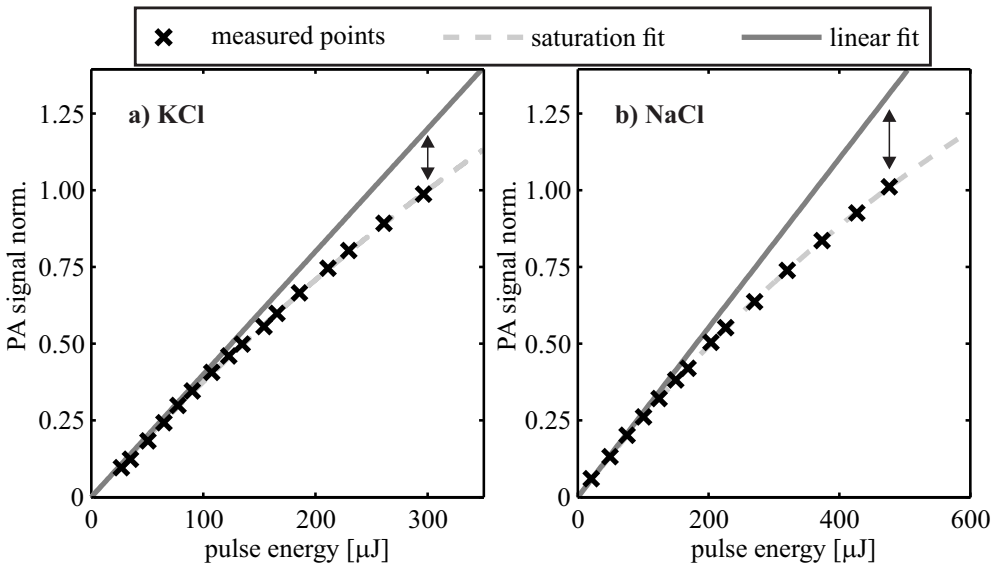

Figure 4.6 Normalized PA signals measured from a) KCl and b) NaCl applying different pulse energies. Double head arrays point the effect of the saturation with maximum pulse energies.

found to have the values of 3.18 ± 0.39 and 795 ± 110 μJ for KCl, and 2.38 ± 0.07 and 860 ± 30 μJ for NaCl. The uncertainties correspond to 95 % confidence bounds of the saturation fits calculated using curve fitting tool of MATLAB (MathWorks inc.). The linear fits correspond to the first term of the Taylor expansion of the saturation equation of the both molecules. The comparison of the linear fit and the measured data points at the maximum energies indicates that the slopes determined in Fig. 4.5 should be 1.203 and 1.294 times larger for KCl and NaCl, respectively. The corrected values for PA cell responses are 2.8 $\mathrm{PaJ^{-1}ppm^{-1}}$ for KCl and 4.3 $\mathrm{PaJ^{-1}ppm^{-1}}$ for NaCl.

The PAS studies of alkali chlorides were completed by measuring the photoacoustic spectra of KCl and NaCl. Potassium chloride was measured at the temperature of 690 °C and NaCl at the temperature of 745 °C, corresponding to the saturated vapor pressure of 50 ppm for both samples. The spectra were measured with the resolution of 2.5 nm in the wavelength region of 210 nm–270 nm and with the resolution of 10 nm from wavelength 270 nm to 330 nm. The average laser pulse energy was 100 μJ at all excitation wavelengths. The measured spectra normalized to correspond to the above-derived responses are presented in Fig. 4.7.

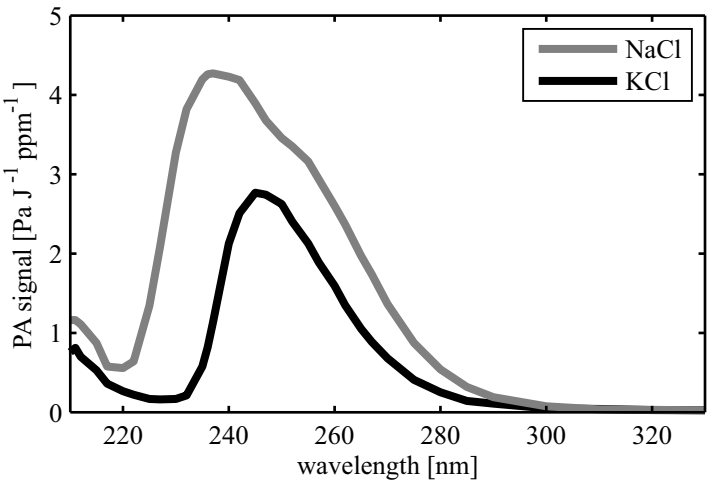

Figure 4.7 Photoacoustic spectra of KCl and NaCl. The maxima of the spectra have been normalized according to previously presented PAS responses.

The shapes of the PA spectra of KCl and NaCl are in good agreement with the shapes of the corresponding high temperature absorption spectra[30,35,36]. KCl spectrum has a maximum at the wavelength of 245 nm from where the PA signal starts to decrease toward longer wavelengths and falls below the detection level at 300 nm. At the shorter wavelengths, KCl spectrum has a local minimum at 227 nm from where the PA signal starts to increase toward the shorter wavelengths. NaCl spectrum has a local maximum at 237 nm, a small bend around 250 nm and the long wavelength end detection limit around 300 nm. At the shorter wavelengths, there is a minimum at 220 nm and a rising slope toward the shorter wavelengths.

The rising slope in both spectra toward shorter wavelengths is assumed to originate from the absorption by the alkali chloride dimers. This assumption is based on the thermodynamic calculations made using the HSC 5.1 database[24] and the reported high temperature absorption spectra measurements[30,35,36]. The saturated vapor pressure of the alkali chloride dimers is approximately 1/3 of the vapor pressure of the monomers in the equilibrium of solid, liquid and gaseous alkali chloride[24]. If the equilibrium vapor is heated without the presence of solid and liquid salt, i.e. the vapor is superheated, the ratio of the dimers starts to decrease. The previous spectra measurements have been done in both above-mentioned cases. Davidovits et al.[30] and Daminelli et al.[35] produced salt vapors in a closed cell and observed a rising slope in their absorption spectra at short wavelengths. Forsberg et al.[36] first produced the vapor at a lower temperature and then heated it before measuring the spectrum. The slope was found missing at short wavelengths in the superheated vapor.

The above mentioned PAS experiment and the observed good correspondence to previous studies verify that PAS is capable of measuring alkali chloride vapors with good sensitivity. Moreover, the developed PA cell enables spectral measurements, which enhance the selectivity of the technique. In its current form, the developed PA cell provides a tool for the laboratory scale experiments of the PAS studies of the alkali chloride vapors within the temperature range of $400 - 1000$ °C.

4.4 Operation of acoustic resonator under corrosive high-temperature conditions

The previously presented measurements were carried out in N_2 atmosphere and by placing the sample powder in the acoustic resonator when the Q-factors of the eigenmodes were found to be constants over the studied temperature ranges. However, the alkali chlorides are known to react with steel materials at high temperatures and to accelerate the formation of a porous oxidation layer on the metal surfaces in oxygen containing conditions[7]. The effect of KCl induced oxidation to the PA cell performance was studied by polishing the resonator and by inserting the KCl powder only in the buffer volumes. The preparations improved the Q-factor of the first radial mode to the value of 350. The PA chamber was next preheated to the temperature of 450 °C and flushed with air. The actual measurement was performed by increasing the temperature of the chamber in steps and allowing the gas to stabilize 15 minutes before measuring the PAS waveforms. The observed Q-factor of the first radial mode as a function of the PA chamber temperature ranging from 450 °C to 750 °C is presented in Fig. 4.8.

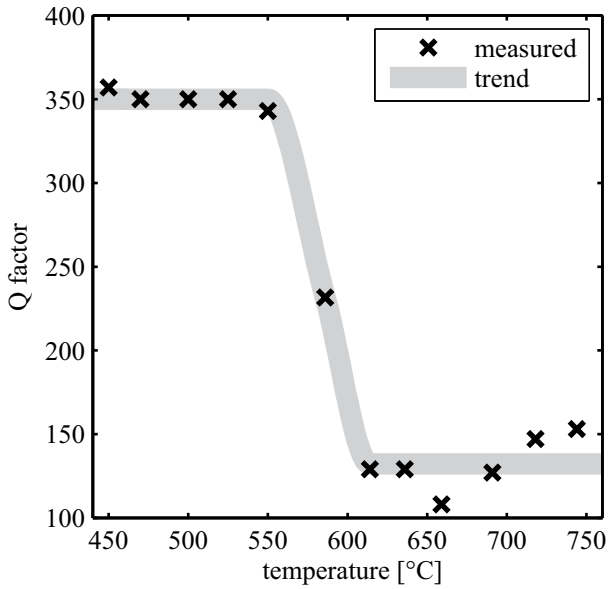

Figure 4.8 Effect of PA chamber wall oxidation in air atmosphere and at elevated temperatures to Q-factor of the resonator.

The oxidation experiment showed that the Q-factor of the resonator decreased sharply around the temperature of 580 °C in air atmosphere. The Q-factor remained at the level of 130 when the temperature of the chamber was decreased after the heating. The formation of the porous oxide layer on the resonator walls was visually confirmed by opening the chamber after the experiment.

The effect of the oxidation on the acoustic properties of the resonator provides new possibilities in the study of high temperature metal oxidation. Parameters, such as threshold temperature, oxygen concentration and salt concentration for oxidation, can be determined for different steel material with above mentioned measurement preparations. The current PA cell could be applied to the oxidation studies by manufacturing the resonator from the studied material or by covering the resonator with thin film made of it. The salt concentration and Q-factor of the resonator can be determined from each measured waveform, which allows the real-time study of the above-mentioned parameters.

Chapter 5

Collinear Photofragmentation and Atomic Absorption Spectroscopy

Photofragmentation and Fragment Detection (PF/FD) techniques detect precursor molecules indirectly providing enhanced selectivity and occasionally enhanced sensitivity compared with the direct detection techniques[93]. PF/FD techniques apply a pump beam to fragment the precursor molecule, and a probe beam to further excite the detected fragment. The fragment detection is done by monitoring fluorescence light from the fragments[94] or the absorption of the applied probe beam[95,96]. When the fragmentation wavelength is short enough, the fragmentation may produce electronic excited fragments, which can be detected by monitoring their fluorescence without applying a separate probe beam[57,58]. Fragment detection can be done applying atom[32,43], molecule[97] or ion[94] fragments.

This chapter presents a PF/FD technique called Collinear Photofragmentation and Atomic Absorption Spectroscopy (CPFAAS) which has been developed during this work. A basic measurement scheme, calibration, the principles of multicomponent detection and three combustion studies are discussed. The combustion studies include one laboratory scale experiment, one intermediate size boiler experiment, and one full-scale boiler experiment. At the end of the chapter, the performance of the CPFAAS technique is compared with other techniques capable of detecting alkalis.

5.1 Principles of CPFAAS

A schematic of CPFAAS measurement setup and the shape of the detected waveform are presented in Fig. 5.1. The setup consists of a pulsed laser, whose emission wavelength is capable of fragmenting the target molecules to atoms via dissociative absorption, and a continuous wave (CW) narrow bandwidth probe laser emitting a wavelength corresponding to the absorption line of the fragment atom. The laser beams are aligned to travel through the sample collinearly along the same optical path. The transmission waveform of the probe laser is recorded in the vicinity of the triggering of the fragmentation pulse, and it consists of three main phases. In phase I., the temporal transmission of the probe laser is determined at $t < 0$. The transmission may fluctuate due to the changes in the sample gas composition or due to the particle flow on the optical path. The base level should be determined for each individual measurement event in fluctuating samples. Phase II. takes place at $t = 0$ when the fragmentation pulse has just passed the sample and the probe laser transmission drops sharply due to the increased number of detected fragment atoms. The relation $-\ln[I(t = 0)/I(t < 0)]$ of the probe laser intensities is directly proportional to the number of fragmented precursor. In phase III., the concentration of the fragment atoms recovers back to the equilibrium when the intensity recovers back to the base level $I(t < 0)$. The recovery of the signal takes place due to the chemical reactions or diffusion. In the case of fast recovery, the transmission fluctuations have no effect on the basic shape of the signal.

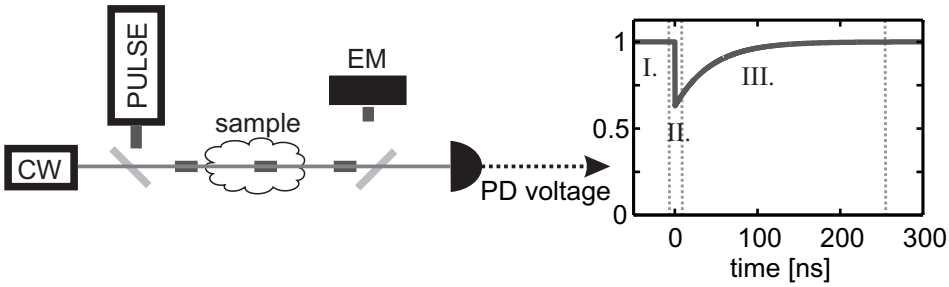

Figure 5.1 Typical measurement arrangement and the shape of the detected waveform in CPFAAS detection. The waveform consists of three main phases: I. Base transmission level before the fragmentation, II. decreased transmission due to the atom fragments released by a fragmentation pulse, and III. the recovery of the distorted gas volume back to the equilibrium state. The base level fluctuation has negligible effect on the detected waveform when Phase III is fast. PD and EM refer to a photo detector and energy meter.

A basic measurement requires at least the acquisition of phases I. and II. but the additional recording of phase III. enables a curve fitting, and enhances the accuracy of the technique. Applying the Beer-Lambert law to describe the intensity at $t = 0$ and an exponential decay for the fragment atoms at $t > 0$ the observed waveform can be described as

$$I(t) = \begin{cases} I_0 + C & t < 0 \\ I_0 \mathrm{exp}\left(-\alpha \mathrm{L_{max}} \mathrm{e}^{(-\mathrm{t}/\tau)}\right) + \mathrm{C} & t \geq 0 \end{cases}, \tag{5.1}$$

where αL_{max} and τ are the maximum absorbance due to the fragment atoms at $t = 0$ and a time constant for the decay process, respectively. The offset parameter C is added to describe the fraction of the probing light that passes the sample without interacting with the fragments due to the misalignment of the beams or the spectral impurity of the probe beam. The curve fitting enhances the detection of the weak signals and the determination of $I(t = 0)$, in particular, when the sample becomes temporarily opaque due to the large concentration of the fragment atoms.

5.2 Calibration of CPFAAS

A CPFAAS measurement consists of two separate absorption events. The target molecules are fragmented in the first absorption and the number of produced fragment atoms is detected in the second absorption. By knowing the fragmentation efficiency γ, i.e. how many fragment atoms a single fragmentation atom release, the number of absorbed fragmentation photons can be calculated based on the number of fragmentation atoms. The number of absorbed fragmentation photons converts to the absorption caused by the target molecule that finally results in the target molecule concentration when the absorption cross section of the target molecule σ_{KCl} and the sample length L are known. The theoretical expression between the target molecule concentration in a pure sample X_{KCl}^{pure} and the observed probe laser absorbance αL_{max} is derived in **Paper 3** in detail and has a form of

$$X_{KCl}^{pure} = -\ln\left(1 - \alpha \mathrm{L_{max}} \frac{\mathrm{hc}}{\gamma \lambda_\mathrm{f}} \frac{1}{\sigma_\mathrm{K}} \frac{\mathrm{A_f}}{\mathrm{E_{in}}}\right) \frac{\mathrm{kT}}{\mathrm{p}} \frac{1}{\sigma_{\mathrm{KCl}} \mathrm{L}}, \tag{5.2}$$

where h, k, c,γ, λ_f, σ_K, E_{in}, A_f and L are Planck's constant, Boltzmann constant,the speed of light, fragmentation efficiency, fragmentation wavelength, the absorption cross

section of the detected fragment atom, input energy of the fragmentation pulse, the cross section area of the fragmentation pulse, and sample length, respectively. The term pure sample refers to samples containing no other compounds absorbing the fragmentation wavelength than the target molecule, and samples where the fragmentation intensity can be assumed to be constant through the measurement path. All other samples are called impure samples.

The impure samples cause the faster attenuation of the fragmentation pulse than the pure samples and, therefore, the number of fragment atoms is smaller than expected. **Paper 3** states that assuming a homogeneously distributed sample the target molecule concentration in the impure sample X_{KCl}^{impure} can be calculated using an equation

$$X_{KCl}^{impure} = \alpha L_{max} \frac{A_f}{E_{in} L} \frac{hc}{\gamma \lambda_f} \frac{kT}{p} \frac{1}{\sigma_K \sigma_{KCl}} \frac{\ln\left(\mathrm{E_{in}}/\mathrm{E_{out}}\right)}{1 - E_{out}/E_{in}}, \tag{5.3}$$

where E_{out} is the energy of the transmitted fragmentation pulse. The difference between Eq. 5.2 and Eq. 5.3 is that the latter takes into account the attenuation of the fragmentation pulse whereas the former is independent of it.

Equation 5.2 was validated in **Paper 3** by comparing KCl concentrations determined by applying it with concentration values determined by using an experimental DOAS technique and the theoretically calculated saturated KCl vapor pressures using HSC 5.1 [24]. In the CPFAAS measurement, KCl molecules were fragmented with 1-ns-long pulses having the wavelength of 266 nm, and the produced K fragments were probed with a narrow bandwidth distributed-feedback (DFB) laser diode. The wavelength of the DFB laser beam was tuned to the absorption maximum of the K reference cell in the vicinity of 766.5 nm (in the air). The probe wavelength was 4 pm off the absorption maximum of the K fragments. The absorption cross section of the K fragments as a function of probe wavelength is shown in Fig. 5.2a. The sample vapor was produced by heating solid KCl in a quartz glass tube. Figure 5.2b presents the measured KCl concentrations as a function of the calculated concentrations.

The comparison of three techniques, which is presented in Fig. 5.2b, validated the values measured with CPFAAS. The mutual deviation between CPFAAS and DOAS determined KCl concentrations was less than 5 % at the concentration $\geq$ 1 ppm. At the lower concentrations, CPFAAS could only be compared with the theoretical calculations of the vapor pressure values due to the relatively high limit of detection of DOAS. The comparison of CPFAAS with the theoretically calculated vapor pressure

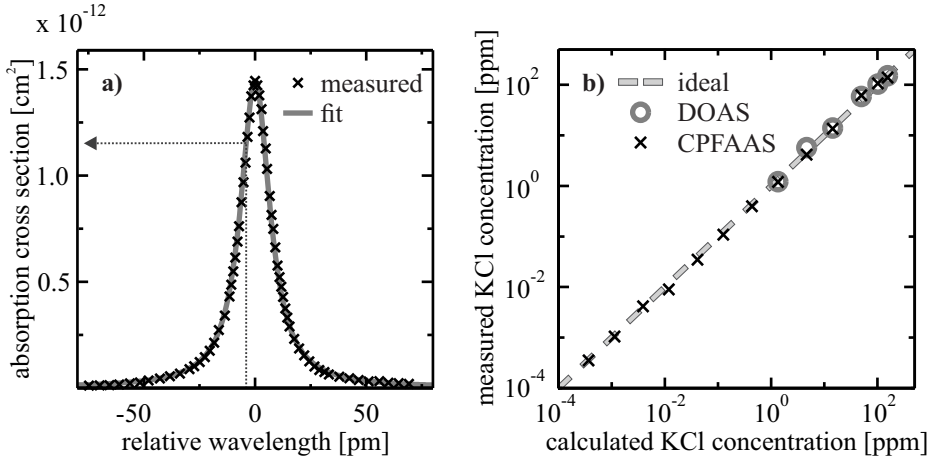

Figure 5.2 a) Measured values and a Voigt fit curve for the absorption peak of the potassium atom fragments. Dotted line presents the center wavelength of the K atoms in low-pressure reference cell in respect to the observed line shape. b) KCl concentrations measured using CPFAAS and DOAS techniques in respect to the calculated concentrations. Dashed line describes ideal correspondence having a slope of one.

values showed the maximum deviation of 20 %. The observed maximum deviation in the KCl concentration corresponds to the temperature difference of 5 °C.

The validity of the Eq. 5.3 has not been verified experimentally. However, its validity in a highly absorbing medium can be modeled using simulated samples. The next section will present simple tools for studying the feasibility of CPFAAS to different samples and demonstrate the response of Eq. 5.3 compared with Eq. 5.2 in impure samples.

5.3 CPFAAS modeling

The modeling of the CPFAAS response is an important tool in the validation of the measurement results and in the designing of CPFAAS based instruments to different applications. The first important factor is the fragmentation ratio of the target molecules in the sample. The local fragmentation ratio indicates whether there is a risk of absorption saturation due to too high fragmentation intensity, and how efficient the fragmentation is as the measurement distance increases. The latter property can

be used to estimate the effect of the inhomogeneity of the sample on the CPFAAS signal. The fragmentation ratio is presented as a relation between the number of produced fragment atoms and the total number of target molecules in the volume drawn by the fragmentation pulse

$$\frac{N_K}{N_{KCl}} = \frac{\frac{E_{absorbed}}{h\nu}}{\frac{pV}{kT}X_{KCl}}, \tag{5.4}$$

where the numerator on the right hand side of the equation is the absorbed energy divided by the photon energy. Assuming linear absorption and taking into account other possible attenuation mechanisms, we get an equation for the local fragmentation ratio at distance L from the light source within a step of dx

$$\frac{N_K}{N_{KCl}} = \frac{E_0 \exp\left(-\mathrm{X_{KCl}}\frac{\mathrm{p}}{\mathrm{kT}}\sigma_{\mathrm{KCl}}\mathrm{L}\right)\exp\left(-\alpha_{\mathrm{rest}}\mathrm{L}\right)\left[1-\exp\left(-\mathrm{X_{KCl}}\frac{\mathrm{p}}{\mathrm{kT}}\sigma_{\mathrm{KCl}}\mathrm{dx}\right)\right]}{h\nu\frac{p}{kT}A_{pulse}dxX_{KCl}}, \tag{5.5}$$

where α_{rest} describes the background extinction. Figure 5.3 shows the fragmentation ratio as a function of distance from the light source and sample concentration when a) $\alpha_{rest} = 0$ and b) $\alpha_{rest} = 0.5$. The latter value is an experimentally determined

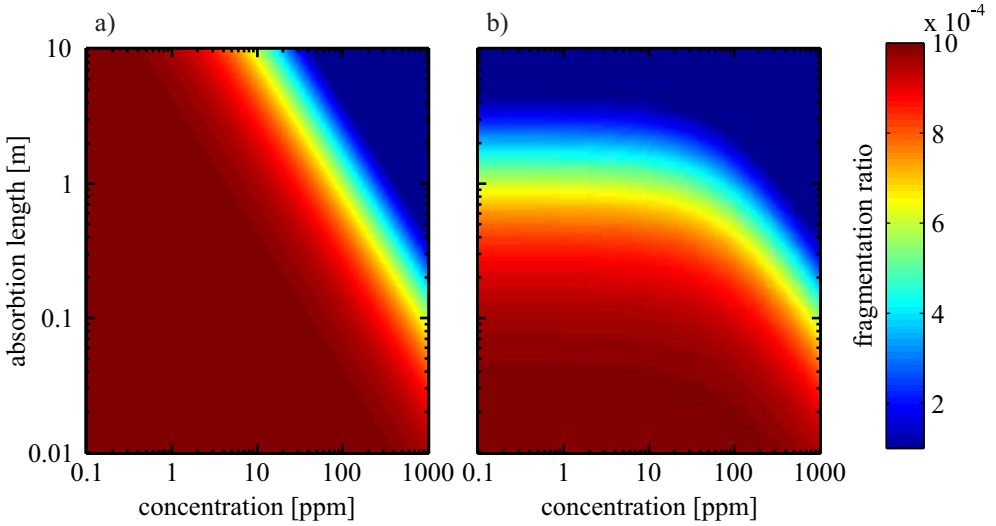

Figure 5.3 Local fragmentation ratios as a function of sample concentration and measurement distance in a) a laboratory and b) approximated power plant conditions. Power plant condition has been approximated adding a constant absorption coefficient of 0.5 1/m to attenuate the fragmentation pulse. Maximum fragmentation ratio using the excitation wavelength of 266 nm, the pulse energy of 80 μJ and a fragmentation pulse diameter of 1 cm was found to be 1/1000.

background extinction coefficient at the wavelength of 266 nm in combustion boilers combusting solid biomass and waste fuels. The fragmentation ratio is calculated using the pulse energy of 80 μJ and the fragmentation pulse diameter of 1 cm.

The calculation resulted in the maximum local fragmentation ratio of 1/1000 at small distances and small sample concentrations with the applied variables. The local fragmentation ratio decreases toward higher concentrations and longer measurement distances. In other words, the CPFAAS detection, which measures the sum of the induced atom fragments through the measurement path, weights the first meter(s) of the sample. The weighting causes distortion in the calculations of the target molecule average concentration when the distribution of the molecules in the sample is inhomogeneous.

It is also possible to generate modeled waveforms from simulated samples when the local fragmentation ratio and the dynamics of the CPFAAS waveform formation are known. The simulated waveforms enable the instrument designing and optimization, and the estimation of the reliability of the measurement results from impure samples. The modeled signal is generated by first forming the simulated measurement conditions and the local absorption coefficients for target molecules and background. Second, the number of induced potassium atoms is calculated spatially in small steps by taking into account the fragmentation pulse attenuation in each modeled point. The energy of the transmitted pulse is determined as an energy value that is left after the modeled pulse has propagated through the whole simulated sample. The total number of potassium atoms affecting the deepness of the dip in the CPFAAS signal is calculated as a sum of the produced K atoms. The concentration of the K atoms is set to decrease exponentially according to the Eq. 5.1. As the time behavior of the signal is fully solved, a C constant is added to the curve. The curve is digitized to simulate the response of an 8-bit digitizer and, finally, some digitizing noise is added. A curve fitting routine is applied to the modeled signal and the KCl concentration is calculated based on the fitting parameters.

The performance of the CPFAAS in impure samples is demonstrated in three modeled samples that are presented in Fig. 5.4. The average background absorption coefficient is set to 0.5 $1/m$ in all examples. In Fig. 5.4 a) KCl is first approximated to have a constant profile through the whole sample with average concentration of 100 ppm and, then, some noise is implemented to it. The average concentration over modeled sample is 98.5 ppm. CPFAAS calibration equations for pure and impure samples result in KCl concentrations of 27.6 ppm and 99.6 ppm, respectively. In case b), the KCl

concentration is assumed to be 50 ppm at the edges and 100 ppm at the center of the sample. The average through the volume b) is 88.9 ppm and CPFAAS calculations result with for pure and impure calibration equations values of 23.4 ppm and 84.9 ppm, respectively. In volume c), the concentration is 50 ppm at the edges and 10 ppm at the center yielding to the average concentration of 24.2 ppm. The pure and impure calibration equations result in 9.6 ppm and 27.8 ppm, respectively, in volume c).

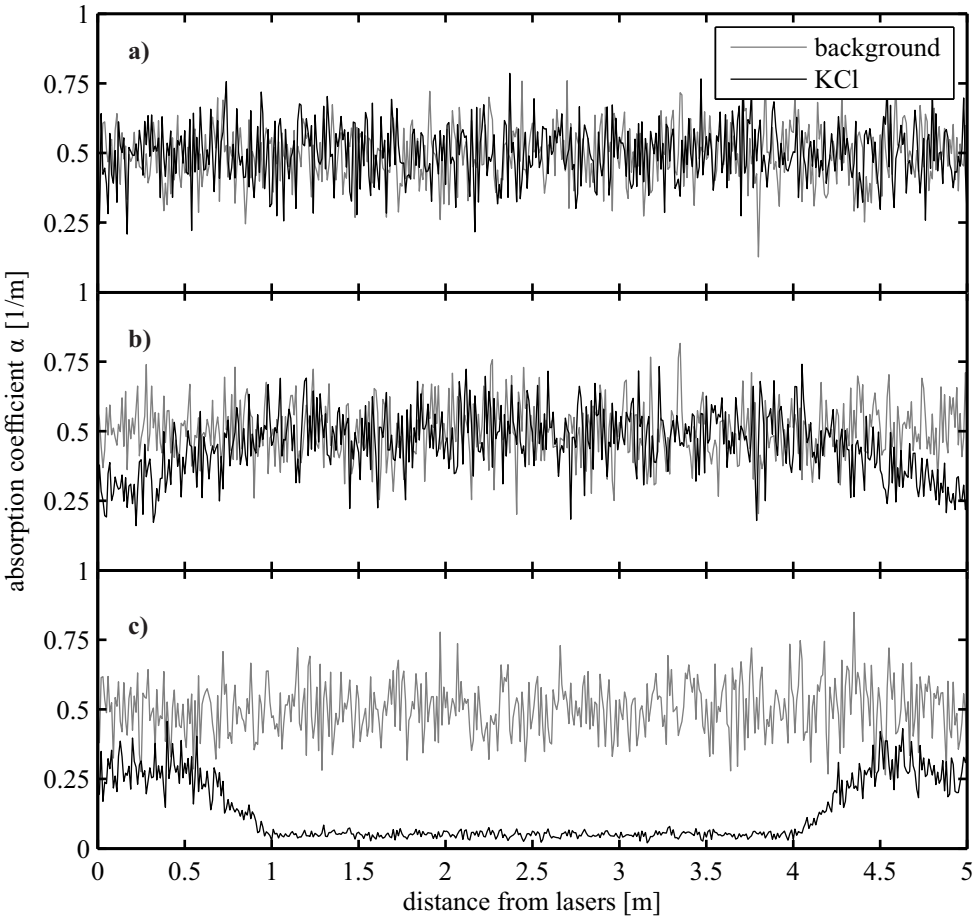

Figure 5.4 Three modeled conditions demonstrating impure and inhomogeneous samples. Gray background line has the average absorption coefficient of 0.5 1/m. Black curves indicate absorption coefficients due to KCl vapor at the wavelength of 266 nm with different concentration profiles: a) constant 100 ppm KCl concentration , b) 50 ppm KCl level at the edges and 100 ppm at the center and c) 50 ppm at the edges and 10 ppm at the center. Some noise is implemented to the curves to simulate boiler conditions.

The above models showed that when the sample has no clear concentration profile, the equation for the impure sample results in a very accurate estimation for the average concentration even in large and strongly absorbing media. The calculation with pure sample calibration equation resulted in clearly too low concentrations. The concentration profiles distort the evaluation of the average concentration but still the impure sample equation results in quite accurate estimations. The inaccuracy of the transmitted pulse energy also has a small effect on the calculated concentration value. For example, a 5 %-distortion in output pulse energy results in a 1 %-change in the calculated concentration.

5.4 Multicomponent analysis

A CPFAAS measurement with two light sources enables the detection of one target molecule. The number of detected molecules can be increased by adding fragmentation and/or probe beams on the measurement path. Two basic measurement arrangements for multicomponent detection are presented in Fig. 5.5. Setup a) applies one probe laser and two fragmentation lasers whose emission pulses pass the sample with small delay with respect to each other. The delay between the pulses should be set long enough so that both dips in the probe beam transmission are clearly distinguishable. Two-fragmentation-pulse setup enables the detection of one fragment atom originating from two different precursors. In **Paper 4**, a similar setup has been applied to the simultaneous detection of KCl and KOH. The use of two fragmentation wavelengths improves the selectivity of the measurement when the absorption bands of the precursors are overlapping.

The second possibility applies two probe beams and one fragmentation pulse as shown in Fig. 5.5 b). The measurement is based on the simultaneous fragmentation of multiple precursors and the probing of the preselected atom fragments. The setup with two probe beams can be applied, for example, in the simultaneous detection of KCl and NaCl. Setup b) induces a signal from both precursors exactly at the same time, while there is a small delay between the detection of different precursors in setup a). The combination of both setups could be used, for example, in the detection of KCl, KOH, NaCl, and NaOH.

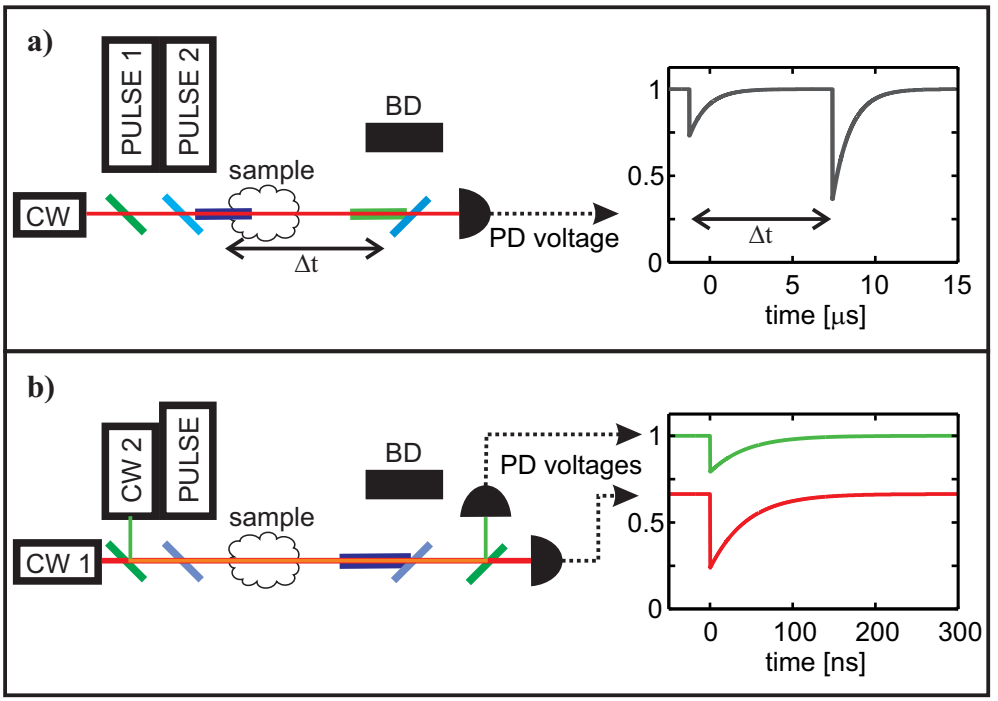

Figure 5.5 Two measurement arrangement enabling multicomponent CPFAAS detection. a) One probe laser and two pulse lasers that produce the same atom fragment from two different precursor molecules. b) Two probe lasers for different atoms and one pulse laser capable of fragmenting different molecules. BD refers to beam dump which can be replaced with an energy meter when required.

5.5 CPFAAS applications

The applicability of the CPFAAS technique to the combustion studies is discussed in this section. The performance of the technique is demonstrated in one laboratory scale application, where the release histories of potassium vapors from small fuel samples were monitored, and in two power plant experiments which were carried out with a mobile instrument built during this work. The laboratory application is discussed in detail in **Paper 4**. The results from power plant experiments have originally been presented in combustion related conferences [98,99].

KCl, KOH and K release measurements for single particle reactor

A single particle reactor (SPR) enables the study of release kinetics from small size fuel samples. Previously, the reactor has been applied to determine CO, CO_2, SO_2 and NO_X emissions from different fuels, and to image the combustion process of the small particles and pellets[100–102]. Controlled combustion conditions and the possibility to collect the combustion residues enable the study of the conversion of fuel to ash. In this work, we applied the optical ports of SPR, which has previously been used for the video imaging, to measure atomic K, KCl and KOH vapor releases from different fuels combusted at different temperatures.

The experiments were done by applying the multicomponent measurement arrangement shown in Fig. 5.5 a). The fragmentation wavelengths were 266 nm and 320 nm for KCl and KOH, respectively. The absorption bands of KCl and KOH overlap at the selected fragmentation wavelengths, but the spectral contrast was good enough so that they could be distinguished by applying a linear equation system. Four curves showing the release histories of KCl and KOH from torrefied wood with and without spectral overlapping correction are presented in Fig. 5.6. The example curves show that the effect of the spectral overlapping on the measured KOH release is minor, and the KCl release curve needs correction only when the concentration of KOH in the flue gas is equal to or larger than the concentration of KCl.

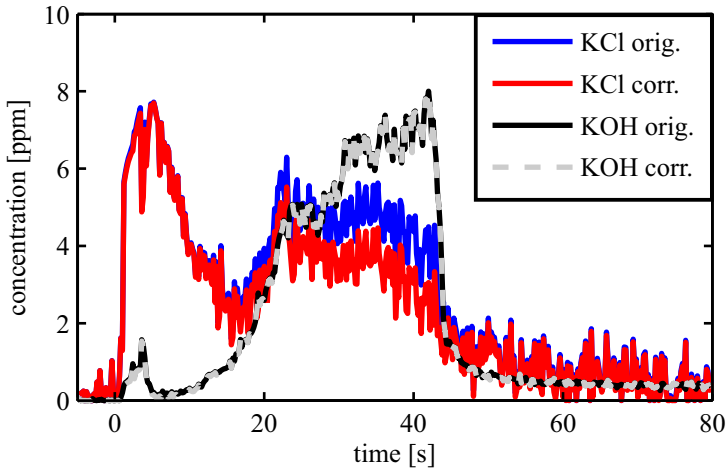

Figure 5.6 The effect of the spectral interference correction on KCl and KOH concentrations measured from a single particle reactor. Original (orig.) and corrected (corr.) concentration curves are presented.

The release histories of K, KCl and KOH vapors from 10 mg torrefied wood (high quality fuel) and straw (low quality fuel) samples combusted at the temperatures of a) 850 °C, b) 950 °C and c) 1050 °C and in 10 % of O_2 are presented in Fig. 5.7 and Fig. 5.8. The content of potassium and chlorine were 574 mg/kg and 11 mg/kg in torrefied wood and 9040 mg/kg and 1900 mg/kg in straw. The presented concentrations have been calculated using the absorption cross sections of $\sigma_{KCl} = 0.74 \cdot 10^{-21}$ cm^2 [36], $\sigma_{KOH} = 0.5 \cdot 10^{-21}$ cm^2, and $\sigma_K = 1.25 \cdot 10^{-21}$ cm^2 (see **Paper 4**). The absorption cross section of KOH is assumed to correspond to that of NaOH at its local absorption maximum near 320 nm [45] due to the lack of an exact value. The measurements were performed with rectangularly shaped beams having the width of 15 mm. The height of the fragmentation beams was 3 mm and the height of probe beam was 1.5 mm. The intensity distribution of the beams was flat. The rectangular shaped beams averaged the spatial variations in the flue gas and enabled the estimation of the total emission of the K vapors during the combustion. The K concentrations were calculated from the changes of the probe beam base transmission level within a combustion experiment and using the value of the K fragments absorption cross section. The effect of the soot and beam steering on the calculated K concentration was determined to be less than 1 ppb by performing a combustion experiment with a probe wavelength that was tuned 200 pm off the resonance line. The absorption of the fragmentation pulses was less than 5 % in SPR measurements and the concentration of KCl and KOH were calculated applying Eq. 5.2.

The CPFAAS measurements indicate that there is a huge difference in the KCl release from torrefied wood and straw. The result is expected, since the chlorine content of straw is two orders of magnitude higher than that of wood. One major source of the chlorine in the straw is the fertilizers whose amount and the chlorine content have been shown to affect the final chlorine content in straw directly [103]. The release histories show also that there are similarities in KOH and K releases between different fuels. Potassium chloride is clearly the main gaseous carrier of K at the temperature of 850 °C, but at the temperatures of 950 °C and 1050 °C the existence of KOH in flue gases is evident. Moreover, the release of the atomic K shows growing trend as the combustion temperature increases. The observations about the amounts and the forms of the different K vapors in the flue gas enable the better understanding of the kinetics of the potassium release and help in developing mathematical tools to model them. The CPFAAS measurements from SPR also provide a fast tool for characterizing how challenging a fuel is in terms of alkalis.

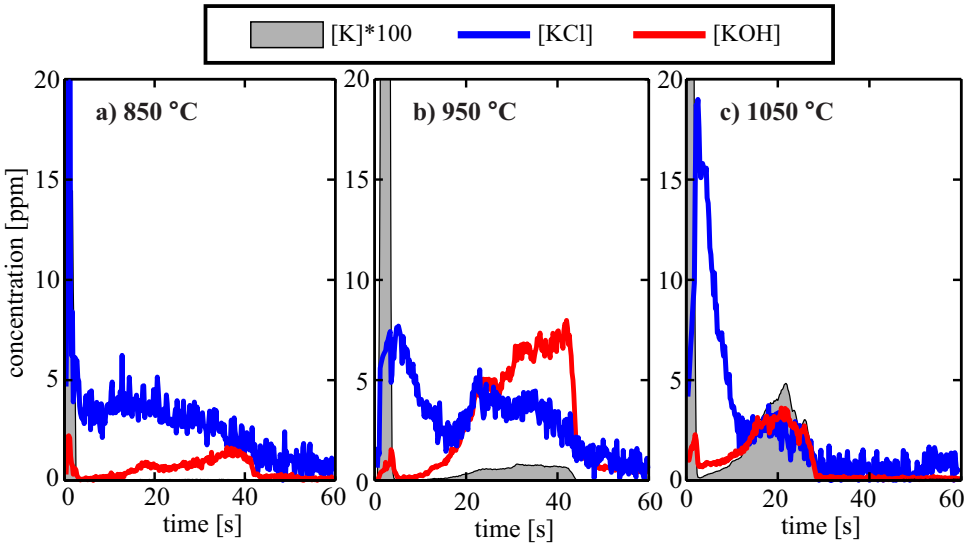

Figure 5.7 Release histories of K, KCl and KOH from three 10 mg torrefied wood samples combusted at temperatures of a) 850 °C,b) 950 °C and c) 1050 °C in 10 % of O_2 in single particle reactor.

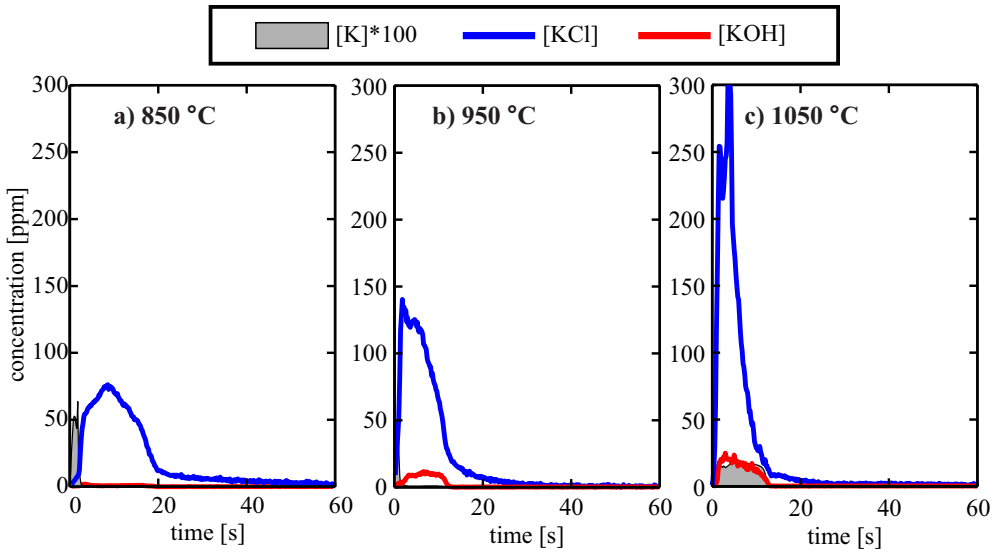

Figure 5.8 Release histories of K, KCl and KOH from three 10 mg straw samples combusted at temperatures of a) 850 °C, b) 950 °C and c) 1050 °C in 10 % of O_2 in single particle reactor.

Full-scale 100 MW_{th} combustion boiler experiments

CPFAAS technique was applied to monitor KCl concentration through a 8-m-wide bubbling fluidized bed boiler a few meters below the secondary super heaters. The flue gas temperature at this region was around 800 °C. The combustion boiler was fired with wastes (REF and sludge) together with bark during the experiments. The content of potassium and chlorine in the mixed fuel were 1670 mg/kg and 3140 mg/kg [104], respectively. Due to the high chlorine content, KCl was expected to be found abundantly from the flue gas. The flue gas temperature at the measurement location was too low for KOH formation.

Large scale combustion boilers are known to be challenging measurement environments for "see-through" applications due to the fluctuation transmissivity. The fluctuations originate from the fly ash stream in the boiler, from beam-steering problems due to the thermal lensing, and from the changing concentration of the light absorbing gases. Therefore the influence of the fluctuations on the applicability of the CPFAAS technique was first studied by determining the transmissivity of a laser beam, having a

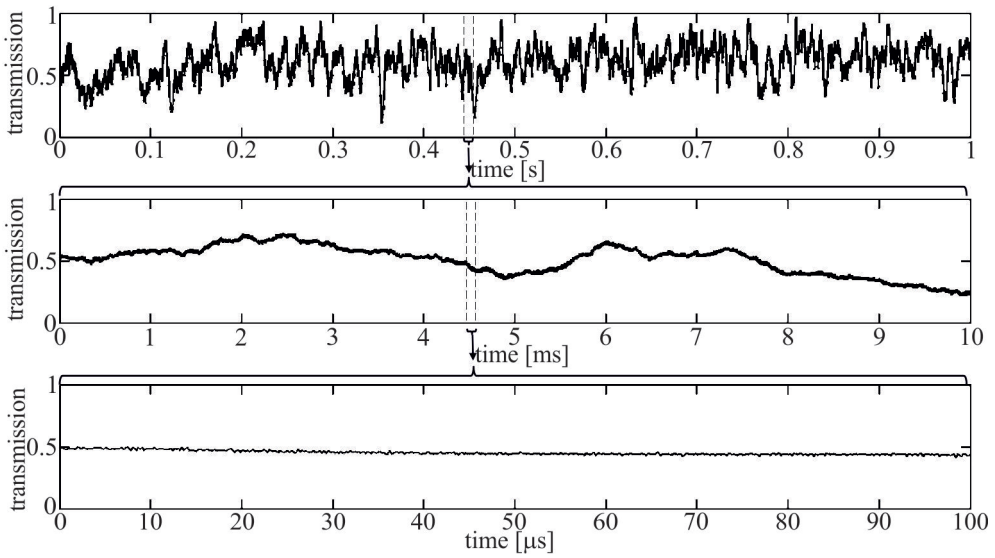

Figure 5.9 Visibility fluctuations through a 8-m-wide combustion boiler in different time scales. The topmost figure presents 1 s time window. The figure in the middle is extracted from the topmost figure and the figure on the bottom is extracted from the on in the middle. Dashed lines indicate the extraction areas.

diameter of 30 mm, through the 8 m wide boiler. The experiment was performed with a CW laser having the emission wavelength of 473 nm and output power of 50 mW. The analog bandwidth of the measurement was limited by a 400-MHz oscilloscope. An example transmission curve is presented in Fig. 5.9.

The topmost curve in Fig. 5.9 shows the normalized transmission of the laser beam in a time scale of 1 s. The curve in the middle is extracted from the first curve to show the fluctuations within a time scale of 10 ms, and the curve at the bottom is extracted from the one in the middle to show fluctuations within 100 μs. The extracted time windows were selected from the points showing the largest gradient in order to demonstrate the worst case scenario. Overall, the experiment showed that the transmission fluctuations are strong but within 5 μs time windows the maximum change in the transmission is less than 1 %. The CPFAAS waveform lasts less than 5 μs in combustion conditions and; therefore, it is immune to the flue gas fluctuations.

The image of the on-line CPFAAS instrument developed for the power plant experiments is shown in Fig. 5.10. The instrument consists of a laser head, a power supply, a controlling computer and a detector head. The laser head and the detector are placed on opposite sides of the boiler and connected with data cables. The size of the laser head is 50 cm x 60 cm x 20 cm (width x length x height). The corresponding dimensions of the detector are 40 cm x 45 cm x 20 cm. The laser and detector heads were connected to the boiler using connection pipes. An air flow through the pipes prevented the combustion gases reaching the instrument heads and ensured the

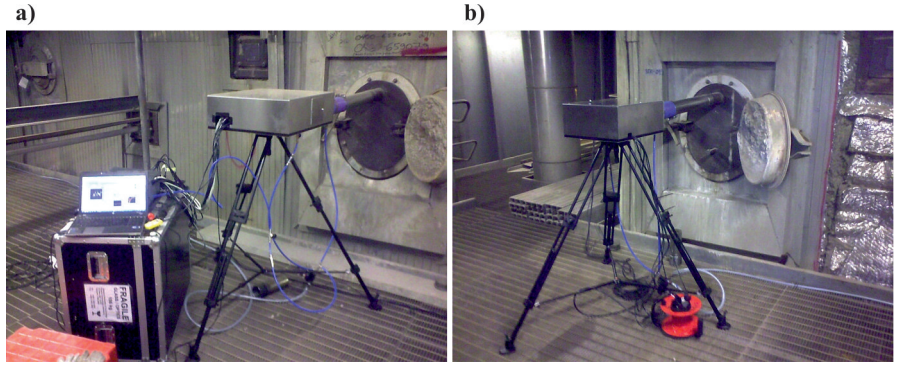

Figure 5.10 A CPFAAS based measurement device for power plant measurements: a) A laser head on tripod, and a controlling computer and a power unit on the transportation box, and b) a detector head on opposite sides of the boiler.

clearness of the viewing ports. The measurement routine, raw data saving, and signal analysis were automated with a LabVIEW code.

The instrument measured 2-μs-long CPFAAS waveforms at the repetition rate of 7 Hz in 200 pulse sequences. The base transmission of the probe beam was fluctuating due to the above-mentioned reasons, but the basic shape of the CPFAAS waveform could be clearly recognized from each individual signal as shown in Fig. 5.11 a). The KCl concentration was calculated from each waveform using the curve fitting and the Eq. 5.3. The UV absorption through the boiler was approximately $99.5 - 99.9$ %.

The observed changes between consecutive calculated concentration readings were less than 10 %; but within 200 pulse sequences, the variation could be even ± 50 %. The large fluctuations occurred in cycles and could be related to the local temperature fluctuations in the boiler, soot blower operation, or fuel feeding. In order to monitor boiler operation, it was more essential to follow the average concentration rather than fast fluctuations. The averaging of single concentration values in time windows of 30 s

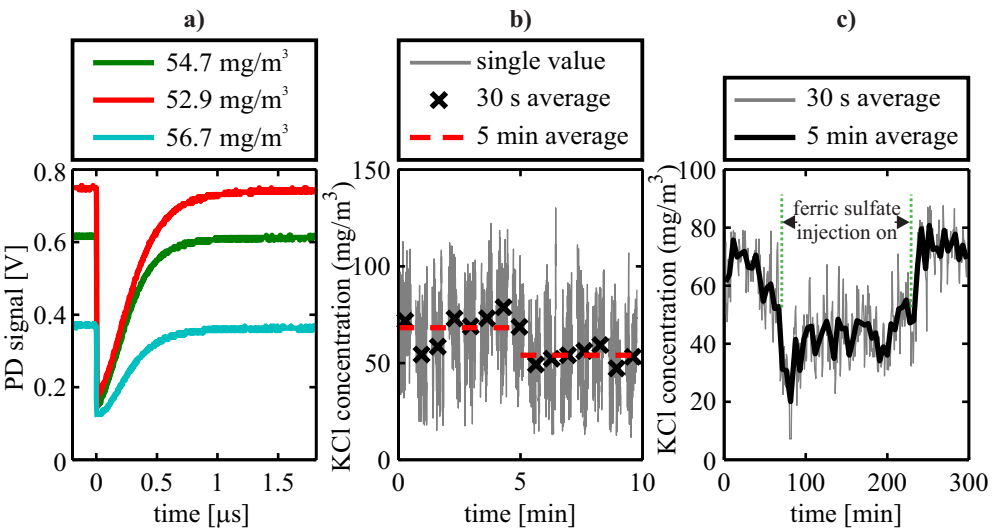

Figure 5.11 On-line measurement data acquired using a portable KCl detector. a) Single signals having different base levels and recovery rates but yielding similar KCl concentrations. b) Fluctuation of single measurements, 30 s average data and 5 min average data. c) 30 s and 5 min average data during ferric sulphate injections to flue gas. The injections cause a decrease in KCl concentration.(The results have been originally presented in *Impact of Fuel Quality on Power Production and the Environment* in Puchberg, Austria, September 23–27, 2012, Ref. 98)

and 5 min is demonstrated in Fig. 5.11 b) and applied in a 5-hour-long measurement in Fig. 5.11 c). The averaging over 30-second time windows was found to eliminate most of the short term fluctuations; but to monitor the boiler operation, the 5 min averaging resulted in a more sufficient output.

The experiments in 100 MW_{th} boiler showed that the CPFAAS technique can be applied in challenging field conditions, and resulted in modeling parameters that can be used in instrument designing. The CPFAAS instrument was capable of detecting the short term fluctuations in a boiler operation, and following the effect of the additive injections on the KCl concentrations. Figure 5.11 c) shows an attempt to reduce KCl concentration with ferric sulfate additive which converts KCl to less harmful K_2SO_4 [105,106]. The instrument detected how the KCl concentration decreased immediately after the additive injection was started and increased when it was stopped.

The measured KCl concentrations were probably affected by the spatial concentration differences in the boiler. Especially, nearby the boiler walls the concentration can be very different than at the center of the boiler. The effect of the inhomogeneous sample is estimated to be less than 10 % based on the models presented in Section 5.3. The accuracy of the boiler measurements can be enhanced for example by extending the instrument connection pipes by 1 m into the boiler. As a result, the cooler layer nearby the walls has a smaller effect on the measurement.

Intermediate size 4 MW_{th} **boiler**

The developed CPFAAS instrument was also applied to study the KCl concentration in a 4 MW_{th} circulating fluidized bed boiler. The measurements were done through a 1-m-wide flue gas channel, where the gas temperature was approximately 825 °C. The boiler combusted wood and straw during the measurement campaign. The content of potassium and chlorine were 390 mg/kg and 50 mg/kg in wood and 7600 mg/kg and 2900 mg/kg in straw [99].

Figure 5.12 presents two measurement periods where the boiler is started-up and the shares of the fuels are changed (a), and ferric sulfate is injected into the boiler to reduce the KCl concentration (b). The HCl concentration is presented in the latter experiment to give a reference for the measured KCl concentration. The UV absorption through the boiler was 50 % during pure wood combustion and 92.5 % during pure straw combustion.

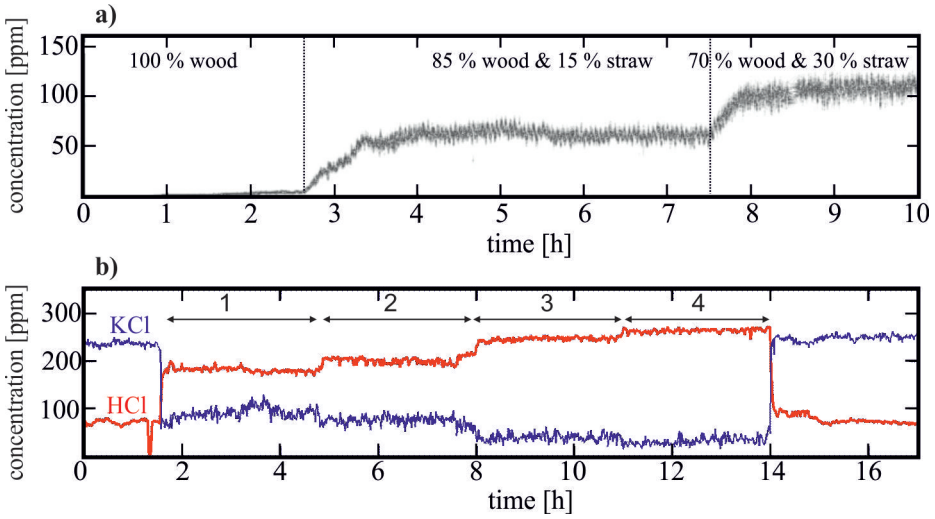

Figure 5.12 Online measurements from 4 MW_{th} CFB boiler. a) The start-up of the boiler fuel with containing wood and straw. The gray curve indicates the temporal variation of KCl concentration in the boiler. b) The effect of the ferric sulphate injection on the flue gas composition. The amount of ferric sulfate in the injected solution was increased in four steps. The boiler combusted 100 % of straw over the whole measurement. The KCl concentration curve indicates the median of the measured KCl concentration values within 30-second time windows. (The results have been originally presented in *European Combustion Meeting* in Lund, Sweden, June 25–28, 2013, Ref. 99)

Figure 5.12 a) shows how the KCl concentration increases in the flue gas as the amount of straw in the fuel increases. The gray line describes the observed concentration distributions of single concentration values within 30-second time windows. At the beginning of the experiment the load of the boiler was increased to 100 % by combusting pure wood. The mixing of straw to the fuel was started 2.5 h from the beginning of the experiment. The share of straw in the fuel achieved a level of 15 % within one hour. Around 7.5 h, the share of straw was further increased up to 30 %. The measured average KCl concentration with the fuel mixtures of 100 % of wood; 85 % of wood and 15 % of straw; and 70 % of wood and 30 % of straw were 5 ppm, 60 ppm and 110 ppm, respectively. The flue gas stream behaved more stably in the smaller boiler than in the previously presented larger boiler. The KCl concentration showed approximately ±10 % fluctuations within 30-second measurement windows while they were ±50 % in the large boiler.

The ferric sulfate injection experiment shows how the additive decreases the KCl concentration and increases the HCl concentration. The conversion originates from the alkali chloride sulphation reaction where alkalis convert to alkali sulfates and the left-over chlorine reacts with water vapor and produces HCl[105,106]. The additive injection was performed with four mixing ratios of ferric sulfate and water. The corresponding sulphation results are shown in Fig. 5.12 b). The measurement showed that the concentration change ΔX_{KCl} was approximately $0.75\Delta X_{HCl}$. Ideally, the concentration changes should have corresponded to each other. The observed difference is assumed to originate from the sulphation of the NaCl in the flue gas, and from the different sampling methods of KCl and HCl. The CPFAAS techniques measured *in-situ* the average through the flue gas channel, whereas HCl was measured using Fourier transform infrared spectrometer (FTIR) and sampling probe that collected gas only from the middle of the channel. Thereby, the possible concentration profiles of the gases in the flue gas channel have influenced the result.

5.6 Comparison of optical alkali detection techniques

This and two previous chapters have discussed the optical techniques for the detection of alkali compounds. They have been found to measure alkalis in different forms and enable different applications. The observed properties have been collected into Table 5.1, and are compared in this section. The measurement techniques for molecules, atoms and particles are compared and discussed separately.

The first three techniques detect alkalis bonded to molecules. The CPFAAS and ELIF techniques have been shown to be capable of detecting different alkalis bonded to chlorides or hydroxides selectively, whereas the DOAS technique measures the sum of KCl and NaCl. In principle, a DOAS measurement applying a broad band UV light source is capable of measuring alkali hydroxides as well, but such an experiment has not been demonstrated. All three techniques utilize transitions from the ground state to repulsive electronic states in the detection of the alkali containing molecules. The DOAS technique measures the direct UV absorption of the molecules, whereas the CPFAAS and ELIF techniques detect the fragment atoms released as a consequence of the UV absorption. The detection of the fragment atoms enhances the sensitivity of the detection but decreases the accuracy in large and strongly absorbing inhomogeneous

Table 5.1. Comparison of optical techniques applied in the detection of alkali compounds. The table lists: the abbreviation of the technique; compounds that a technique detects; the order of the sensitivity (Sen.); if the detection requires calibration or is absolute (CAl.); has a technique been applied in power plant measurements, Yes or No (PP); has a technique been applied in single particle reactor or corresponding studies, Yes or No (SPR) ; and how the detection is oriented in respect to light source.

Technique	Detects	Sen.	Cal.	PP	SPR	Detection
CPFAAS	KCl,KOH,NaCl,NaOH	10^{-10}	abs.	Y	Y	see-through
ELIF	KCl,KOH,NaCl,NaOH	10^{-10}	calib.	Y	Y	single-port/side
DOAS	KCl + NaCl	10^{-6}	abs.	Y	N	see-through
TDLS	K,Na	10^{-12}	abs.	Y	Y	see-through
PLIF	K,Na	10^{-9}	calib.	N	Y	side
LIBS	$[K]_{tot}$,$[Na]_{tot}$	10^{-8}	calib.	N	Y	single-port/side
PAS	KCl,NaCl	10^{-8}	calib.	N	N	acoustic

samples as discussed in Section 5.3. The direct absorption is insensitive to sample anomalies and indicates the average concentration through the measurement path.

The wavelengths used in CPFAAS and ELIF have different properties in alkali detection. The wavelengths of 266 nm and 320 nm, which were used in this work in the CPFAAS detection of KCl and KOH, release alkali atoms on their electronic ground levels, whereas the wavelength of 193 nm, which is used in the ELIF detection, releases alkali atoms on their excited levels. The latter alkalis can be detected with fluorescence spectroscopy which theoretically provides the sensitivity in the order of single atoms. The alkali atoms on their ground level are detected using atomic absorption spectroscopy which enables the detection at the level of parts per trillions (ppt). On the other hand, the more sensitive fluorescence detection requires a calibration, whereas the absorption measurement is absolute. The wavelength of 193 nm is also absorbed by O_2 and CO_2, which are abundant in combustion gases. Therefore, it has a shorter penetration depth into the sample than the longer wavelengths of 266 nm and 320 nm.[107–109] The short penetration depth decreases the accuracy of the determination of the average gas concentration in large sample volumes where the target gas is distributed inhomogeneously. In small or homogeneous samples the short penetration depth is not an issue, since the ELIF technique applies a single port alignment, i.e. the fluorescence light is collected from the same direction where the excitation is done. The CPFAAS and DOAS techniques operate with see-through alignment and require a sufficient visibility through the sample.

In the detection of alkali containing molecules, it can be concluded that the ELIF technique provides extremely good sensitivity with good accuracy from small samples with a measurement length of ~ 0.5 m or smaller. In large and highly absorbing samples, the DOAS technique provides the best accuracy and relatively good sensitivity in the order of parts per million. The CPFAAS technique combines the benefits of ELIF and DOAS; and enables the diagnostics of small and intermediate size samples up to several meters with good accuracy and the sensitivity of parts per billion.

The fourth and fifth techniques in Table 5.1 enable the accurate detection of the atomic alkalis. PLIF applies an ICCD camera in the imaging of fluorescence light from the side of the sample and, therefore, provides the spatial mapping of the alkali atoms in the studied volume. The PLIF technique is applied in the detection of alkalis only in the single particle scale combustion experiments and is not directly applicable to full scale power plant measurements. TDLS is a see-through measurement technique and provides calibration-free absolute concentration measurements. The technique has been demonstrated in the detection of K atoms with the wavelength modulation frequency of 1.3 kHz[21], but modern laser sources would allow to increase the frequency up to 10 kHz[110]. Both techniques provide better accuracy in the atom detection than CPFAAS, which is capable of evaluating alkali concentration only in non-fluctuating conditions as a changing base transmission. However, the probe laser of the CPFAAS setups, which were developed in this work, allows the TDLS measurement as well, but it was not performed in this work.

LIBS is the only optical *in-situ* technique allowing the measurement of the total amount of alkalis in atomic forms, in molecules, and in sub-micron particles. The measurement volume is in the order of 1 mm^3 in the LIBS detection. The LIBS signal can be recorded in any direction in respect to the measured point. The simultaneous single particle combustion experiment of LIBS and CPFAAS or ELIF could be used to estimate the ratio of the alkalis in vapors and particles. This kind of purely optical comparison measurement could verify or correct previous observations measured applying the sampling SI technique and the ELIF techniques[111].

The PAS technique provides the sensitive detection of alkali chlorides and has potential in real-time high-temperature metal oxidation studies, for example. However, its application to study alkalis from combustion gases would require a sampling line and the analysis of PAS signal at multiple excitation wavelengths.

Chapter 6

Summary

Optical spectroscopy has been applied to develop diagnostic techniques for alkali vapors in high-temperature gases. Optical measurements are sensitive, selective, and can be used without sampling. They thereby provide good measurement tools for the detection of reactive alkali compounds in different samples at sub-ppm concentration level. Alkalis induce corrosion and slagging problems in combustion applications, and their real-time monitoring would help to control their concentrations and optimize the processes. The topic of the Thesis is closely related to the combustion research and, therefore, the work includes experimental study from laboratory and power plants.

At the beginning of the Thesis, the reader was introduced to the topic by discussing the importance of combustion in modern society and current trends in combustion. The introduction also presented the alkali related problems and the need for their real-time monitoring. The absorption properties of the main alkali vapors found in combustion were discussed in Chapter 2. The previously applied alkali detection techniques were reviewed and some of their applications were highlighted in Chapter 3.

This Thesis presented two novel optical measurement techniques in Chapter 4 and Chapter 5. The techniques have been presented in detail in the journal papers that are the base of this Thesis. The first technique applies Photoacoustic Spectroscopy (PAS) in high-temperature gas analysis. The developed photoacoustic (PA) cell has been

presented and demonstrated by measuring KCl in **Paper 1**. Chapter 4 highlighted a few details about the cell and the signal processing, and determined the PA response of KCl and NaCl vapor. Moreover, the application of the PA cell in a high temperature salt induced metal oxidation research was discussed.

Chapter 5 focused on discussing a technique called Collinear Photofragmentation and Atomic Absorption Spectroscopy (CPFAAS), which has been developed within the framework of this Thesis. **Paper 2** and **Paper 3** presented the technique and its calibration equations. Moreover, the calibration equation of the pure samples was validated experimentally. The principles and calibration equations of the technique were presented in Chapter 5. Moreover, modeling tools for instrument designing and the validation of the impure sample calibration equation, and the basics of measurement setups for multicomponent diagnostics were presented. **Paper 4** discussed an application of the CPFAAS technique in the simultaneous detection of K, KCl and KOH vapors from the combustion gas emanated from a small amount of solid fuel. The combusted fuel was spruce bark, and the combustion temperatures were 850 °C, 950 °C and 1050 °C. Chapter 5 presented similar release histories recorded from two additional fuels: torrefied wood and straw. Two fuels were selected to demonstrate the difference in amount of the alkalis released from straw compared with that of refined wood fuel. The applicability of CPFAAS to long term measurements in power plant conditions was validated in two measurement campaigns performed with an automatized instrument. The techniques, which were developed in this work, were compared with other optical techniques for alkalis at the end of Chapter 5.

The presented applications, modeling and comparison with other detection methods showed that CPFAAS and PAS enable new measurement capabilities from high temperature gases. PAS is a sufficient tool for laboratory scale experiments but is not readily applicable to combustion monitoring. CPFAAS has more application possibilities since it can be applied *in-situ*, and it provides wide dynamic range. The CPFAAS experiments presented in this work focused on the detection of potassium vapors but similar measurements of other alkali vapors can be done with modern narrow-bandwidth laser sources. The experiments were carried out in the temperatures from 410 °C to 1050 °C and in atmospheric pressure, which are normal conditions in fluidized bed boilers combusting solid biomass fuels. The CPFAAS measurements in pulverized coal combustors and glass furnaces, where temperatures and pressures are higher than those applied in this work, would be interesting, but a fundamental

work to determine the absorption cross sections of the alkali vapors in such conditions is first needed. Moreover, the CPFAAS detection of heavy metal compounds, which can be photofragmented, should be plausible. The presented methods are both new and their full potential remains to be shown. Hopefully, this Thesis gave a good base to understand the methods and encouraged to apply them in new applications.

References

[1] I. E. Agency, "Key world energy statistics," (2012).

[2] "World energy outlook 2009," International Energy Agency, Paris, France (2009).

[3] "The renewable energy directive (2009/28/ec)," The directive is available for download in all European languages at `http://eur-lex.europa.eu/LexUriServ/LexUriServ.do?uri=CELEX:32009L0028:EN:NOT`. (Ref. 2.5.2011).

[4] L. Beurskens and M. Hekkenberg, "Renewable energy projections as published in the national renewable energy action plans of the european member states," Tech. rep., Energy research Centre of the Netherlands (2011).

[5] *Kansallinen energia- ja ilmastostrategia Taustaraportti.*

[6] H. Nielsen, F. Frandsen, K. Dam-Johansen, and L. Baxter, "The implications of chlorine-associated corrosion on the operation of biomass-fired boilers," Progress in energy and combustion science **26**, 283–298 (2000).

[7] J. Lehmusto, B. Skrifvars, P. Yrjas, and M. Hupa, "High temperature oxidation of metallic chromium exposed to eight different metal chlorides," Corrosion Science **53**, 3315–3323 (2011).

[8] M. Aho, P. Vainikka, R. Taipale, and P. Yrjas, "Effective new chemicals to prevent corrosion due to chlorine in power plant superheaters," Fuel **87**, 647–654 (2008).

[9] J. Sandberg, C. Karlsson, and R. Fdhila, "A 7 year long measurement period investigating the correlation of corrosion, deposit and fuel in a biomass fired circulated fluidized bed boiler," Applied Energy **88**, 99–110 (2011).

[10] P. Monkhouse, "On-line spectroscopic and spectrometric methods for the determination of metal species in industrial processes," Progress in Energy and Combustion Science **37**, 125–171 (2011).

[11] M. R. McCurdy, Y. Bakhirkin, G. Wysocki, R. Lewicki, and F. K. Tittel, "Recent advances of laser-spectroscopy-based techniques for applications in breath analysis,"

Journal of Breath Research **1**, 014001 (2007).

[12] G. Wysocki, Y. Bakhirkin, S. So, F. K. Tittel, C. J. Hill, R. Q. Yang, and M. P. Fraser, "Dual interband cascade laser based trace-gas sensor for environmental monitoring," Applied optics **46**, 8202–8210 (2007).

[13] W. M. Haynes, ed., *CRC Handbook of Chemistry and Physics* (CRC Press/Taylor and Francis Boca Raton, FL., 2013), 94th ed.

[14] S. M. Jasinski, "2011 minerals yearbook - potash," Tech. rep., U.S. Geological Survey (2011).

[15] I. F. I. Association, "Fertilizer indicator - may 2013," .

[16] J. M. Hollas, *Modern Spectroscopy* (Wiley, 2004), 4th ed.

[17] J. E. Sansonetti, W. C. Martin, and S. Young, "Handbook of basic atomic spectroscopic data," Journal of Physical and Chemical Reference Data **34**, 1559–2260 (2005).

[18] R. Y. R. J. Kramida, A. and N. A. T. (2012), "Nist atomic spectra database (ver. 5.0)," Online (2013).

[19] W. Demtröder, *Laser Spectroscopy* (Springer-Verlag, 1996).

[20] V. Härinen, "Plasma excited atomic resonance line spectroscopy as a method for real-time detection of alkali metals in combustion gases," Ph.D. thesis, Tampere University of Technology (2003).

[21] E. Schlosser, T. Fernholz, H. Teichert, and V. Ebert, "In situ detection of potassium atoms in high-temperature coal-combustion systems using near-infrared-diode lasers," Spectrochimica Acta Part A: Molecular and Biomolecular Spectroscopy **58**, 2347–2359 (2002).

[22] M. Blander, *Alkali halide vapors: Thermodynamic properties of Alkali Halide Vapors* (Academic Press, 1979).

[23] "Merc millipore: 104928 Potassium Chloride [Material Safety Data Sheet]," The material data sheet is available for download at `http://www.merckmillipore.com`. (Ref. 31.8.2013).

[24] A. Roine, "Outukumpu hsc chemistry for windows version 5.1," Outokumpu Research, Pori, Finland (2003).

[25] S. C. van Lith, P. A. Jensen, F. J. Frandsen, and P. Glarborg, "Release to the gas phase of inorganic elements during wood combustion. part 2: influence of fuel composition," Energy & Fuels **22**, 1598–1609 (2008).

[26] R. Ram, M. Dulick, B. Guo, K.-Q. Zhang, and P. Bernath, "Fourier transform infrared emission spectroscopy of NaCl and KCl," Journal of molecular spectroscopy **183**, 360–373 (1997).

[27] H. Levi, "Doctoral dissertation," Ph.D. thesis, University of Berlin (1934).

[28] R. Oldenborg, J. Gole, and R. Zare, "Chemiluminescent spectra of alkali-halogen reactions," The Journal of Chemical Physics **60**, 4032–4042 (1974).

[29] R. S. Berry, *Alkali halide vapors: Optical Spectra of the Alkali Halide Molecules* (Academic Press, 1979).

[30] P. Davidovits and D. Brodhead, "Ultraviolet absorption cross sections for the alkali halide vapors," The Journal of Chemical Physics **46**, 2968–2973 (1967).

[31] S. Kubodera, P. Wisoff, and R. Sauerbrey, "Absorption spectra of alkali halide molecules in the vacuum ultraviolet," The Journal of Chemical Physics **92**, 5867–5874 (1990).

[32] J. Silver, D. Worsnop, A. Freedman, and C. Kolb, "Absolute photodissociation cross sections of gas phase sodium chloride at room temperature," The Journal of chemical physics **84**, 4378–4384 (1986).

[33] T. S. Rose, M. J. Rosker, and A. H. Zewail, "Femtosecond real-time probing of reactions. iv. the reactions of alkali halides," The Journal of chemical physics **91**, 7415–7436 (1989).

[34] T.-M. R. Su and S. J. Riley, "Alkali halide photofragment spectra. III. alkali chloride bond energies and excited state symmetries at 266 nm," The Journal of Chemical Physics **72**, 6632–6636 (1980).

[35] G. Daminelli, D. Katskov, R. Mofolo, and P. Tittarelli, "Atomic and molecular spectra of vapours evolved in a graphite furnace. part 1. alkali halides," Spectrochimica Acta Part B: Atomic Spectroscopy **54**, 669–682 (1999).

[36] C. Forsberg, M. Broström, R. Backman, E. Edvardsson, S. Badiei, M. Berg, and H. Kassman, "Principle, calibration, and application of the in situ alkali chloride monitor," Review of Scientific Instruments **80**, 023104 (2009).

[37] M. Oppenheimer and R. S. Berry, "Ultraviolet spectra of alkali halides in inert matrices," The Journal of Chemical Physics **54**, 5058–5073 (1971).

[38] K. J. Kaufmann, J. L. Kinsey, H. B. Palmer, and A. Tewarson, "Chemiluminescent emission spectra and possible upper-state potentials of KCl and KBr," The Journal of Chemical Physics **61**, 1865– 1867 (1974).

[39] R. L. Kuczkowski, D. R. Lide, and L. C. Krisher, "Microwave spectra of alkali hydroxides: evidence for linearity of CsOH and KOH," The Journal of Chemical Physics **44**, 3131–3132 (1966).

[40] A. Kumar, M. Park, J. Y. Huh, H. M. Lee, and K. S. Kim, "Hydration phenomena of sodium and potassium hydroxides by water molecules," The Journal of Physical Chemistry A **110**, 12484–12493 (2006).

[41] R. F. Porter and R. C. Schoonmaker, "Gaseous species in the vaporization of potassium hydroxide," The Journal of Physical Chemistry **62**, 234–237 (1958).

[42] T. Blomberg, "Correlation of the corrosion rates of steels in a straw fired boiler with the thermodynamically predicted trend of KOH (g) in the flue gases," Biomass and Bioenergy **39**, 489–493 (2012).

[43] R. C. Oldenborg and S. L. Baughcum, "Photofragment fluorescence as an analytical technique: application to gas-phase alkali chlorides," Analytical Chemistry **58**, 1430–

1436 (1986).

[44] M. Vasiliu, S. Li, K. A. Peterson, D. Feller, J. L. Gole, and D. A. Dixon, "Structures and heats of formation of simple alkali metal compounds: Hydrides, chlorides, fluorides, hydroxides, and oxides for Li, Na, and K," The Journal of Physical Chemistry A **114**, 4272–4281 (2010).

[45] D. E. Self and J. M. Plane, "Absolute photolysis cross-sections for $NaHCO_3$, NaOH, NaO, NaO_2 and NaO_3: implications for sodium chemistry in the upper mesosphere," Physical Chemistry Chemical Physics **4**, 16–23 (2002).

[46] D. C. Dayton, R. J. French, and T. A. Milne, "Direct observation of alkali vapor release during biomass combustion and gasification. 1. application of molecular beam/mass spectrometry to switchgrass combustion," Energy & Fuels **9**, 855–865 (1995).

[47] U. Jäglid, J. G. Olsson, and J. B. Pettersson, "Detection of sodium and potassium salt particles using surface ionization at atmospheric pressure," Journal of aerosol science **27**, 967–977 (1996).

[48] J. G. Olsson, U. Jäglid, J. B. Pettersson, and P. Hald, "Alkali metal emission during pyrolysis of biomass," Energy & Fuels **11**, 779–784 (1997).

[49] K. O. Davidsson, K. Engvall, M. Hagström, J. G. Korsgren, B. Lönn, and J. B. Pettersson, "A surface ionization instrument for on-line measurements of alkali metal components in combustion: Instrument description and applications," Energy & fuels **16**, 1369–1377 (2002).

[50] K. A. Christensen and H. Livbjerg, "A field study of submicron particles from the combustion of straw," Aerosol science and technology **25**, 185–199 (1996).

[51] K. Iisa, Y. Lu, and K. Salmenoja, "Sulfation of potassium chloride at combustion conditions," Energy & Fuels **13**, 1184–1190 (1999).

[52] P. J. van Eyk, P. J. Ashman, Z. T. Alwahabi, and G. J. Nathan, "Quantitative measurement of atomic sodium in the plume of a single burning coal particle," Combustion and Flame **155**, 529–537 (2008).

[53] M. Broström, H. Kassman, A. Helgesson, M. Berg, C. Andersson, R. Backman, and A. Nordin, "Sulfation of corrosive alkali chlorides by ammonium sulfate in a biomass fired CFB boiler," Fuel Processing Technology **88**, 1171–1177 (2007).

[54] H. Kassman, J. Pettersson, B.-M. Steenari, and L.-E. Åmand, "Two strategies to reduce gaseous KCl and chlorine in deposits during biomass combustioninjection of ammonium sulphate and co-combustion with peat," Fuel Processing Technology **105**, 170–180 (2013).

[55] B. Li, Z. Sun, Z. Li, M. Aldén, J. G. Jakobsen, S. Hansen, and P. Glarborg, "Post-flame gas-phase sulfation of potassium chloride," Combustion and flame **160**, 959–969 (2013).

[56] U. Gottwald and P. Monkhouse, "Single-port optical access for spectroscopic measurements in industrial flue gas ducts," Applied Physics B **69**, 151–154 (1999).

[57] U. Gottwald, P. Monkhouse, N. Wulgaris, and B. Bonn, "In-situ study of the effect of operating conditions and additives on alkali emissions in fluidised bed combustion,"

Fuel processing technology **75**, 215–226 (2002).

[58] C. Erbel, M. Mayerhofer, P. Monkhouse, M. Gaderer, and H. Spliethoff, "Continuous in situ measurements of alkali species in the gasification of biomass," Proceedings of the Combustion Institute **34**, 2331–2338 (2013).

[59] B. L. Chadwick, G. Domazetis, and R. J. Morrison, "Multiwavelength monitoring of photofragment fluorescence after 193 nm photolysis of NaCl and NaOH: application to measuring the sodium species released from coal at high temperatures," Analytical Chemistry **67**, 710–716 (1995).

[60] C. Erbel, "Beiträge zur entwicklung der ELIF-messtechnik," Ph.D. thesis, Technical University of München (2013).

[61] B. L. Chadwick, P. G. Griffin, and R. J. Morrison, "Quantitative detection of gas-phase NaOH using 355-nm multiple-photon absorption and photofragment fluorescence," Applied spectroscopy **51**, 990–993 (1997).

[62] L.-J. Hsu, Z. T. Alwahabi, G. J. Nathan, Y. Li, Z. Li, and M. Aldén, "Sodium and potassium released from burning particles of brown coal and pine wood in a laminar premixed methane flame using quantitative laser-induced breakdown spectroscopy," Applied spectroscopy **65**, 684–691 (2011).

[63] Y. He, J. Zhu, B. Li, Z. Wang, Z. Li, M. Aldén, and K. Cen, "In-situ measurement of sodium and potassium release during oxy-fuel combustion of lignite using laser-induced breakdown spectroscopy: Effects of O_2 and CO_2 concentration," Energy & Fuels **27**, 1123–1130 (2013).

[64] G. S. Hurst, M. Payne, S. Kramer, and J. Young, "Resonance ionization spectroscopy and one-atom detection," Reviews of Modern Physics **51**, 767–819 (1979).

[65] L. Grossman, G. Hurst, M. Payne, and S. L. Allman, "Saturated photodissociation of CsI," Chemical Physics Letters **50**, 70–73 (1977).

[66] B. Kaldvee, "Development and application of single-ended picosecond laser diagnostics," Ph.D. thesis, Lund University (2010).

[67] A. G. Bell, "On the production and reproduction of sound by light," American Journal of Sciences **20**, 305–324 (1880).

[68] A. G. Bell, *Upon the production of sound by radiant energy* (Gibson Brothers, printers, 1881).

[69] A. Rosencwaig, *Photoacoustics and Photoacoustic Spectroscopy* (Robert E. Krieger Publishing company, 1980).

[70] V. P. Zharov, *Laser Optoacoustic Spectroscopy* (Springer-Verlag, Berlin, 1986).

[71] W. R. Harshbarger and M. B. Robin, "Opto-acoustic effect. revival of an old technique for molecular spectroscopy," Accounts of chemical research **6**, 329–334 (1973).

[72] J. Saarela, T. Sorvajärvi, T. Laurila, and J. Toivonen, "Phase-sensitive method for background-compensated photoacoustic detection of NO_2 using high-power LEDs," Optics Express **19**, A725–A732 (2011).

[73] J. Kalkman and H. Van Kesteren, "Relaxation effects and high sensitivity photoacoustic detection of NO_2 with a blue laser diode," Applied Physics B **90**, 197–200 (2008).

[74] J. Saarela, J. Toivonen, A. Manninen, T. Sorvajärvi, and R. Hernberg, "Wavelength modulation waveforms in laser photoacoustic spectroscopy," Applied optics **48**, 743–747 (2009).

[75] I. Calasso and M. Sigrist, "Selection criteria for microphones used in pulsed nonresonant gas-phase photoacoustics," Review of Scientific Instruments **70**, 4569–4578 (1999).

[76] A. Miklós, P. Hess, and Z. Bozóki, "Application of acoustic resonators in photoacoustic trace gas analysis and metrology," Review of scientific instruments **72**, 1937–1955 (2001).

[77] S. Schäfer, A. Miklós, and P. Hess, "Quantitative signal analysis in pulsed resonant photoacoustics," Applied optics **36**, 3202–3211 (1997).

[78] M. Pushkarsky, M. Webber, and C. Patel, "Ultra-sensitive ambient ammonia detection using CO_2-laser-based photoacoustic spectroscopy," Applied Physics B **77**, 381–385 (2003).

[79] F. Harren, F. Bijnen, J. Reuss, L. Voesenek, and C. Blom, "Sensitive intracavity photoacoustic measurements with a CO_2 waveguide laser," Applied Physics B **50**, 137–144 (1990).

[80] C. Brand, A. Winkler, P. Hess, A. Miklós, Z. Bozóki, and J. Sneider, "Pulsed-laser excitation of acoustic modes in open high-q photoacoustic resonators for trace gas monitoring: results for C_2H_4," Applied optics **34**, 3257–3266 (1995).

[81] Brüel&Kjær, *Microphone Handbook – Vol. 1: Theory*, Nærum, Denmark (1996).

[82] A. Kosterev, Y. A. Bakhirkin, R. Curl, and F. Tittel, "Quartz-enhanced photoacoustic spectroscopy," Optics Letters **27**, 1902–1904 (2002).

[83] J. Kauppinen, K. Wilcken, I. Kauppinen, and V. Koskinen, "High sensitivity in gas analysis with photoacoustic detection," Microchemical journal **76**, 151–159 (2004).

[84] N. Bilaniuk, "Optical microphone transduction techniques," Applied Acoustics **50**, 35–63 (1997).

[85] B. Fischer and E. Wintner, "Sound recording by laser interferometry," in *Conference on Lasers and Electro-Optics/International Quantum Electronics Conference*, Baltimore, Maryland United States, May 31 - June 5, 2009.

[86] J. Hillenbrand and G. M. Sessler, "High-sensitivity piezoelectric microphones based on stacked cellular polymer films (l)," The Journal of the Acoustical Society of America **116**, 3267–3270 (2004).

[87] A. Manninen, J. Sand, J. Saarela, T. Sorvajärvi, J. Toivonen, and R. Hernberg, "Electromechanical film as a photoacoustic transducer," Optics Express **17**, 16994–16999 (2009).

[88] H. Jalink and D. Bicanic, "Concept, design, and use of the photoacoustic heat pipe cell," Applied Physics Letters **55**, 1507–1509 (1989).

[89] D. Bicanic, M. Chirtoc, M. Lubbers, and H. Jalink, "A photoacoustic detector of the total carbon content in soil water solutions," Measurement Science and Technology **4**, 1016–1020 (1993).

[90] J. Stenberg, R. Hernberg, and J. Vattulainen, "Analysis of pollutant chemistry in combustion by *in situ* pulsed photoacoustic laser diagnostics," Applied optics **34**, 8400–8408 (1995).

[91] H. A. Beck, Z. Bozóki, and R. Niessner, "Screening of pentachlorophenol-contaminated wood by thermodesorption sampling and photoacoustic detection," Analytical chemistry **72**, 2171–2176 (2000).

[92] O. Svelto, *Principles of Lasers* (Springer, 1998), 4th ed.

[93] J. Simeonsson and R. Sausa, "Laser photofragmentation/fragment detection techniques for chemical analysis of the gas phase," TrAC Trends in Analytical Chemistry **17**, 542–550 (1998).

[94] O. Johansson, J. Bood, M. Alden, and U. Lindblad, "Detection of hydrogen peroxide using photofragmentation laser-induced fluorescence," Applied spectroscopy **62**, 66–72 (2008).

[95] D. Ehrlich and R. Osgood Jr, "Metal-atom resonance-line lasers," Quantum Electronics, IEEE Journal of **16**, 257–268 (2002).

[96] S. Edelstein and P. Davidovits, "Cross Sections for the Alkali-Metal-Halogen Molecule Reactions: Na, K, Rb, and Cs with I," The Journal of Chemical Physics **55**, 5164 (1971).

[97] J. Simeonsson and R. Sausa, "Trace analysis of NO_2 in the presence of NO by laser photofragmentation/fragment photoionization spectrometry at visible wavelengths," Applied spectroscopy **50**, 1277–1282 (1996).

[98] T. Sorvajärvi, J. Roppo, J. Silvennoinen, and J. Toivonen, "Optical detection of KCl vapor using collinear photofragmentation spectroscopy," in *Impact of Fuel Quality on Power Production and the Environment*, Puchberg, Austria, September 23 - 27, 2012.

[99] T. Sorvajärvi, J. Maunula, J. Silvennoinen, and J. Toivonen, "Optical detection of KCl vapor in 4 MW CFB boiler during straw combustion and ferric sulfate injection," in *European Combustion Meeting*, Lund, Sweden, June 25 - 28, 2013.

[100] J. Giuntoli, W. de Jong, A. H. Verkooijen, P. Piotrowska, M. Zevenhoven, and M. Hupa, "Combustion characteristics of biomass residues and biowastes: fate of fuel nitrogen," Energy & Fuels **24**, 5309–5319 (2010).

[101] N. Vähä-Savo, N. DeMartini, and M. Hupa, "Combustion of black liquor–solid biomass mixtures in a single particle reactor - characteristics and fate of nitrogen," Energy & Fuels **25**, 4944–4951 (2011).

[102] O. Karlström, A. Brink, and M. Hupa, "Time dependent production of NO from combustion of large biomass char particles," Fuel **103**, 524–532 (2013).

[103] B. Sander, "Properties of danish biofuels and the requirements for power production," Biomass and Bioenergy **12**, 177–183 (1997).

[104] M. Hedman, J. Maunula, J. Roppo, T. Sorvajärvi, J. Toivonen, and P. Vainikka, "Measurement and control of the corrosivity of the environment in combustion of solid recovered fuel in BFB boiler," in *Impact of Fuel Quality on Power Production and the Environment*, Puchberg, Austria, September 23 - 27, 2012.

[105] P. Glarborg and P. Marshall, "Mechanism and modeling of the formation of gaseous alkali sulfates," Combustion and Flame **141**, 22–39 (2005).

[106] M. Aho, P. Vainikka, R. Taipale, and P. Yrjas, "Effective new chemicals to prevent corrosion due to chlorine in power plant superheaters," Fuel **87**, 647–654 (2008).

[107] J. Vattulainen, L. Wallenius, J. Stenberg, R. Hernberg, and V. Linna, "Experimental determination of SO_2, C_2H_2, and O_2 UV absorption cross sections at elevated temperatures and pressures," Applied spectroscopy **51**, 1311–1315 (1997).

[108] D. Ityaksov, H. Linnartz, and W. Ubachs, "Deep-UV absorption and Rayleigh scattering of carbon dioxide," Chemical Physics Letters **462**, 31–34 (2008).

[109] S. F. Rice and R. G. Hanush, "Absorptivity of carbon dioxide and molecular oxygen at 193 nm at high temperatures up to 1600 $^{\circ}$C," Applied spectroscopy **56**, 1621–1625 (2002).

[110] O. Witzel, A. Klein, C. Meffert, S. Wagner, S. Kaiser, C. Schulz, and V. Ebert, "VCSEL-based, high-speed, in situ TDLAS for in-cylinder water vapor measurements in IC engines," Optics Express **21**, 19951–19965 (2013).

[111] P. Monkhouse, U. Gottwald, K. Davidsson, B. Lönn, K. Engvall, and J. Pettersson, "Phase discrimination of alkali species in PCFB combustion flue gas using simultaneous monitoring by surface ionisation and photofragmentation fluorescence," Fuel **82**, 365–371 (2003).

Appendices

Paper 1

Tapio Sorvajärvi, Albert Manninen, Juha Toivonen, Jaakko Saarela, and Rolf Hernberg.

Resonant photoacoustic cell for pulsed laser analysis of gases at high temperature.

Review of Scientific Instruments **80**, 123103 (2009)

doi: 10.1063/1.3266974

Resonant photoacoustic cell for pulsed laser analysis of gases at high temperature

Tapio Sorvajärvi, Albert Manninen, Juha Toivonen, Jaakko Saarela, and Rolf Hernberg[a)]
Department of Physics, Optics Laboratory, Tampere University of Technology, P.O. Box 692, FI-33101 Tampere, Finland

(Received 28 July 2009; accepted 2 November 2009; published online 7 December 2009)

A new approach to high temperature gas analysis by means of photoacoustic (PA) spectroscopy is presented. The transverse modes of the resonant PA cell were excited with a pulsed laser and detected with a microphone. Changes in the properties of the PA cell resulting from a varying temperature are discussed and considered when processing the PA signal. The feasibility of the proposed method was demonstrated by studying PA response from saturated vapor of potassium chloride (KCl) in the temperature range extending from 410 to 691 °C. The PA spectrum, the detection limit, and the signal saturation of KCl vapor are discussed. At 245 nm excitation wavelength and 300 μJ pulse energy, the achieved detection limit for KCl is 15 ppb. © *2009 American Institute of Physics.* [doi:10.1063/1.3266974]

I. INTRODUCTION

Photoacoustic spectroscopy (PAS), a well established diagnostic method with a large dynamic range,[1,2] can be readily applied to the analysis of gases at the trace level, as well as for the studies of liquids and solids.[3] It relies on the indirect detection of heat generated by thermal relaxations or dissociation of the molecules in the absorbing sample. More specifically, in the closed volume, generated heat causes changes of the gas pressure. Modulating periodically the intensity of the incident light at acoustic frequencies results in a production of acoustic wave at the modulation frequency and/or its higher harmonics. On the other hand, a short acoustic pulse characterized by a broad frequency spectrum is generated whenever the excitation is accomplished using the pulse excitation. The sound waves are detected by acoustic transducers such as microphones,[4,5] quartz tuning forks,[6] silicon cantilevers,[7–9] and piezoelectric elements.[10] Recently, a novel type of transducer that makes use of an electromechanical film has been developed and tested.[11]

A special feature of PAS is the fact that the ultimate detection sensitivity depends on the amount of energy deposited in the absorbing sample. For a given sample, the latter is equal to the product of the number of absorbing molecules and the intensity of incident radiation. Hence, the detection sensitivity can be enhanced by increasing the power of the incident radiation. Improvement of several orders of magnitude has been achieved in comparison with traditional absorption spectroscopy.

Due to the limited operational temperature range of acoustic transducers, PAS is often used at room temperature conditions. Special cell designs are required if PAS is to be applied at elevated temperatures; the examples are the "heat-pipe"[12,13] and a special signal tube[14,15] that have been used at temperatures as high as 630 and 1000 °C, respectively.

In the study described in this paper, we present the resonant PA cell that can be used for analysis of gases at high temperatures. In addition, the signal processing method that normalizes variations of the resonator's quality factor is discussed. The pulsed optical parametric oscillator (OPO) laser served as the excitation source and the performance of the resonant PA cell was tested by measuring the PA response of KCl vapor. KCl is a major compound responsible for increased corrosion and fouling of the superheater tubes in biomass-fired power plants.[16] The PA response of the KCl vapor was studied as a function of the excitation wavelength, the concentration of the sample, and the excitation pulse energy. The PA measurements were performed within the temperature range extending from 410 to 691 °C using the excitation wavelengths from 210 to 340 nm emitted by OPO.

II. EXPERIMENTAL SETUP

Figure 1 shows the resonant PA cell designed for high temperature analysis of gases. Basically, the PA cell consists of the five major components: (i) the acoustic resonator, (ii) the signal tube, (iii) the microphone base, (iv) the buffer volumes, and (v) the extension tubes that enable the windows to be placed outside the heating oven. All major components were fabricated from the acid-proof steel. The PA cell is placed in the sublimation oven which can be heated up to 900 °C. The PA impulse was excited in the cylindrical acoustic resonator, the length and diameter of which are 85 and 25 mm, respectively. In order to maximize the sound reflection, the walls of the resonator were polished. The PA signal was detected with a 4939, Brüel & Kjær microphone. The 6 mm inner diameter and 400-mm-long signal tube mounted to the wall of the acoustic resonator ends at the microphone base, where it is by means of an acoustic adapter connected air tightly to the microphone. The adapter was

[a)]Deceased.

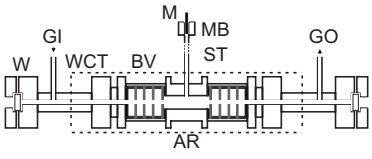

FIG. 1. The resonant PA cell for high temperature studies of gases: window (w), gas inlet (GI), gas outlet (GO), extension tube (ET), buffer volumes (BV), acoustic resonator (AR), signal tube (ST), microphone base (MB), and microphone (m). The section of the PA cell within the area defined by broken line in Fig. 1 is placed in the oven which can be heated up to 900 °C. The buffer rings and the spacer, which constitute the buffer volumes, are pointed out with lighter and darker shades of gray, respectively.

made from electrically isolating polymer. The acoustic background, originating from the gas inlet/outlet as well as due to the absorption radiation in to the windows, were isolated from the acoustic resonator by placing four acoustic buffers at each side of the resonator. The acoustic buffers consist of rings having a length, an inner diameter, and an outer diameter of 14.2, 50, and 56 mm, respectively. The rings were separated by 2-mm-thick spacers each provided with a central hole 6 mm in diameter. Similar spacers were also used between the resonator and the adjacent buffer volume rings. The rings and the spacers were tightened together inside the buffer holder tubes, whose inner diameter is 56 mm and length is 65 mm, that, on their turn, were connected to the acoustic resonator and to the extension tubes. The hermeticism of each joint was ensured with a copper gasket. The windows are kept 160 mm away from the oven to prevent the vapor condensing on their surfaces. They were connected to the extension tubes by means of copper gaskets on each side and by tightening them between metal flanges and the extension tubes.

The schematic diagram of the setup used for the PA measurements is shown in Fig. 2. The PA pulses were generated using a wavelength tunable (210–2300 nm) solid state OPO laser (NT342/1/UVE, Ekspla Ltd.). This laser produces 5-ns-long pulses at a repetition rate of 10 Hz. Depending on the wavelength of the specific emission line of the laser, the output energy in the UV region of a single pulse varied between 1 and 4 mJ. The cross sectional profiles of pulses varied from a pulse to pulse and their divergence was shown

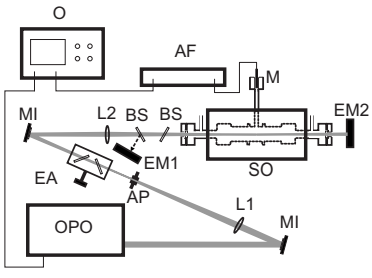

FIG. 2. Schematic representation of the experimental setup: tunable solid-state laser (OPO), mirror (MI), aperture (AP), variable high-energy attenuator (EA), lens (L1 & L2), beamsplitter (BS), energy meter (EM1 & EM2), sublimation oven (SO), programmable amplifier (AF), and oscilloscope (o). The gray line describes the path and the focusing of the laser pulses and the broken line the position of the PA cell inside the oven.

to be wavelength dependent. The cross sectional profile of the pulses was combined by focusing them with lens L1 (f=+750 mm) through a 1.5-mm-aperture AP. The average pulse energy was restricted using a high-energy variable attenuator EA (935–5-OPT, Newport Co.). After passing the attenuator, laser pulses were refocused with lens L2 (f=+500 mm) in such a way that the radiation pulses traverse the cell without interacting with the inner walls of the PA cell. At the site of the PA resonator, the cross section of the pulse was less than 1 mm^2. The energy of the pulse was monitored ahead and behind the PA cell with energy meters EM1 (PD10, Ophir Optronics Ltd.) and EM2 (PE9, Ophir Optronics Ltd.), respectively. The optical alignment was adjusted to fulfill the following requirements: (i) minimal acoustic background caused by laser pulse interaction with the PA cell, (ii) minimal excitation of the azimuthal and combination modes, (iii) uniform cross-sectional profiles of the laser pulses, and (iv) maximal energy throughput behind the PA cell.

The signal detected by the microphone was first preamplified (preamplifier 2670, Brüel & Kjær) and then amplified and filtered using the SR650 programmable amplifier from Stanford Research System Inc. Typical settings for amplification factor and a pass band were 80 dB and 5–99.9 kHz, respectively. The amplified and filtered signals were averaged and recorded with an oscilloscope (Waverunner6100A, LeCroy Co.) triggered by the Q-switch synchronized TTL output of the OPO laser. The time window of the oscilloscope was set to 20 ms, begun at 1.2 ms after the triggering in order to eliminate the electrical disturbances caused by the Q-switch of the laser.

Suprapur (99.999%) KCl from Merck KGaA was chosen to demonstrate the feasibility of the resonant PA cell for studies at high temperature. This compound has dissociative electron transitions at wavelengths shorter than 280 nm. The first absorption band with a maximum at 246 nm consists of two dissociative transitions corresponding to the dissociation to neutral atoms, and neutral potassium atom and chlorine atom excited to its first excitation level. The peak at 193 nm associated with the third electronic transition of KCl results from the dissociation of molecule and the excitation of the potassium atom.[17] The PA signal from the KCl molecules is induced because of an increased number of the particles as well as due to the kinetic energy of the fragments.[18] The KCl powder was deposited at both ends of the acoustic resonator. As the temperature of the PA cell increased, the vapor pressure of the sample rises. The concentration of the sample was calculated using the commercial thermochemical database (HSC 5.1, Outokumpu Research Oy) based on the known relationship between the vapor pressure and the temperature. Since the PA cell is actually an isolated system, it was assumed that the sample's concentration is that of the saturated vapor pressure. The temperature of the sublimation oven was actively controlled by PID temperature controller (Eurotherm), while the temperature of the cell was monitored with a K type thermocouple and a thermocouple monitor (SR630, Stanford Research Systems). During the heating process, the PA cell was continuously flushed with a nitrogen; the flow rate was 1.5 l/min. The nitrogen flow was stopped when a

desired temperature of the PA cell was reached. The 20 min long interval was allowed for the concentration of KCl to stabilize; the actual measurement was initiated once this equilibrium has been achieved. The distribution of the KCl vapor could be assumed uniform during the actual measurement, since the longitudinal modes, excited due to the spatial variations of concentration, were vanished from the PA signal during the 20 min interval.

III. SIGNAL PROCESSING

The resonant properties of the PA cell are susceptible to alterations of ambient conditions. The temperature and pressure changes affect the resonant frequency. Furthermore, modifications of resonator wall's acoustic reflection properties influence the quality (Q) factors of the resonator. Thereby, a signal processing technique that takes into account variations of frequencies and Q factors is needed to enable the comparison of the PA signals detected at different temperatures.

In finding the appropriate signal processing method, the dynamics of the acoustic resonator has been considered. The sound pressure at a position $\mathbf{r}$ (m) at the time t (s) is given by the wave equation

$$\frac{\partial^2 p(\mathbf{r},t)}{\partial t^2} - c_s^2 \nabla^2 p(\mathbf{r},t) = (\gamma - 1)\frac{\partial H(\mathbf{r},t)}{\partial t}, \tag{1}$$

where c_s (m/s), γ, and H (W/m^3) are the sound velocity, the adiabatic constant of the buffer gas, and the heat power density, respectively. The solutions to this homogenous wave equation in single pulse excitation are

$$p(\mathbf{r},t) = \sum_{j=1}^{k} p_j(\mathbf{r}) A_j e^{i(\Omega_j t + \phi_j)}, \tag{2}$$

where A_j (Pa) and ϕ_j (rad) are the amplitude and the phase of the jth mode, respectively. The complex frequency of the jth eigenmode is expressed as $\Omega_j = \omega_j + i g_j$, where ω_j (Hz) and g_j (Hz) are the angular frequency and the damping factor of the jth mode, respectively. $p_j(\mathbf{r})$ is the dimensionless spatial distribution of the jth eigenmode.[2,19]

Single pulse excitation induces an acoustic impulse propagating cylindrically away from the optical path. Short acoustic pulse has a broad frequency spectrum and excites several resonator's eigenmodes simultaneously. In a cylindrical resonator, the frequencies f (Hz) of the eigenmodes are given by

$$f_{nml} = \frac{c_s}{2}\sqrt{\left(\frac{\alpha_{nm}}{R}\right)^2 + \left(\frac{l}{L}\right)^2}, \tag{3}$$

where n, m, and l are the integers expressing the orders of the radial, azimuthal, and longitudinal modes, respectively. R (m) and L (m) are the radius and the length of the resonator. α_{nm} is the nth zero of the derivative of the mth order Bessel function divided by π. Assuming the propagation of the laser pulse along the cylinder axis of the resonator, the azimuthal modes are precluded, leaving the radial modes to be the only excited transverse modes. Following the excitation, the modes oscillate independently and decay due to the cell losses.[2] The amplitudes of the excited modes at excitation time are given by

$$A_j = \frac{(\gamma - 1) L F_j p_j(\mathbf{r})}{V} \beta E_L, \tag{4}$$

where V (m^3), F_j, β (1/m), and E_L (J) are the volume of the resonator, the normalized overlap integral of the jth eigenmode, the PA absorption coefficient of the sample, and the energy of the laser pulse, respectively. The overlap integral describes how efficient is the excitation of the jth mode, or in the words, the extent of the overlap between the spatial distribution of the jth eigenmode $p_j(\mathbf{r})$ and the spatial distribution of the laser pulse.[2,19]

From Eq. (4), it is seen that the amplitudes of the eigenmodes are independent of the frequencies and Q factors of the eigenmodes. Thereby, the amplitudes of the eigenmodes are comparable quantities at different conditions. Let us next consider the amplitude of the first radial mode A_1. Since only the real pressure amplitudes can be measured, the imaginary part of the pressure is ignored and the pressure oscillation is written as

$$p_1 = A_1 \cos(\omega_1 t + \phi_1) e^{-g_1 t} = \frac{1}{2} A_1 (e^{i(\omega_1 t + \phi_1)} + e^{-i(\omega_1 t + \phi_1)}) e^{-g_1 t}. \tag{5}$$

Due to the intrinsic symmetry, only the positive side of the frequency spectrum has been used. The Fourier transform of the positive side of Eq. (5) is

$$P_1(\omega) = \frac{1}{2} A_1 \int_0^{T_0} e^{i(\omega_1 t + \phi_1) - g_1 t} e^{-i\omega t} dt = \frac{A_1 e^{i\phi_1}}{-2(g_1 + i(\omega - \omega_1))} (e^{[-g_1 + i(\omega_1 - \omega)]T_0} - 1). \tag{6}$$

Furthermore, in a time window T_0, the exponential term for a damped oscillation approaches zero and the magnitude of P_1 (Pa/Hz) at $\omega = \omega_1$ can be approximated by

$$|P_1(\omega_1)| = \frac{A_1}{2 g_1} = \frac{A_1}{\Delta \omega_1}, \tag{7}$$

where $\Delta \omega_1 = 2 g_1$ is the full width at half maximum value of the power spectrum of the resonance mode of interest. When the Q factors of the resonator are high, they are defined as $Q_j = \omega_j / \Delta \omega_j$. Thereby, by applying Eq. (7) to the signal processing, the effect of the Q factors on the intensity of the signal is normalized.

IV. RESULTS AND DISCUSSION

The proposed method was applied to study the PA response of the saturated KCl vapor at different operating temperatures. All measurements were performed at the atmospheric pressure. An example of PA signal, measured at 691 °C, is shown in Fig. 3. The plotted signal represents an average of 200 consecutive signals excited at 245 nm using an average pulse energy of 100 μJ. The temporal signals begin to oscillate as the first wavefront reaches the microphone at the end of the signal tube. The time delay between the acoustic excitation and the first obtained wavefront is

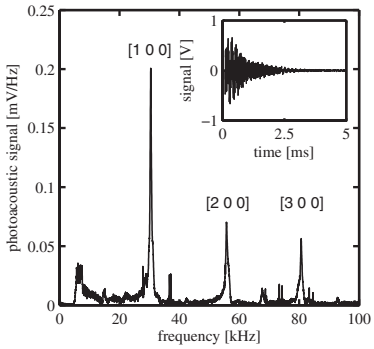

FIG. 3. Typical PA signal in the time and the frequency domains. The three lowest radial modes are marked in the frequency spectrum with expression [n m l].

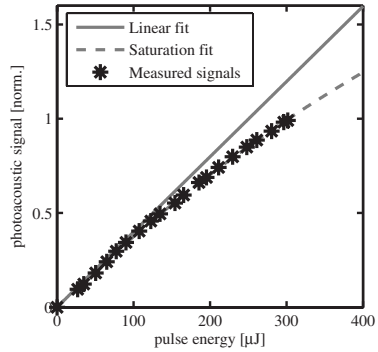

FIG. 5. The strength of the normalized PA signal plotted as a function of the average pulse energy. The PA signal from KCl saturates when pulse energies exceeding 130 μJ.

approximately 1.2 ms. Following the first detected wavefront, the PA signal decreases due to the cell losses. In the frequency domain, the signal consists of sharp peaks centered at frequencies of the radial modes of the cell. Measured Q-values for the first three radial modes were 100, 150, and 150. The Q-value of 270 was obtained for the first radial mode at a room temperature after the polishing of the resonator. The deviation in the strength of the PA signal at different heating occasion with similar parameters is less than four percent. In Fig. 4, the PA response of the KCl vapor is displayed as a function of the excitation wavelength. The spectrum was recorded at 691 °C when the corresponding equilibrium concentration was 50 ppm. The average pulse energies varied between 80 and 120 μJ depending on the excitation wavelength. The values along the vertical axis were calculated using Eq. (7). Furthermore, the calculated values were normalized to the average pulse energy, the amplification factor (80 dB), and the sensitivity of the microphone (4.13 mV/Pa). The measured PA spectrum is in good agreement with the absorption spectra of KCl found in Refs. 17 and 20. OPO laser was a necessary tool to determine the PA spectrum of the KCl vapor for the first time. However,

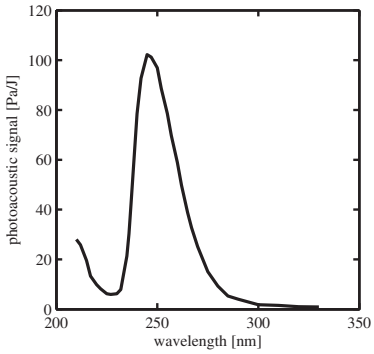

FIG. 4. The PA spectrum of KCl at 690 °C. The absorption band between wavelengths of 235 and 280 nm consists of two dissociative electron transitions, which are irresolvable at high temperatures. The absorption at shorter wavelengths results from the third electron transition of the KCl molecule.

other lasers emitting single wavelength, such as excimer laser KrF emitting 248 nm, Nd:YAG lasers emitting crystals 4th harmonic corresponding to 266 nm, and flash lamps used with proper filter are also applicable to the sensitive detection of KCl.

The relation between the PA signal and the average excitation energy is shown in Fig. 5. The saturation curve was measured at 245 nm excitation wavelength at 691 °C. The obtained relationship between the PA signal and the average excitation energy at the energies lower than 130 μJ is linear, as it was assumed in Eq. (4). However, at high energies, the PA signal begins to saturate. At 300 μJ, the departure from the linearity is approximately 18%. The strength of the PA signal is in good agreement with the saturation equation $\mathrm{PA}_{\mathrm{signal}}=a[1-\exp(-bE_L)]$, with $a=3.09\pm0.33$ and $b=0.0013\pm0.0002\ 1/\mu\mathrm{J}$. The uncertainties corresponds to 95% confidence bounds of the fitting. The saturation equation was derived from a standard rate equation for the two level system[21] assuming: (i) that the dissociation time is very short and (ii) the recombination time of the fragments is much longer than the laser pulse duration. Under such assumptions, the effects of the stimulated and spontaneous emissions from the upper state can be ignored. The linear fit was calculated from the first term of the Taylor expansion of the saturation equation.

The sensitivity and the dynamic range of the PA cell are illustrated in Fig. 6. The PA signals were measured at 245 nm using 300 μJ average pulse energy in the temperature range between 410 and 691 °C, which corresponds to 1 ppb–50 ppm equilibrium concentrations of KCl. The temperature interval were chosen to produce measurable concentrations, in which the absorption of light is less than 10% through the PA cell. The values along the vertical axis are calculated by averaging 1000 consecutive PA signals and then using Eq. (7). The detection limit, determined from a noise signal measured at 23 °C, when the laser radiation was blocked, is independent of wavelength and temperature.

Measured noise signal was transformed into frequency domain and standard deviation of frequency amplitudes near 27.1 kHz was calculated. The latter value is the frequency of the first radial mode at 470 °C at which the equilibrium KCl

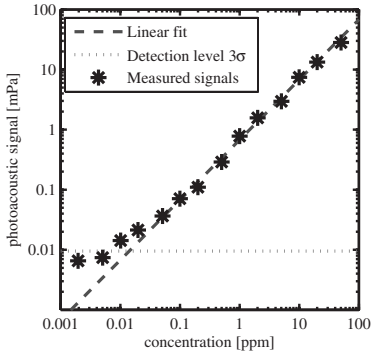

FIG. 6. The PA signal obtained from the saturated KCl vapor for different concentrations. The extrapolated detection limit is 15 ppb.

concentration is 20 ppb. Finally, standard deviation data was multiplied by factor of three. Because measured signals have been multiplied by $\Delta\omega$, according to Eq. (7), the detection limit must also be scaled with this factor. Therefore, the detection level was multiplied by $\Delta\omega$ measured at 470 °C.

Experimental data in Fig. 6 exhibits a good linearity with concentration even though the Q factor is varying from 100–140. The lowest detectable KCl concentration determined as the intersection of the 3σ noise level and the linear plot is 15 ppb. The slope between concentration and signal was 0.68 ± 0.03 mPa/ppm and the correlation factor 0.997. The sensitivity achieved here with the PA cell, in witch the absorption length is 8.5 cm, is two orders of magnitude better than that reported for direct absorption method with 5 m absorption length.[16] Excellent sensitivity combined with the short absorption length and broad dynamic range covering more than three orders of magnitudes justifies the continuation of the research efforts toward a practical PA based instrument capable of field measurements.

V. CONCLUSIONS

The resonant PA cell for high temperature gas measurements was proposed and its feasibility was demonstrated. Several radial modes of the PA cell were excited simultaneously using a pulsed laser. The PA signals were processed using a novel method that minimizes the effect of changes in Q factor. The KCl vapor was studied successfully at temperatures between 410 and 691 °C at which the equilibrium concentration of this gas varies from 1 ppb to 50 ppm. The plot of the processed signals is linear with respect to the concentration of the KCl vapor; the detection limit is 15 ppb. By proper selection of wavelengths and cell temperatures, the method is readily applicable to high temperature analysis of other gases as well.

ACKNOWLEDGMENTS

The research was supported by ChemCom, a mainly Tekes financed project coordinated by the Process Chemistry Centre at Åbo Akademi University. Other ChemCom funders are Andritz Oy, Foster Wheeler Energia Oy, International Paper Inc., Metso Power Oy, Oy Metsä-Botnia Ab, Clyde Bergemann GmbH, and UPM-Kymmene Oyj. Likewise, the authors acknowledge Graduate School of Modern Optics and Photonics, and Finnish Academy of Science and Letters.

[1] P. L. Meyer and M. W. Sigrist, Rev. Sci. Instrum. **61**, 1779 (1990).
[2] A. Miklós and P. Hess, Rev. Sci. Instrum. **72**, 1937 (2001).
[3] A. Rosencwaig, *Photoacoustics and Photoacoustic Spectroscopy* (Robert E. Krieger Publishing Company Inc., Malabar, Florida, 1990).
[4] I. G. Calasso and M. W. Sigrist, Rev. Sci. Instrum. **70**, 4569 (1999).
[5] M. A. Gondal and J. Mastromarino, Appl. Opt. **40**, 2010 (2001).
[6] A. A. Kosterev, Y. A. Bakhirkin, R. F. Curl, and F. K. Tittel, Opt. Lett. **27**, 1902 (2002).
[7] J. Kauppinen, K. Wilcken, I. Kauppinen, and V. Koskinen, Microchem. J. **76**, 151 (2004).
[8] T. Laurila, H. Cattaneo, V. Koskinen, J. Kauppinen, and R. Hernberg, Opt. Express **13**, 2453 (2005).
[9] J. Saarela, J. Toivonen, A. Manninen, T. Sorvajärvi, and R. Hernberg, Appl. Opt. **48**, 743 (2009).
[10] J. Hodgkinson, M. Johnson, and J. P. Dakin, J. Appl. Phys. **98**, 084908 (2005).
[11] A. Manninen, J. Sand, J. Saarela, T. Sorvajärvi, J. Toivonen, and R. Hernberg, Opt. Express **17**, 16994 (2009).
[12] H. Jalink and D. Bicanic, Appl. Phys. Lett. **55**, 1507 (1989).
[13] D. Bicanic, M. Chirtoc, M. Lubbers, and H. Jalink, Meas. Sci. Technol. **4**, 1016 (1993).
[14] J. Stenberg, R. Hernberg, and J. Vattulainen, Appl. Opt. **34**, 8400 (1995).
[15] H. A. Beck, Z. Bozóki, and R. Niessner, Anal. Chem. **72**, 2171 (2000).
[16] P. Henderson, P. Szakálos, R. Pettersson, C. Andersson, and J. Högberg, Mater. Corros. **57**, 128 (2006).
[17] P. Davidovits and D. C. Brodhead, J. Chem. Phys. **46**, 2968 (1967).
[18] G. J. Diebold, *Photoacoustic, Photothermal and Photochemical Processes in Gases* (Springer, Berlin, 1989).
[19] S. Schäfer, A. Miklós, and P. Hess, Appl. Opt. **36**, 3202 (1997).
[20] G. Daminelli, D. A. Katskov, R. M. Mofolo, and P. Tittarelli, Spectrochim. Acta, Part B **54**, 669 (1999).
[21] O. Svelto, *Principle of Lasers* (Springer, New York, 1998).

Paper 2

Tapio Sorvajärvi, Jaakko Saarela, and Juha Toivonen

Optical detection of potassium chloride vapor using collinear photofragmentation and atomic absorption spectroscopy.

Optics Letters **37**, 4011–4013 (2012)
doi: 10.1364/OL.37.004011

Optical detection of potassium chloride vapor using collinear photofragmentation and atomic absorption spectroscopy

Tapio Sorvajärvi,* Jaakko Saarela, and Juha Toivonen

Optics Laboratory, Department of Physics, Tampere University of Technology, P.O. Box 692, FI-33101 Tampere, Finland
**Corresponding author: tapio.sorvajarvi@tut.fi*

Received July 9, 2012; accepted August 15, 2012;
posted August 22, 2012 (Doc. ID 172031); published September 20, 2012

A sensitive and selective optical technique to detect potassium chloride (KCl) vapor is introduced. The technique is based on the photofragmentation of KCl molecules, using a pulsed UV laser, and optical probing of the temporarily increased amount of potassium atoms with a near-infrared laser. The two laser beams are aligned to go through the sample volume along the same optical path. The performance of the technique is demonstrated by detecting KCl concentrations from 25 ppb to 30 ppm in a temperature-controlled cell. © 2012 Optical Society of America

OCIS codes: 120.1740, 350.5130, 300.6210.

Environmental aspects and the increasing price of fossil fuels has increased the interest in renewable fuels for power production. One good alternative, as a largely CO_2 neutral fuel, is biomass that can be harvested, for example, as residues of the forest industry. However, the combustion of the biomass causes serious corrosion and slagging problems in combustion boilers. One cause of the problems are alkali chloride vapors, which are formed during combustion due to the high content of alkalis and chlorine in the biomass [1]. In order to study the alkali chloride vapor-related problems and monitor their concentration in process gases, a reliable monitoring technique is needed.

The benefits of the optical techniques in gas sensing are typically their sensitivity, selectivity, and capability of measuring gas components in situ, i.e., detection without sampling [2]. The optical measurements of the alkali chlorides are based on their dissociative electronic transition at wavelengths shorter than 300 nm [3]. During the past few decades, two different optical in situ techniques have been proposed for detection of alkali chlorides: excimer laser induced fluorescence (ELIF) [4] and differential optical absorption spectroscopy (DOAS) [5]. In the ELIF technique, alkali chloride molecules are dissociated using 193 nm light to excited alkali atoms and chlorine atoms. As the excited alkali atoms relax back to their ground states, they emit photons at alkali-specific wavelength. The ELIF technique enables the detection of alkali chlorides at the parts per billion (ppb) level but has limitations in penetration depth to the sample due to the strong absorption of 193 nm light by the combustion gases. The DOAS technique measures the whole UV absorption spectrum of the sample that is then compared to spectral shapes of the alkali chlorides to resolve the total content of the alkali chlorides (NaCl + KCl). It enables the analysis of large measurement volumes but has limited dynamic range and requires several-meter sample lengths to be capable of detecting alkali chloride concentrations on the order of parts per million (ppm).

In this Letter, we present a sensitive and selective optical technique for the detection of potassium chloride (KCl) vapor. The technique is based on the photofragmentation of the KCl molecules using a UV pulse and the detection of the released potassium (K) atoms with a narrow-linewidth continuous-wave probe laser. The wavelength of the probe laser, i.e., probe wavelength, is tuned to correspond the electron transition of the K atom. The two laser beams are aligned collinearly on the same optical path through the sample volume. Therefore, the probe laser is capable of detecting the udden increase of the K atoms right after the UV pulse has propagated through the sample volume. A similar technique has previously been used to study the recombination rate of the dissociated metal salts [6,7]. In the previous studies, the dissociation was induced with a flash lamp or a pump laser and the probing was achieved using a hollow cathode lamp or a resonance lamp. In this Letter, the two collinear light beams are utilized for the first time to measure the concentration of the metal salt through the whole sample volume.

The technique was demonstrated using the experimental setup shown in Fig. 1. The photofragmentation was induced with a pulsed UV laser (NT342/1/UVE, Ekspla), emitting 5 ns long pulses with 10 Hz repetition rate at wavelength of 245 nm. The absorption of the KCl molecules at 245 nm dissociates the molecules to ground-state potassium ($4^2S_{1/2}$) atoms and chlorine atoms that settle either on their ground state ($3P_{3/2}$) or the first excited state ($3P_{1/2}$) [3]. The energy of the UV pulses was monitored before and after the sample volume using energy

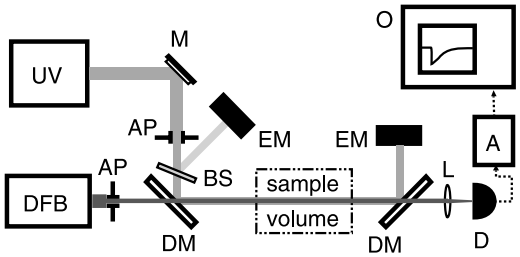

Fig. 1. Experimental setup for real-time detection of vaporous potassium chloride: ultraviolet laser, UV; probe laser, DFB; mirror, M; aperture, AP; beam splitter, BS; dichroic mirror, DM; energy meter, EM; lens, L; detector, D; amplifier, A; oscilloscope, O.

0146-9592/12/194011-03$15.00/0

sensors (PD10 & PE9, Ophir). The wavelength of the probe laser (LD-0767-0015-DFB-1, Toptica) was tunable around potassium absorption near 766.5 nm, corresponding to the $4^2S_{1/2} - 4^2P_{3/2}$ transition. The probe wavelength was monitored by means of a wavemeter (WA-1500-NIR, EXFO Burleigh) having an accuracy of 0.1 pm. The UV and the probe laser beams were combined and separated using dichroic mirrors (FF310-Di01, Semrock). The diameters of the UV and the probe laser beams were limited to 5 mm and 2.5 mm, respectively. After passing the sample volume, the probe laser beam was detected using a silicon photodiode (DET-210, Thorlabs). The signal from the photodiode was amplified with a factor of 25 using an amplifier (SR445, Stanford Research Systems) and recorded with an oscilloscope (WaveRunner6000A, LeCroy).

The KCl vapor was produced by sublimating KCl powder (99.999%, Merck) in the 85 mm long middle part of the high temperature cell that has previously been used for photoacoutic detection of KCl [8]. The buffer gas in the cell was air and its pressure was kept at atmospheric pressure in all measurements. The concentration of the KCl vapor was calculated using a commercial thermochemical database HSC 5.1 (Outokumpu Research). Due to the open ends of the middle section of the cell, KCl vapor diffused also to the other parts of the cell. Therefore, an effective sample length for KCl vapor was determined using the direct UV absorption. At the temperature of 630 °C, corresponding to equilibrium KCl concentration of 30 ppm, the absorption of 245 nm light through the cell was 7.5%. By applying the Beer–Lambert law to the measured absorption and using $2.0 * 10^{-21}$ m^2 absorption cross section for KCl [3], the effective sample length was determined to be 170 mm.

Two measured transmission curves of the probe laser in the vicinity of the UV excitation are presented in Fig. 2. The curves are averages of 100 individual measurement events whose bandwidths were limited to a frequency range of 0–20 MHz in order to eliminate the high-frequency electrical interference caused by the electro-optic Q-switch of the UV laser. The measurements were performed using an average UV pulse energy of 58 μJ and the cell temperature of 590 °C that corresponds to an equilibrium KCl concentration of 2 ppm.

The lower curve in Fig. 2 shows a typical behavior of the probe laser transmission when the probe wavelength is tuned to the absorption maximum of the K atoms released in photofragmentation. At the beginning of the curve, the transmission is at a constant level I_0. The UV excitation takes place at $t = 0$, when a small part of the KCl molecules is dissociated and the amount of the atomic K is increased. The fast increase in K atom concentration is seen as a sharp dip in the transmission curve. The K atom concentration achieves its maximum right after the UV pulse has passed the sample and starts to relax back to the thermal equilibrium. The relaxation of the vapor is observed as the recovery of the transmission intensity back to the original I_0 level. Applying Beer–Lambert law and assuming an exponential decay for the induced K atoms, the observed temporal transmission intensity $I(t)$ can be described as

$$I(t) = \begin{cases} I_0 & t < 0 \\ I_0 \exp(-\alpha L_{\max} e^{(-t/\tau)}) & t \geq 0 \end{cases}, \quad (1)$$

where $\alpha L_{\max}$ and τ are the maximum absorbance of the released K atoms at $t = 0$ and a time constant for the decay process, respectively. According to the Beer–Lambert law, the $\alpha L_{\max}$ is directly proportional to the increased amount of the K atoms that in turn is proportional to the dissociating UV intensity and the KCl concentration. The short timescale of the observed dip enables accurate measurements also in fluctuating samples.

The technique is sensitive to the probe wavelength. The upper curve in Fig. 2 shows how the dip is almost

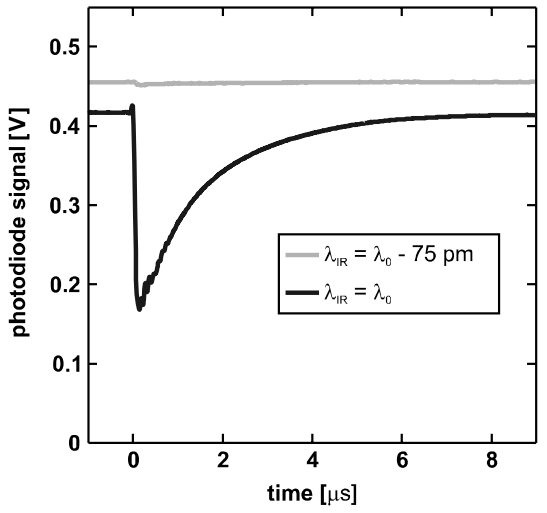

Fig. 2. Two transmission curves of the probe laser with different probe wavelength through sample vapor having KCl concentration of 2 ppm. The UV excitation takes place at $t = 0$.

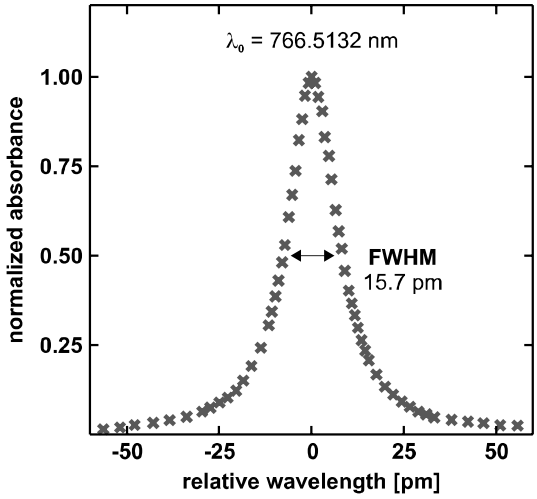

Fig. 3. Normalized maximum absorbance of the probe laser right after the UV excitation with respect to its wavelength around 766.5132 nm. The FWHM of the peak was measured to be 15.7 pm.

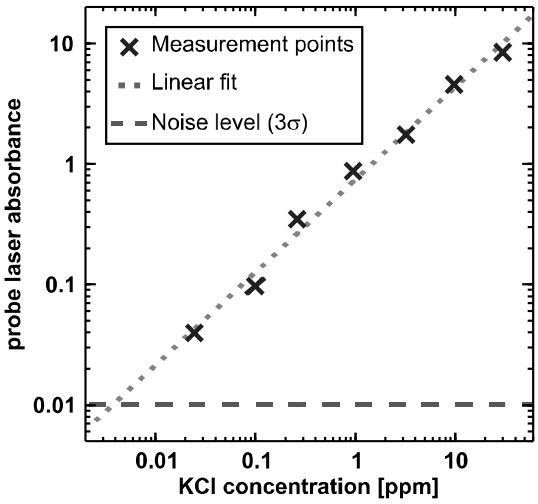

Fig. 4. Maximum absorbance of probe laser beam as a function of KCl concentration. 3σ detection limit was determined to be 4 ppb with 170 mm sample length.

disappeared from the transmission curve when the wavelength is tuned 75 pm off from the absorption maximum of the K atoms released in photofragmentation. The normalized $\alpha L_{\max}$ value is presented as a function of probe wavelength near the K atom absorption maximum in Fig. 3. The maximum of the $\alpha L_{\max}$ spectrum is at 766.5132 nm and the FWHM of the observed lineshape is 15.7 pm. The other possible effects causing temporal change in the transmission intensity of the probe laser, e.g., thermal lensing, are not observed. The shape and the center wavelength of the measured spectrum verify that the observed dip in the transmission curve originates from the absorption of the K atoms released in photofragmentation. The technique detects selectively molecules that are releasing K atom(s) due to the photofragmentation at the selected UV wavelength.

Figure 4 shows $\alpha L_{\max}$ as a function of the KCl concentration that was varied in the range of 25 ppb–30 ppm. In this set of measurements, the average UV pulse energy was increased to 150 μJ. Thereby, a higher amount of KCl molecules were dissociated and a better sensitivity was achieved. The detection limit for $\alpha L_{\max}$ was determined as $-\ln(3\sigma/I_0)$, where σ is the standard deviation of the unfiltered photodiode signal before the UV excitation. This corresponds to a detection limit of 4 ppb for the KCl vapor. The UV absorbance was less than 0.1 in all the measurements, which allows us to assume a uniform dissociation efficiency throughout the sample.

In conclusion, a sensitive and selective optical technique for detection of KCl vapor has been presented. The dynamics of the measured curves were studied and the observed dip was verified to origin from the absorption of the potassium atoms released in photofragmentation. The detection limit of the technique was determined to be 4 ppb with 170 mm sample length. Moreover, the dynamic range of three orders of magnitude was demonstrated. The results are encouraging for combustion research applications.

This work has been carried out within the project ChemCom 2.0 as part of activities of the Tampere University of Technology. Funding by the National Technology Agency of Finland and industrial partners Andritz Oy, Metso Power Oy, Oy Metsä-Botnia Ab, Foster Wheeler Energia Oy, UPM-Kymmene Oyj, Clyde Bergemann GmbH, and International Paper, Inc. is gratefully acknowledged.

References

1. H. Nielsen, F. Frandsen, K. Dam-Johansen, and L. Baxter, Progr. Energy Combust. Sci. **26**, 283 (2000).
2. P. Monkhouse, Progr. Energy Combust. Sci. **37**, 125 (2011).
3. P. Davidovits and D. C. Brodhead, J. Chem. Phys. **46**, 2968 (1967).
4. R. Oldenborg and S. Baughcum, Anal. Chem. **58**, 1430 (1986).
5. C. Forsberg, M. Broström, R. Backman, E. Edvardsson, S. Badiei, M. Berg, and H. Kassman, Rev. Sci. Instrum. **80**, 023104 (2009).
6. S. Edelstein and P. Davidovits, J. Chem. Phys. **55**, 5164 (1971).
7. D. Ehrlich and R. Osgood, Jr., IEEE J. Quantum Electron. **16**, 257 (1980).
8. T. Sorvajärvi, A. Manninen, J. Toivonen, J. Saarela, and R. Hernberg, Rev. Sci. Instrum. **80**, 123103 (2009).

Paper 3

Tapio Sorvajärvi, and Juha Toivonen.

Principles and calibration of collinear photofragmentation and atomic absorption spectroscopy.

Applied Physics B
Accepted for Publication Sep. 2013
available online
doi: 10.1007/s00340-013-5633-9
Open access

Appl. Phys. B
DOI 10.1007/s00340-013-5633-9

Applied Physics B
Lasers and Optics

Principles and calibration of collinear photofragmentation and atomic absorption spectroscopy

Tapio Sorvajärvi · Juha Toivonen

Received: 17 May 2013 / Accepted: 27 August 2013

Abstract The kinetics of signal formation in collinear photofragmentation and atomic absorption spectroscopy (CPFAAS) are discussed, and theoretical equations describing the relation between the concentration of the target molecule and the detected atomic absorption in case of pure and impure samples are derived. The validity of the equation for pure samples is studied experimentally by comparing measured target molecule concentrations to concentrations determined using two other independent techniques. Our study shows that CPFAAS is capable of measuring target molecule concentrations from parts per billion (ppb) to hundreds of parts per million (ppm) in microsecond timescale. Moreover, the possibility to extend the dynamic range to cover eight orders of magnitude with a proper selection of fragmentation light source is discussed. The maximum deviation between the CPFAAS technique and a reference measurement technique is found to be less than 5 %. In this study, potassium chloride vapor and atomic potassium are used as a target molecule and a probed atom, respectively.

1 Introduction

Photofragmentation and fragment detection (PF/FD) techniques improve selectivity and sensitivity in gas sensing [1]. They are based on the fragmentation of the detected molecule and the sensing of the released fragment. Molecule [2], atom [3], and ion [4] fragments have been used in sensing the target molecules. Fragments are detected utilizing their emission [5–7] or absorption [8, 9] properties.

Recently, a technique called collinear photofragmentation and atomic absorption spectroscopy (CPFAAS) was demonstrated in the detection of alkali chloride vapors [10]. The technique utilizes a UV laser pulse to dissociate alkali chloride molecules to alkali and chlorine atoms, and a narrow bandwidth laser diode to monitor the concentration of the alkali atom. The collinear alignment of the two beams through the sample volume enables the detection of temporally increased alkali atom concentration within the volume determined by the UV beam. The large absorption cross-sections and the narrow absorption profiles of the alkali atoms favor their detection, also when interfering fragments, such as O_2, exist.

In this paper, a theoretical approach for signal formation in CPFAAS is discussed, and relations between detected fragment atom absorption and target molecule concentration in different conditions are derived. The theoretically derived relation for pure sample is validated by comparing KCl vapor concentrations measured with the CPFAAS technique to concentrations determined with two other independent reference techniques. The linearity of the CPFAAS technique with respect to the target molecule concentration and the absolute limits of the CPFAAS detection at low and high concentration ends are also discussed.

2 Theoretical approach

CPFAAS is based on the fragmentation of a fraction of the target molecules with a light pulse and the detection of the released fragments within the gas volume drawn by the pulse with a collinearly aligned continuous wave probe

T. Sorvajärvi (✉) · J. Toivonen
Optics Laboratory, Department of Physics, Tampere University of Technology, P.O. Box 692, 33101 Tampere, Finland
e-mail: tapio.sorvajarvi@tut.fi

Published online: 15 September 2013

beam. The probe beam consists of monochromatic light, whose wavelength is preselected to correspond to the absorption line of the probed atom fragment. The transmission of the probe beam is monitored continuously in the vicinity of the fragmentation, which enables the determination of the transmission base level I_0 at $t < 0$, the fragmentation-induced increased absorption at $t = 0$, and the recovery of the gas sample back to the thermal equilibrium at $t > 0$. Applying the Beer–Lambert law to describe the transmission of the probe beam and assuming an exponential decrease for the concentration of the produced fragments at $t > 0$, the transmission intensity I of the probe beam can be expressed as:

$$I(t) = \begin{cases} I_0 + C & t < 0 \\ I_0 \exp\left(-\alpha L_{\max} e^{(-t/\tau)}\right) + C & t \geq 0 \end{cases}, \quad (1)$$

where $\alpha\ L_{\max}$ and τ are the maximum absorbance due to the fragment atoms at $t = 0$ and a time constant for the decay process, respectively. The offset parameter C is added to describe the fraction of the probing light that passes the sample without interacting with the fragments due to the misalignment of the beams or the spectral impurity of the probe beam.

The dependence of the detected quantity $\alpha\ L_{\max}$ on a definable quantity target molecule concentration X_{KCl} can be studied by eliminating C and assuming that the recovery of the fragments is negligible during the excitation time, e.g., relaxation time is much longer than the excitation pulse, when the transmission intensity at $t = 0$ can be written as

$$I(t = 0) = I_0 \exp(-\alpha L_{\max}) = \exp\left(-\frac{N_K}{V_f}\sigma_K L\right), \quad (2)$$

where N_K, V_f, σ_K and L are the total number of produced fragment atoms, a volume in which the fragmentation has occurred, the absorption cross-section of the fragment atoms at the probe wavelength and sample length, respectively. N_K is directly proportional to the number of the absorbed fragmentation photons by the target molecules and can be rewritten as a relation between absorbed energy by target molecule $E^{\mathrm{abs}}_{\mathrm{KCl}}$ and the energy of a single fragmentation photon $E_{\mathrm{photon}} = hc/\lambda_f$ multiplied with the photofragmentation efficiency γ at the fragmentation wavelength

$$N_K = \gamma \frac{E^{abs}_{KCl}}{\frac{hc}{\lambda_f}} \quad (3)$$

where h, c and λ_f are Planck's constant, speed of light, and the wavelength of the fragmenting pulse, respectively. The photofragmentation efficiency depends on the target molecule and the fragmentation wavelength. For example, the photofragmentation of NO_2 produces O atoms with fragmentation efficiency of $0 \leq \gamma \leq 1$ in the vicinity of 400 nm [11], and the fragmentation of $SeBr_2$ produces Br atoms with $\gamma = 2$ in the vicinity of 350 nm [12]. Alkali chlorides are known to have $\gamma = 1$ for production of ground state alkali atoms in the vicinity of 250 nm [13].

On the other hand, total fragmentation energy absorbed by a sample is a sum of energy absorbed by the target molecule and energy lost due to other extinction mechanisms E^{ext}

$$E^{abs}_{\mathrm{KCl}} + E^{\mathrm{ext}} = E_{\mathrm{in}} - E_{\mathrm{out}}, \quad (4)$$

where E_{in} and E_{out} are the energy of the fragmentation pulse at the input and at the output of the sample, respectively. By solving $E^{\mathrm{abs}}_{\mathrm{KCl}}$ out from Eq. 3, N_K out from Eq. 2 and dividing both sides in Eq. 4 with $E_{\mathrm{in}} - E_{\mathrm{out}}$ we get:

$$R_{\mathrm{KCl}} + R_{\mathrm{other}} = 1 \left| \begin{array}{l} R_{\mathrm{KCl}} = \alpha L_{\max} \frac{hc}{\gamma \lambda_f} \frac{V_f}{\sigma_K L (E_{\mathrm{in}} - E_{\mathrm{out}})} \\ R_{\mathrm{other}} = \frac{E^{\mathrm{ext}}}{E_{\mathrm{in}} - E_{\mathrm{out}}} \end{array} \right. , \quad (5)$$

where R_{KCl} and R_{other} describe the percentages of the total absorbed fragmentation energy by target molecule absorption and by other extinction mechanisms, respectively.

In measurement conditions, where target molecule absorption is dominant extinction mechanism, i.e., sample is pure, we can approximate that $R_{\mathrm{KCl}} = 1$, which yields to

$$\begin{aligned} \alpha L_{\max} \frac{hc}{\gamma \lambda_f} \frac{V_f}{\sigma_K L} &= E_{\mathrm{in}} - E_{\mathrm{out}} \\ 1 - \alpha L_{\max} \frac{hc}{\gamma \lambda_f} \frac{V_f}{\sigma_K L E_{\mathrm{in}}} &= \frac{E_{\mathrm{out}}}{E_{\mathrm{in}}}. \end{aligned} \quad (6)$$

Recalling that the fragmentation takes place only in the volume drawn by the fragmentation pulse and assuming a flat intensity distribution for the fragmentation pulse, the volume V_f can be expressed as $V_f = A_f\, L$, where A_f is the cross-section area of the fragmenting pulse. Moreover, we can apply the Beer–Lambert law to describe the relation $E_{\mathrm{out}}/E_{\mathrm{in}}$, and get

$$\begin{aligned} 1 - \alpha L_{\max} \frac{hc}{\gamma \lambda_f} \frac{A_f}{\sigma_K E_{\mathrm{in}}} &= \exp(-\alpha_{\mathrm{KCl}} L) \\ 1 - \alpha L_{\max} \frac{hc}{\gamma \lambda_f} \frac{A_f}{\sigma_K E_{\mathrm{in}}} &= \exp\left(-X_{\mathrm{KCl}} \frac{N}{V} \sigma_{\mathrm{KCl}} L\right), \end{aligned} \quad (7)$$

where α_{KCl}, N/V, and σ_{KCl} are target molecule absorption coefficient, total molecule density in the sample and the absorption cross-section of the target molecule at λ_f, respectively. Finally, by applying the ideal gas law to describe molecule density and solving X_{KCl} out from Eq. 7, we get a relation

$$X_{\mathrm{KCl}} = -\ln\left(1 - \alpha L_{\max} \frac{hc}{\gamma \lambda_f} \frac{1}{\sigma_K} \frac{A_f}{E_{\mathrm{in}}}\right) \frac{kT}{p} \frac{1}{\sigma_{\mathrm{KCl}} L}, \quad (8)$$

where p, k_B and T are sample pressure, the Boltzmann constant, and sample temperature, respectively. Equation 8 describes how a measurable parameter $\alpha\ L_{\max}$ and a measurement setup specific variable fragmentation energy density E_{in}/A_f can be used to calculate the target molecule concentration from the pure samples. Other parameters in Eq. 8 are physical constants or sample specific parameters.

In measurement conditions, where the fragmentation pulse attenuates strongly while propagating through the sample, the density of the produced fragment atoms is smaller at the end of the sample than at the beginning. The strong attenuation of the fragmentation pulse in pure samples means high target molecule concentration and is taken into account in Eq. 8 as a logarithm dependence between X_{KCl} and $\alpha\ L_{\max}$. In impure samples, the fragmentation pulse attenuates due to multiple extinction mechanisms, e.g., absorption by target molecule, absorption by other gas components, and scattering from particles. Beer–Lambert law determines that the attenuation of the fragmentation pulse can be expressed in common case as

$$\ln\left(\frac{E_{\text{in}}}{E_{\text{out}}}\right) = \sum_{i=1}^{\text{n}} \epsilon_{\text{i}} L = \epsilon_{\text{tot}} L, \tag{9}$$

where ε_i and ε_{tot} are the extinction coefficient of the single extinction agent and the total extinction coefficient, respectively. In order to solve the share of the target molecule absorption out from the total extinction, we can multiply the both sides in Eq. 9 by R_{KCl} and get

$$\begin{aligned} \ln\left(\frac{E_{\text{in}}}{E_{\text{out}}}\right) R_{\text{KCl}} &= R_{\text{KCl}} \epsilon_{\text{tot}} L \\ \ln\left(\frac{E_{\text{in}}}{E_{\text{out}}}\right) R_{\text{KCl}} &= \alpha_{\text{KCl}} L. \end{aligned} \tag{10}$$

Inserting the previously presented quantities R_{KCl} and α_{KCl} to Eq. 10, we get

$$\ln\left(\frac{E_{\text{in}}}{E_{\text{out}}}\right) \alpha L_{\max} \frac{\text{hc}}{\gamma \lambda_{\text{f}}} \frac{V_{\text{f}}}{\sigma_{\text{K}} L (E_{\text{in}} - E_{\text{out}})} = \text{X}_{\text{KCl}} \frac{\text{p}}{\text{kT}} \sigma_{\text{KCl}} L. \tag{11}$$

Finally, solving X_{KCl} from Eq. 11 results

$$X_{\text{KCl}} = \alpha L_{\max} \frac{A_f}{E_{\text{in}} L} \frac{hc}{\gamma \lambda_f} \frac{kT}{p} \frac{1}{\sigma_K \sigma_{\text{KCl}}} \frac{\ln(\text{E}_{\text{in}}/\text{E}_{\text{out}})}{1 - E_{\text{out}}/E_{\text{in}}}. \tag{12}$$

Equation 12 presents a common relation between the target molecule concentration X_{KCl} in pure and impure samples, and the measured quantity $\alpha\ L_{\max}$, the measurement setup specific variable E_{in}/A_f and the background extinction correction coefficient determined by measurable energy values E_{in} and E_{out}. Other parameters in Eq. 12 are sample dependent or physical constants. In case of small extinction, a linear assumption can be applied to the logarithm term in Eq. 12, when the correction coefficient is reduced and we get an approximation

$$X_{\text{KCl}} = \alpha L_{\max} \frac{A_f}{E_{\text{in}} L} \frac{hc}{\gamma \lambda_f} \frac{kT}{p} \frac{1}{\sigma_{\text{K}} \sigma_{\text{KCl}}}. \tag{13}$$

The same approximation is also achieved when a linear assumption is applied to Eq. 8.

We can conclude that when the change in the intensity of the fragmentation pulse through the sample is undetectable, the interfering extinction mechanisms have negligible effect to the signal formation and Eq. 13 or Eq. 8 can be applied in signal processing. In case of detectable extinction, Eq. 8 should be used, when the target molecule absorption is known to be the dominant extinction mechanism in the sample, in order to minimize measurement errors due to the fluctuations between independent detectors. Finally, Eq. 12 should be used when the content of the sample is unknown or it is known to contain many different extinction agents.

3 Experiments

The validity of the theoretical derivation in pure samples was studied experimentally using a measurement setup shown in Fig. 1. The setup allowed the comparison of CPFAAS and two reference techniques in the determination of KCl concentration from sample volume. In the CPFAAS technique, a quadrupled Nd:YAG laser (FQSS 266-200, Crylas GmBh.) emitting 1 ns pulses at a 20 Hz repetition rate at the wavelength of 266 nm was used for the fragmentation of the KCl molecules. The output beam of the fragmentation laser was expanded with a factor of 10 and then limited with an aperture having a diameter of 2.8 mm in order to achieve a flat beam profile. The energy of the pulses entering the sample was monitored with an energy meter (PD10, Ophir). The K atoms released in fragmentation were probed with a distributed feedback (DFB) laser emitting light at the wavelength of 766.5 nm (in air)

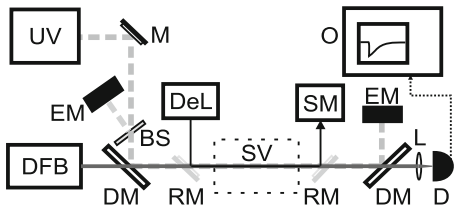

Fig. 1 Experimental setup for the detection of vaporous potassium chloride: fragmentation laser (UV); probe laser (DFB); Deuterium lamp (DeL); mirror (M); beam splitter (BS); dichroic mirror (DM); removable mirror (RM); sample volume (SV); spektrometer (SM); energy meter (EM); lens (L); detector (D); oscilloscope (O)

(Nanoplus GmbH). The wavelength of the probe laser was tuned to the absorption maximum of K vapor in a reference cell (SC-K-19 × 75-Q-W, Photonics Technologies) having inner pressure of 10^{-7} Torr and a temperature of 60 °C. The operation of the DFB laser was considered stable, as no short-term wavelength drifting compared to the K absorption maximum was observed. The UV and IR laser beams were combined on the same optical path using a dichroic mirror (FF310-Di01, Semrock). After passing the sample volume, the laser beams were separated and directed to a pulse energy meter (PE9, Ophir) and to an amplified photodiode (PDA10A, Thorlabs) with an analog bandwidth of 0–150 MHz. Probe laser transmission curves were recorded using an oscilloscope (Waverunner6000, LeCroy).

KCl sample vapor was produced by sublimating KCl powder in 80-cm-long quartz glass tube with an inner diameter of 36 mm. The powder was spread evenly at the bottom of the 50 cm long heated section of the tube. The middle point temperature of the oven ranged from 410 to 762 °C during the experiments. The ends of the quartz tube were open that led us to assume a constant pressure of 1 atm through the whole sample tube. As a first reference technique for KCl concentration, we measured the temperature profile in the oven using a K-type thermocouple and then calculated the corresponding saturated KCl vapor pressure profile through the tube using a thermochemical database (HSC 5.1, Outokumpu). The average concentration over the heated section was found to be less than half of the local maximum KCl concentration at the center of the tube.

Differential optical absorption spectroscopy (DOAS) was used as a second reference technique. DOAS applies a known reference spectrum to solve the concentration of the sample out from a measured absorption spectrum. Previously, DOAS has been applied to measure, e.g., KCl monomers at parts per million (ppm) level [14]. Instead of using KCl monomer spectrum, the combination spectrum of KCl monomers and dimers [13] was applied in this study due to the method of sample generation. DOAS measurement was done using a deuterium lamp (AvaLight-DH-S-BAL, Avantes) emitting broadband UV light and a spectrometer (AvaSpec-2048, Avantes). The broadband light beam was aligned on the same optical path with CPFAAS beams using removable mirrors. The DOAS measurements were done after each CPFAAS measurement in order to get a reference from same sample conditions. DOAS spectra were measured using 300 ms exposure time and were repeated 10 times at every temperature.

4 Results

Three CPFAAS transmission curves and their curve fittings according to Eq. 1 are presented in Fig. 2. The transmission curves were measured through the measurement cell having middle point temperatures and corresponding to calculated KCl equilibrium concentrations of (a) 456 °C and 3.8 ppb, (b) 534 °C and 126 ppb, and (c) 762 °C and 155 ppm. The signals were excited using UV pulse energies of 16μJ in measurements (a) and (b), and 1.6 μJ in measurement (c). Curve fittings yielded (a) $\propto L_{max} = 0.0056$ and $\tau = 28$ ns (b) $\propto L_{max} = 0.17$ and $\tau = 42$ ns (c) $\propto L_{max} = 13$ and $\tau = 82$ ns. Offset parameter C was determined to be 6 % of I_0 in each measurement according to transmission curve measured from KCl concentration of 155 ppm.

The fitting function showed good correspondence to the observed transmission curves in all measured conditions. The relation $\propto L_{max}/E_0$ increased with respect to the KCl concentration as was expected in Eq. 8. The relaxation time constant τ became longer when the sample temperature was increased. A similar behavior between elevated temperature and K atom decay time in O_2-rich conditions has been previously reported by Husain et al. [15]. The amount of produced K atoms was found to have negligible effect to τ when measuring transmission curve in similar condition with different E_{in} values. The oscillation observed in the vicinity of the fragmentation occurred at the frequency of the analog bandwidth limit of the used amplified photodiode. The oscillations had negligible effect to the curve fittings due to their periodic behavior and short occurrence time.

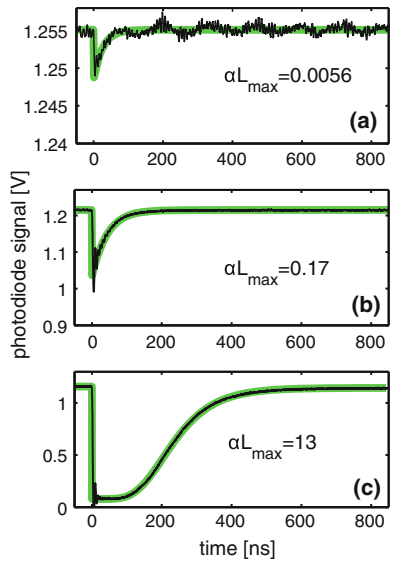

Fig. 2 Three example signals and their *curve* fittings measured from KCl equilibrium concentrations of **a** 3.8 ppb, **b** 126 ppb and **c** 155 ppm using UV pulse energies of 16, 16, and 1.6 μJ, respectively

Table 1 Variables used to calculate KCl concentrations in CPFAAS technique

Variable	Value
σ_{KCl}	0.74×10^{-21} m^2 [13]
σ_K	1.15×10^{-16} m^2
A	6.16×10^{-6} m^2
E_p	16 μJ, 1.6 μJ[a]
L	0.50 m
γ	1 [13]

[a] Lower pulse energies were used when KCl concentration was 0.4 ppm or higher in order to avoid signal saturation

In the previous chapter 2, the relation between observed $\propto L_{max}$ and target molecule was discussed in pure an impure samples. In this study, the only extinction agent for the fragmentation pulse is KCl vapor and, therefore, Eq. 8 is applied in following calculations. The equation includes physical constants and measurement setup dependent variables. The variable values used in these experiments are presented in Table 1. The absorption cross-section of the K atom fragments at their probing wavelength was determined by utilizing the lineshape of the K atom fragments, having linewidth of 15.7 pm, determined previously [10] and the Einstein coefficient [16] for the used $4^2S_{1/2} - 4^2P_{3/2}$ electron transition. The probing wavelength was measured to be 4 pm off from the peak absorption of K fragments due to the different conditions between the reference cell and the sample cell. 4 pm offset yielded 20 % reduction to σ_K when compared to its peak value. The fragmentation pulse energies were decreased at the temperatures of $T \geq 566$ °C corresponding to the calculated equilibrium concentration of $X_{KCl} \geq 0.4$ ppm in order to avoid signal saturation during the comparison measurements done with the DOAS technique. The signal saturation refers in this study to the broadening of the recovering transmission tail outside the measurement window.

KCl concentrations determined using CPFAAS technique, i.e., curve fitting parameter $\propto L_{max}$ and Eq. 8, are compared to values measured using DOAS in Fig. 3. The presented values are the averages of 10 individual measurements and the errorbars correspond to their +/- standard deviations. The standard deviation of the KCl concentrations determined by using the CPFAAS technique was smaller than 2 % of average values in all presented conditions and are indistinguishable in Fig. 3.

DOAS and CPFAAS techniques were found to result similar KCl concentration values over the measured concentration range. The measurement range was limited at the low concentration end by the sensitivity of DOAS technique and at the high concentration end by the instability of the sample vapor due to the partial melting of the KCl powder. The good correspondence between the DOAS technique and the CPFAAS technique showing less than 5 % mutual variation validates the theoretically derived Eq. 8 within the measured concentration range.

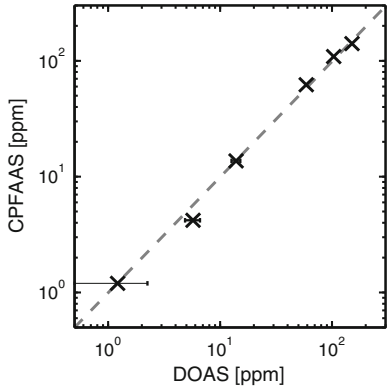

Fig. 3 Comparison between KCl concentrations measured using DOAS and CPFAAS techniques. *Dashed line* having a slope of one indicates ideal correspondence

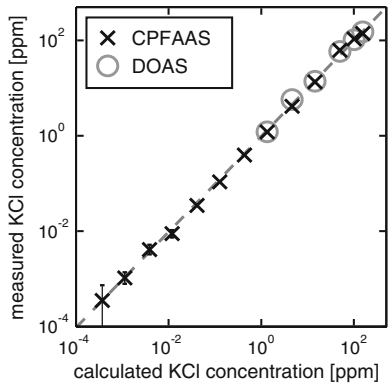

Fig. 4 Comparison between calculated equilibrium KCl concentrations and KCl concentration measured using CPFAAS and DOAS techniques. The *dashed line* having a slope of one is added to the figure to emphasize the ideal correspondence between the techniques

The linearity of CPFAAS at sub-ppm concentrations was studied by comparing the measured values to the calculated equilibrium concentrations. The equilibrium calculations were first shown to result reasonable concentrations by comparing the calculated values to the two used measurement techniques at concentrations of $X_{KCl} > 1$ ppm. The comparison between the high concentration values showed that the equilibrium calculations result reasonable values and, therefore, they could be used as a reference for CPFAAS also at low concentrations. The comparison

between equilibrium calculations and CPFAAS in a concentration range of 0.4 ppb–150 ppm is shown in Fig. 4. Also, the previously presented values measured with DOAS are added to Fig. 4 as circles to show the similarity of the results. The X_{KCl} values determined with CPFAAS are averages of 10 measurements in which 10 single transmission curves were averaged before using the curve fitting tool. Error bars correspond to the ±standard deviations of the 10 single KCl concentration value at every measurement point.

An ideal correspondence line having slope of one was added to Fig. 4 in order to emphasize the differences between the KCl concentrations determined with the three different techniques. The difference between KCl concentrations determined using CPFAAS and the equilibrium calculations was less than 20 % throughout the whole measurement range. The observed fluctuation between the measured and the calculated concentrations is reasonable, especially when taking into account the possible temperature fluctuations in the sample cell due to the open ends. The 20 % change in equilibrium concentration corresponds to the temperature change of 5 °C.

The experimental results showed that the assumed CPFAAS curve shape fits well with the measured curves, and the technique can be used to determine the concentration of the sample with a good accuracy without the need for a separate calibration. The absorption dip in the non-averaged single CPFAAS transmission curves could be obtained from sample having KCl concentration of 1 ppb, which enables fast and sensitive diagnostics in microsecond timescale. The CPFAAS technique was also shown to provide at least 5 orders of magnitude dynamic range with linear response respect to the sample concentration. The theoretical saturation limit of the technique is achieved when the whole fragmentation pulse is absorbed to the sample. Assuming the minimum detectable transmissivity of the pulse is 1/1,000, we get a saturation limit of 2,500 ppm for KCl with the used measurement arrangement. At the low concentration end, the absolute detection limit is achieved when the fragmentation pulse starts to saturate the target gas absorption and $\propto L_{max}$ is indistinguishable from the detector noise. In a previous study, it was shown that the absorption of KCl is linear up to 100 μJ excitation energy when the diameter of the UV beam is 1 mm^2 and the fragmentation wavelength is 245 nm [17]. Scaling these saturation values to the values used in this study, it is found that the detection limit could still be improved with a factor of 100 by properly selecting of the fragmentation light source. According to these estimations, it is possible to achieve 8 orders of magnitude dynamic range in the detection of KCl by tuning the fragmentation pulse energy.

5 Conclusions

The principles and the signal formation in the CPFAAS technique were discussed, and the theoretical relations between absorption by the fragment atoms and the target molecule concentration were introduced in different measurement conditions. The theoretical treatment of pure samples was verified with experiments including the comparison between the assumed and the measured shape of the probe laser transmission curve in the vicinity of the fragmentation, and with the comparison between sample concentrations determined using CPFAAS and two independent reference techniques. The sample gas in these experiments was KCl vapor that was produced by sublimating KCl powder in a quartz glass tube using temperatures from 410 to 762 °C.

The demonstrated linear response over five orders of magnitude and discussed achievable dynamic range of eight orders of magnitude are important properties when strongly fluctuating samples are analyzed. Moreover, the capability of detecting 1 ppb sample concentration within 1 μs provides an excellent time resolution. CPFAAS can be applied to measure target molecule concentrations from small laboratory scale samples due to its good sensitivity and large sample volumes due to its immunity against strong attenuation of the fragmentation pulse. The absolute limits for detection are the electrical noise of the detector at the low concentration end and the non-detectable transmissivity of the fragmentation pulse at the high concentration end.

Acknowledgments This work has been partly carried out within the consortium FUSEC (2011–2014) with support from National Technology Agency of Finland (Tekes), Andritz Oy, Metso Power Oy, Foster Wheeler Energia Oy, UPM-Kymmene Oyj, Clyde Bergemann GmbH, International Paper Inc. and Top Analytica Oy Ab. T. Sorvajärvi acknowledges support from the graduate school of Tampere University of Technology.

References

1. J. Simeonsson, R. Sausa, TrAC Trends Anal. Chem. **17**(8), 542 (1998)
2. J. Simeonsson, R. Sausa, Appl. Spectrosc. **50**(10), 1277 (1996)
3. R. Oldenborg, S. Baughcum, Anal. Chem. **58**(7), 1430 (1986)
4. O. Johansson, J. Bood, M. Alden, U. Lindblad, Appl. Spectrosc. **62**(1), 66 (2008)
5. J. Silver, D. Worsnop, A. Freedman, C. Kolb, J. Chem. Phys. **84**, 4378 (1986)
6. D.E. Self, J.M. Plane, Phys. Chem. Chem. Phys. **4**(1), 16 (2002)

7. C. Erbel, M. Mayerhofer, P. Monkhouse, M. Gaderer, H. Spliethoff, Proc. Combust. Inst. **34**, 2331 (2013)
8. S. Edelstein, P. Davidovits, J. Chem. Phys. **55**, 5164 (1971)
9. D. Ehrlich, R. Osgood Jr, IEEE J. Quantum Electron. **16**(3), 257 (2002)
10. T. Sorvajärvi, J. Saarela, J. Toivonen, Opt. Lett. **37**(19), 4011 (2012)
11. C.M. Roehl, J.J. Orlando, G.S. Tyndall, R.E. Shetter, G.J. Vazquez, C.A. Cantrell, J.G. Calvert, J. Phys. Chem. **98**(32), 7837 (1994)
12. R. Samuel, Rev. Mod. Phys. **18**(1), 103 (1946)
13. P. Davidovits, D.C. Brodhead, J. Chem. Phys. **46**(8), 2968 (1967)
14. C. Forsberg, M. Broström, R. Backman, E. Edvardsson, S. Badiei, M. Berg, H. Kassman, Rev. Sci. Instrum. **80**, 023104 (2009)
15. D. Husain, Y. Lee, P. Marshall, Combust. Flame **68**(2), 143 (1987)
16. D. Morton, Astrophys. J. Suppl. Ser. **149**(1), 205 (2003)
17. T. Sorvajärvi, A. Manninen, J. Toivonen, J. Saarela, R. Hernberg, Rev. Sci. Instrum. **80**, 123103 (2009)

Paper 4

Tapio Sorvajärvi, Nikolai DeMartini, Jussi Rossi, and Juha Toivonen.

In-situ measurement technique for simultaneous detection of K, KCl and KOH vapors released during combustion of solid biomass fuels in single particle reactor.

Applied Spectroscopy
Accepted for Publication

Tampereen teknillinen yliopisto
PL 527
33101 Tampere

Tampere University of Technology
P.O.B. 527
FI-33101 Tampere, Finland

ISBN 978-952-15-3188-0
ISSN 1459-2045